PhD degree in Systems Medicine (curriculum in Molecular Oncology)

European School of Molecular Medicine (SEMM)

University of Milan, Faculty of Medicine

THE ROLE OF TELOMERIC RNA AT DYSFUNCTIONAL TELOMERES AND ITS IMPACT ON SENESCENCE AND AGING

Julio Aguado Pérez

IFOM, Milan

Matricola n. R10800

Supervisor Dr. Fabrizio d'Adda di Fagagna
IFOM, Milan

Internal co-supervisor Dr. Marco Foiani
IFOM, Milan

External co-supervisor Dr. Joachim Lingner
EPFL, Lausanne

Academic year 2017-2018

Some Figures presented in this doctoral dissertation are already part of published reports. I have listed them below:

Figures 13, 15, 16, 17, 18, 19, 20b-c, 21 and 22 are part of a report of Rossiello F, **Aguado J**, et al. in Nature Communications (Rossiello et al., 2017).

Figures 7, 8, 9 and 10 are part of a report of Nguyen Q[*], **Aguado J**[*] et al. in Nature Protocols (Nguyen et al., 2018). [*]Co-first authors.

Table of Contents

List of Abbreviations

4OHT	4-hydroxytomaxifen
53BP1	p53 binding protein 1
a-NHEJ	Alternative non-homologous end joining
Ago2	Argonaute 2
ALT	Alternative lengthening of telomeres
APB	ALT-Associated PML Body
aRNA	Aberrant RNA
ASO	Antisense Oligonucleotide
ATM	Ataxia telangiectasia mutated
ATM pS1981	Autophosphorylation of ATM at serine 1981
ATR	Ataxia telangiectasia and Rad3-related
ATRIP	ATR-interacting protein
B2M	Beta-2 microglobulin
BRCA1	Breast cancer 1
BrdU	5-bromodeoxyuridine
c-NHEJ	Classical non-homologous end joining
CCF	Cytoplasmic chromatin fragment
CO-FISH	Chromosome orientation fluorescence *in situ* hybridization
CST	CTC1-STN1-TEN1 complex
DAPI	4'-6-Diamidino-2-phenylindole
DDR	DNA-damage response
DDRNA	DNA damage response RNA
dilncRNA	Damage-induced long non-coding RNA
diRNA	DSB-induced RNA

DNA-PKcs	DNA-PK catalytic subunit
DSB	DNA double-strand break
ECTR	Extrachromosomal telomeric repeat
ER	Estrogen receptor
EZH2	Enhancer of Zeste Homolog 2
FBS	Fetal bovine serum
FDA	Food and Drug Administration
FTI	Farnesyltransferase inhibitor
H3K9me3	Histone H3 trimethylated at lysine 9
HBS	HEPES-buffered saline
HGPS	Hutchinson–Gilford Progeria Syndrome
HP1α	Heterochromatin Protein 1 alpha
HR	Homologous recombination
hTERT	Human telomerase reverse transcriptase
hTR	Human telomerase RNA
IL-1A	Interleukin-1A
IL-6	Interleukin-6
IL-8	Interleukin-8
IR	Ionizing radiation
KAT5	Lysine acetyl transferase 5
LAP2α	Lamina-associated polypeptide-α
LNA	Locked nucleic acid
lncRNA	Long non-coding RNA
m7G	7-methylguanosine
MDC1	Mediator of DNA damage checkpoint 1
MEF	Mouse embryonic fibroblast

miRNA	microRNA
MRN	Mre11-Rad50-Nbs1 complex
NEAA	Non-essential amino acid
NF-κB	Kappa-light-chain-enhancer of activated B cells
NHEJ	Non-homologous end joining
nt	nucleotide
OB	Oligonucleotide/oligosaccharide binding
PARP1	Poly(ADP-ribose) polymerase 1
PBS	Phosphate Buffered Saline
PFA	Paraformaldehyde
piRNA	Piwi interacting RNA
POT1	Protection of telomeres 1
pRB	Retinoblastoma protein
RAP1	Repressor/activator protein 1
RNA Pol II	RNA Polymerase II
RNAi	RNA interference
ROS	Reactive oxygen species
RPA	Replication protein A
Rplp0	Ribosomal protein large P0
rRNA	Ribosomal RNA
RT	Room temperature
SA-β-gal	Senescence-associated-β-galactosidase
SAHF	Senescence-associated heterochromatin foci
SASP	Senescence-associated secretory phenotype
SDF	Senescence-associated DNA-damage foci
SDS	Sodium dodecyl sulphate

siRNA	Small interfering RNA
sncRNA	Small non-coding RNA
snoRNA	Small nucleolar RNA
snRNA	Small nuclear RNA
sRNA	Small RNA
SSB	Single-strand break
ssDNA	Single-stranded DNA
ssRNA	Single-stranded RNA
T-SCE	Telomere-sister chromatid exchange
TERRA	Telomeric repeat-containing RNA
TEsR	Target-Enrichment of small RNAs
TIF	Telomere induced foci
TIN2	TRF1-interacting nuclear factor 2
TMM	Telomere maintenance mechanism
TopBP1	Topoisomerase II binding protein 1
TRF1	Telomeric-repeat-binding factor 1
TRF2	Telomeric-repeat-binding factor 2
tRNA	Transfer RNA
tTR	Tetracyclin-controlled transactivator
TZAP	Telomeric zinc finger-associated protein
UV	Ultraviolet light
XRCC4	X-ray repair cross-complementing protein 4

Figures Index

Abstract

A novel class of small non-coding RNAs discovered in our laboratory, termed DNA damage response RNAs (DDRNAs), has been demonstrated to be locally generated upon DNA double strand break (DSB) induction, and to be necessary for full DNA Damage Response (DDR) activation (Francia et al., 2012, Francia et al., 2016). DDRNAs are generated following DSB induction upon transcription of the damaged locus and the synthesis of an RNA precursor further processed by the endoribonucleases DICER and DROSHA (Michelini et al., 2017). DSBs generated by different sources such as ionizing radiation, enzymatic DNA cleavage, or oncogene-induced replicative stress, induce the generation of DDRNAs (Francia et al., 2012).

The aim of my PhD project was to investigate the mechanism underlying DDRNA-dependent DDR activation specifically at telomeres, important chromosomal regions required for genomic stability that, if disrupted, are associated with aging-related diseases. In this dissertation, I show that telomere dysfunction, like DSBs, induces the transcription of telomeric DDRNAs and their precursors from both DNA strands of the telomere. Such transcripts are necessary for DDR activation and maintenance at dysfunctional telomeres. Most importantly, the use of sequence-specific antisense oligonucleotides (ASOs) allows the inhibition of telomere transcripts' functions, thereby specifically inhibiting telomeric DDR.

Furthermore, I show that telomere dysfunction in senescence, induced by either critically short telomeres or irreparable telomeres after ionizing radiation, induces the transcription of telomeric DDRNAs, whose inhibition leads to a decrease of the cyclin dependent kinase inhibitors p21 and p16.

Telomere dysfunction is a key feature in Hutchinson–Gilford Progeria Syndrome (HGPS), and other premature aging syndromes. Hallmarks of HGPS are accumulation of DNA damage, chromosomal instability, and accelerated telomere shortening and dysfunction (Gonzalo et al., 2017). Here I show that progerin, a truncated form of the Lamin A protein whose expression causes HGPS, induces the transcription of telomeric DDRNAs and their

precursors, both *in vitro* and *in vivo*. Furthermore, inhibition of progerin-driven telomere transcripts improves the growth potential of progerin-overexpressing and HGPS patient-derived cells. Excitingly, this inhibition also increases the lifespan of an HGPS mouse model, opening the possibility for the use of this approach as a viable therapy to treat HGPS.

1 INTRODUCTION

1.1 The DNA damage response

Cell viability is threatened every time DNA lesions of any kind occur. Every human cell experiences tens of thousands of lesions per day (Lindahl and Barnes, 2000), which have the potential of blocking DNA replication and transcription and if unsuccessfully repaired can lead to mutations with serious consequences.

Some alterations in DNA can originate through physiological processes like DNA replication, leading for instance to the introduction of DNA mismatches, or cell metabolism, which is responsible for the production of reactive oxygen species (ROS) derived from oxidative respiration, leading to oxidative DNA modifications (Valko et al., 2006).

Endogenously-produced ROS and nitrogen chemicals often lead to the formation of DNA single-strand breaks (SSBs) and, when two of them occur in close proximity, DNA double-strand breaks (DSBs) can occur. DSBs can also be generated as a result of fork stalling following oncogene-induced replication stress (Di Micco et al., 2007). Importantly, although DSBs arise less frequently than the above-mentioned lesions, they are the most challenging lesions for the cell machinery to repair and can therefore be severely toxic (Khanna and Jackson, 2001).

In addition to endogenous DNA damage sources, there are also several exogenous sources with the potential to compromise the integrity and stability of the genome. Some well-studied sources are ultraviolet light (UV) (the most prevalent environmental DNA-damaging agent causing approximately 100,000 lesions per exposed cell per hour), ionizing radiation (IR) and various genotoxic compounds (e.g. chemotherapics such as neocarzinostatin, bleomycin) (Ward, 1988, Iliakis et al., 2003, Povirk, 1996, Rastogi et al., 2010).

1.1.1 The DNA damage response pathway

To handle the threats of DNA lesions, cells have developed mechanisms – known as DNA-damage response (DDR) pathways – to detect DNA damage and amplify the signal of its

presence, and promote its repair (Harper and Elledge, 2007, Harrison and Haber, 2006, Polo and Jackson, 2011). When a DNA lesion arises, a DDR is activated, and cell-cycle progression is arrested in order to avoid the propagation of DNA alterations (known as the checkpoint function). Meanwhile, the cell coordinates a mechanism of DNA damage repair to maintain genome integrity.

Exposed SSBs or DSBs induce the activation of a DDR (**Figure 1**). These two DNA lesions are sensed by complexes that recruit and activate the protein kinases ataxia telangiectasia and Rad3-related (ATR) or ataxia telangiectasia mutated (ATM), respectively, at sites of DNA damage (Shiloh, 2003, Bartek and Lukas, 2007).

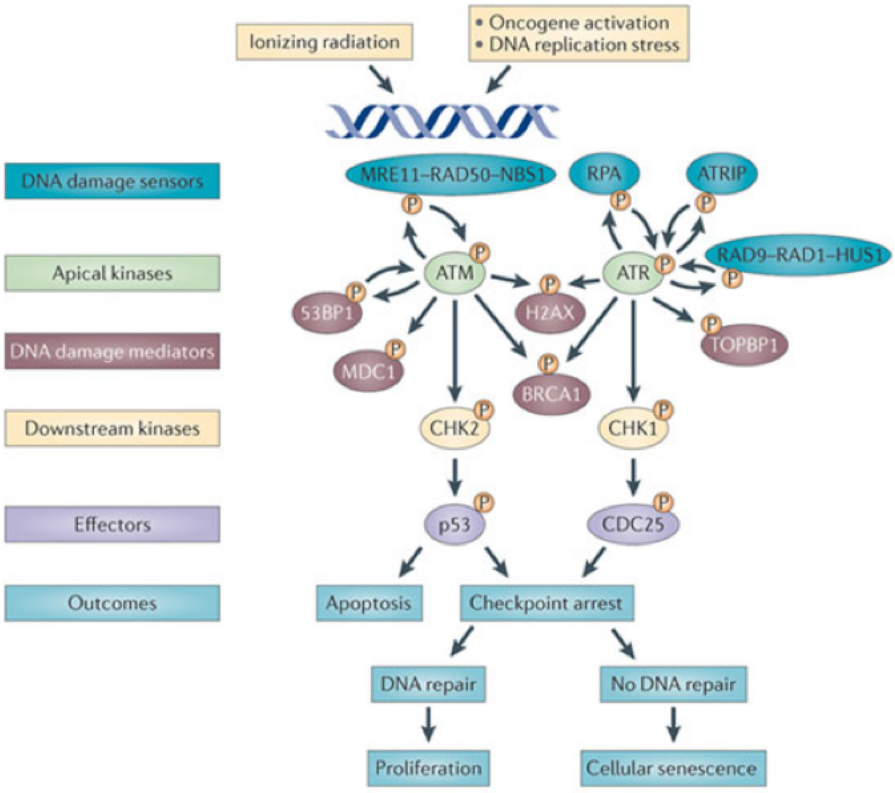

Adapted from (Sulli et al., 2012)

Figure 1. The DNA damage checkpoint response cascade.

DSBs are initially recognized by the Mre11-Rad50-Nbs1 (MRN) complex, while ssDNA is coated by RPA and the RAD9–RAD1–HUS1 (9-1-1) complex. These initial sensors allow the recruitment and activation of the apical kinases ATM and ATR, which in turn phosphorylate the histone variant H2AX at Ser139 (known as γH2AX) to recruit to the site of damage other DDR proteins such as MDC1, 53BP1 and BRCA1. The downstream kinases CHK2 and CHK1 are respectively phosphorylated by ATM and ATR, which ultimately

spread the signal to effector proteins such as p53 and CDC25. The three potential outcomes of the DDR are cell death by apoptosis or a checkpoint arrest, which can be successfully resolved by repair of the damaged site (leading to a resumption of cell proliferation) or enter a permanent arrest known as cellular senescence caused by persistent DNA damage.

ATR and ATM are members of the family of phosphatidylinositol 3-kinase-like kinases, which tend to phosphorylate their substrates on a serine or threonine followed by glutamine: S/TQ motif (known as pS/TQ once phosphorylated) (Bensimon et al., 2010). The recruitment of ATR or ATM to DSBs induces the phosphorylation of the histone variant H2AX at serine 139 (so-called γH2AX). γH2AX serves for the retention of other DDR proteins at sites of DNA damage (Martin et al., 2009), which leads to a positive feedback loop that propagates γH2AX formation for megabases in cis along the chromatin (Iacovoni et al., 2010). Formation of γH2AX at the site of DNA breaks is cytologically detectable in the form of discrete bright foci when damaged cells are stained with antibodies against γH2AX or other DNA damage markers.

When single-stranded DNA (ssDNA) is exposed, replication protein A (RPA) binds to it and serves as an initial signal for ATR-interacting protein (ATRIP) and ATR recruitment (Zou and Elledge, 2003, Ball et al., 2005), a process boosted by the recruitment of the RAD9–RAD1–HUS1 (9-1-1) complex and topoisomerase II binding protein 1 (TopBP1) to the chromatin where ssDNA sites arise, ultimately allowing the spreading of the DDR signalling (Cimprich and Cortez, 2008).

ATM, in the absence of DSBs, remains inactive in the form of a homodimer (Shiloh and Ziv, 2013). However, when a DSB arises, it undergoes a conformational change leading to its monomerization that allows the specific recognition of chromatin flanking DSBs by interacting with the Mre11-Rad50-Nbs1 (MRN) complex. This interaction favours the acetylation of ATM by lysine acetyl transferase 5 (KAT5) (Sun et al., 2005), which in turn allows the full activation of ATM through its autophosphorylation at serine 1981 (ATM pS1981). Activated ATM then amplifies DDR signalling by phosphorylating (and

recruiting to the site of DNA break) the proteins mediator of DNA damage checkpoint 1 (MDC1), p53 binding protein 1 (53BP1) and breast cancer 1 (BRCA1) (Bekker-Jensen et al., 2005, Stucki et al., 2005).

It is known that ATR and ATM cross talk with each other to a certain extent. For instance, ATM favours the activation of ATR by enhancing DNA end resection (Jazayeri et al., 2006). On the other hand, ATR is known to phosphorylate H2AX upon DNA replication stress induction, which may recruit and activate ATM to the chromatin where stressed replication forks are generated (Ward and Chen, 2001).

Activation of ATR and ATM leads to the phosphorylation of the downstream protein kinases CHK1 and CHK2 respectively, although it has been reported that CHK1 can also be phosphorylated by ATM (Bekker-Jensen et al., 2006). Activated CHK1 and CHK2 ultimately phosphorylate their respective targets CDC25 and p53 leading to cell death by apoptosis or activation of a checkpoint arrest. This proliferative arrest can be transient, in case the damaged genomic site is successfully repaired, or permanent, known as cellular senescence, where the DNA damaged site persists.

1.1.2 DNA double-strand break repair pathways

As DSBs are extremely toxic lesions, their successful repair is critical to maintain the integrity and stability of the genome and cell survival. Defects in the DNA repair pathways can lead to cell death or chromosomal rearrangements that have the potential of generating cancer. Cells have two major pathways to repair DSBs (**Figure 2**): homologous recombination (HR) and non-homologous end joining (NHEJ) (Chapman et al., 2012, Chang et al., 2017).

NHEJ is a fast DNA repair pathway, where the rejoining of DNA ends is available throughout all phases of the cell cycle. ATM has been reported to contribute to NHEJ (Zha et al., 2011). When DSBs arise at DNA replication forks in the S phase of the cell cycle or after DNA replication in G2 phase, the second major DSB repair pathway, HR, is preferentially used (Karpenshif and Bernstein, 2012). As opposed to NHEJ, HR requires

both the homologous DNA as a repair template sequence (often from sister chromatids) and ssDNA ends to search for a homologous sequence.

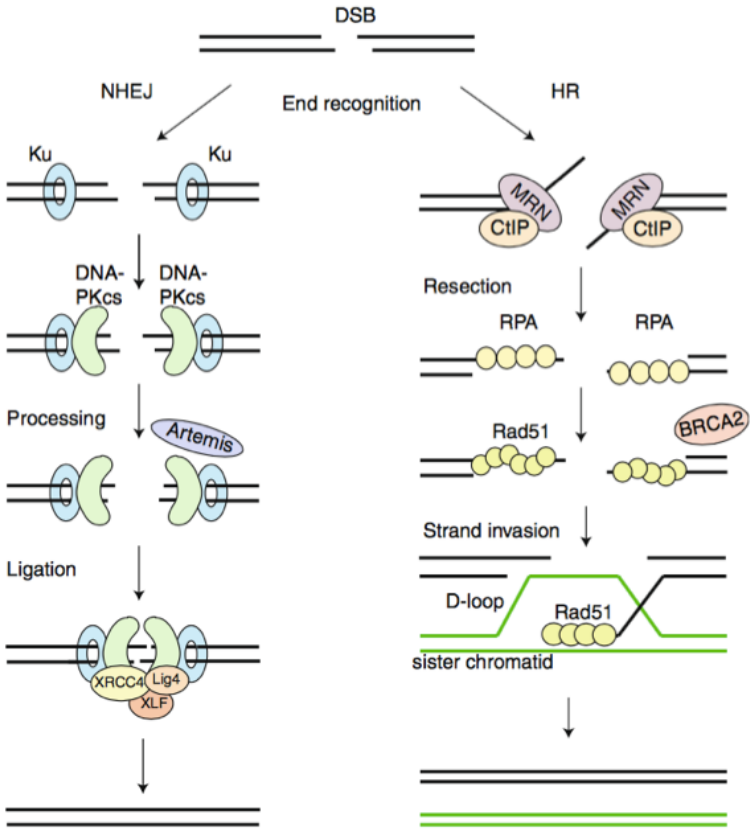

Adapted from (Brandsma and Gent, 2012)

Figure 2. The major DNA repair pathways: NHEJ and HR.

NHEJ: DNA ends are initially recognised by the KU70/80 heterodimer, which recruits and activates DNA-PKcs and brings the nuclease Artemis to trim DNA ends. Next, the XRCC4-DNA Ligase IV-XLF complex seals the lesion. **HR:** DNA binding and resection is performed by the MRN-CtIP-complex to generate ssDNA, which is first coated by RPA and subsequently displaced by Rad51, a process mediated by BRCA2 and RAD52. RAD51-loaded ssDNA allows the strand invasion on the homologous template leading to the formation of a D-loop that results in *de novo* DNA synthesis.

NHEJ is the only repair pathway cells can use during G0, G1 and the early stages of S phase when homologous templates are yet not available (Lieber, 2010). The KU70/80 heterodimeric complex binds to DNA ends, which allows the recruitment and autophosphorylation of DNA-PK catalytic subunit (DNA-PKcs) in a complex with the endonuclease Artemis (Goodarzi et al., 2006, Gu et al., 2010). If necessary, synthesis of de novo DNA in humans is carried out by two members of the POLX family, DNA

polymerase μ (Pol μ) and Pol λ (Moon et al., 2014), and DNA ligase IV associated with X-ray repair cross-complementing protein 4 (XRCC4) and XLF, which stimulates DNA ligase IV enzyme activity (Grawunder et al., 1997), ligate the DNA ends.

As HR uses a homologous DNA template for repair, it is generally restricted to the late S phase (after DNA replication takes place) and G2 phase of the cell cycle (Karpenshif and Bernstein, 2012). An early event in HR is the resection of the DSB in the 5'-to-3' direction, which generates 3'-ssDNA tails. The DNA-binding activity of the MRN complex and the exonuclease activity of its subunit NBS1, together with CtIP and BLM, promote this resection process that enables the strand invasion of the 3'ssDNA. ssDNA is coated by RPA, which controls its accessibility to the RAD51 recombinase (Morrical, 2015). A number of HR mediators, such as BRCA2 and RAD52, mediate the displacement of RPA to allow RAD51 to bind to ssDNA (Zelensky et al., 2014). RAD51-loaded ssDNA catalyses the invasion into a homologous DNA duplex to generate a displacement loop (D-loop). Then, the ATP-dependent DNA translocase Rad54 allows the invading 3'DNA end to be extended by DNA polymerases to generate homologous DNA from the intact DNA duplex (Li and Heyer, 2009) and lastly DNA ligation takes place. This process often generates joint molecules, such as double Holliday junctions, which are generally dissolved by the RecQ helicases BLM and WRN proteins (Wu and Hickson, 2003) or by the MUS81-EME1 nuclease complex (Wyatt and West, 2014) to allow separation of the sister chromatids during mitosis.

When, for various reasons, classical NHEJ (c-NHEJ) is impaired, an alternative mechanism called alternative NHEJ (a-NHEJ), also known as microhomology-mediated end joining and Pol θ-mediated end joining (Saito et al., 2016), is used. Given the extremely low frequency of human mutations in the NHEJ pathway, it is yet unclear whether a-NHEJ is an independent DNA repair pathway or whether its components usually serve other molecular pathways and only become relevant to DNA repair when NHEJ is compromised (Chang et al., 2017). Importantly, a-NHEJ is believed to require

microhomology DNA regions that range between 2 bp and 20 bp as opposed to the HR pathway, which usually requires longer lengths of DNA homology. The mechanisms of a-NHEJ are yet unclear, however it is known to employ polymerase Pol θ (Wyatt et al., 2016) and may also require the activity of poly(ADP-ribose) polymerase 1 (PARP1), CtIP, DNA ligase 3 and XRCC1 and the MRN complex (Sfeir and Symington, 2015).

1.2 The role of non-coding RNAs in DDR and DNA repair

1.2.1 Non-coding RNAs

Non-coding RNAs (ncRNA), which are defined as RNA molecules that are not translated into proteins, have been reported to exert a wide range of functions (St Laurent et al., 2015, Vickers et al., 2015). The growing list of the ncRNA landscape includes ribosomal RNAs (rRNAs), transfer RNAs (tRNAs), small nuclear RNAs (snRNAs), small nucleolar RNAs (snoRNAs), long non-coding RNAs (lncRNAs), microRNAs (miRNAs), small interfering RNAs (siRNAs) and piwi interacting RNAs (piRNAs). In addition to the above-mentioned well-established ncRNAs, increasing evidence supports the existence of a large variety of ncRNAs playing fundamental roles in diverse biological processes. Most studies are focused on the study of lncRNAs and just a small subset is focused on small RNAs (sRNAs). Among sRNA studies, most research so far has focused on miRNAs (Vickers et al., 2015). Since there is mounting evidence of sRNAs playing critical roles in cellular biology, new methods and sequencing techniques are needed to address the fundamental but challenging questions of: (i) whether or not (or in which biological context) sRNA exist; (ii) how many different sRNA isoforms there are and what are their lengths, sequences and quantities; (iii) what are the precursors of a mature sRNA; and (iv) what is the differential expression of low abundant sRNAs in different biological conditions.

1.2.2 The link between ncRNAs and DDR

In the recent years, strong evidence supports a conserved link between DNA damage and ncRNAs across species (d'Adda di Fagagna, 2014).

In the plant *Arabidopsis thaliana*, small ncRNAs (sncRNAs), named DSB-induced RNAs (diRNAs), have been shown to orchestrate DNA repair by HR in a derived cell line where an inducible DSB was generated. These diRNAs are specifically induced upon DSB generation (Wei et al., 2012). They have the RNA sequence corresponding to the DNA-damaged locus, are transcribed by RNA Polymerase IV, and their expression is dependent on the components of the RNA interference (RNAi) machinery Dicer-like proteins and

Argonaute 2 (Ago2). Moreover, upon DSB generation, the expression of HR genes remains unaltered, which demonstrates a miRNA-independent mechanism (Wei et al., 2012).

In *Drosophila melanogaster*, transfection of a linearized plasmid has been reported to induce the generation of sncRNAs (21 nucleotides (nt)), which contain the corresponding DNA sequence of the transfected plasmid ends and are able to silence the transcription of the homologous DNA sequences (Michalik et al., 2012), and more recently have been demonstrated to be dispensable for DNA repair (Schmidts et al., 2016). Furthermore, in *Neurospora crassa*, sncRNAs termed qiRNAs (for QDE-2-interacting small RNAs) were reported to be transcribed from the rDNA locus in response to DNA damage (Lee et al., 2009). Importantly, a single-stranded RNA (ssRNA) named aberrant RNA (aRNA) was reported to be required as precursor RNAs for qiRNA generation (Lee et al., 2010).

Our laboratory has recently demonstrated, in line with the above-mentioned observations, the direct involvement of non-canonical sncRNAs in the modulation of the DDR in mammalian cells. Ionizing radiation, enzymatic DNA cleavage or oncogene-induced replicative stress induce the generation of DNA damage response RNAs (DDRNAs, 20-35 nt), which are generated at DSBs and contain the sequence corresponding to the damaged genomic locus (Francia et al., 2012). The biogenesis of DDRNAs is dependent on the endoribonucleases DROSHA and DICER, and when either of them are inactivated, the formation of DDR foci containing upstream signalling proteins, such as ATM pS1981, 53BP1 and MDC1, is impaired while γH2AX foci remain unaltered (**Figure 3** and (Francia et al., 2012)). Recent additional evidence from our laboratory supports the notion that DDRNAs are dispensable for the direct recognition of DNA damage and H2AX phosphorylation, and are critical for the recruitment of DDR proteins downstream of γH2AX to form DDR foci at DSBs (Francia et al., 2016). Importantly, this effect is not observed upon depletion of GW182 proteins, effectors of the RNAi machinery, demonstrating a miRNA-independent mechanism.

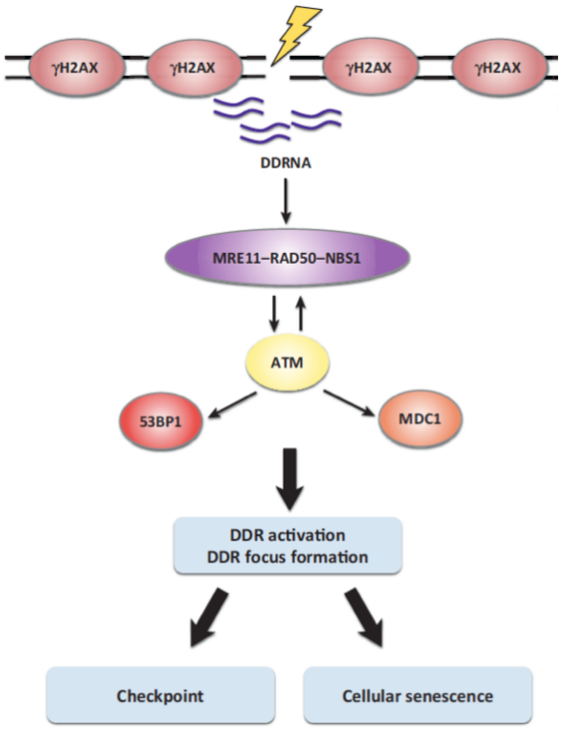

Adapted from (d'Adda di Fagagna, 2014)

Figure 3. DNA Double-strand breaks (DSB) trigger the DNA damage checkpoint response cascade. DNA ends are initially recognized by the MRN complex (MRE11-RAD50-NBS1) which recruits and activates the apical protein kinase ATM. Its activation promotes the phosphorylation of the histone variant H2AX on Ser139 (known as γH2AX). This process is sustained by the recruitment of other downstream mediators like 53BP1 and MDC1. Most importantly, a new class of small non-coding RNAs (ncRNAs), named DNA damage response RNAs (DDRNAs), has been shown to be transcribed upon DSB induction orchestrating events downstream γH2AX.

In addition, more recent data from our laboratory indicates the existence of a longer precursor transcribed by RNA Polymerase II (RNA Pol II) from and towards the broken DNA ends upon DSB generation, which is then processed by DROSHA and DICER to generate DDRNAs (Michelini et al., 2017). In only apparent contrast, RNA Pol II-dependent transcription in gene-coding genomic regions is known to be silenced upon DNA damage (Pankotai et al., 2012, Iannelli et al., 2017, Shanbhag et al., 2010). These apparently mutually exclusive scenarios can be reconciled by a unique hypothesis in which, upon DSB generation, the relaxation of chromatin surrounding the break allows the recruitment of apical DDR proteins and the RNA transcription machinery to the DSB. This

would subsequently favour the transcription and processing of DDRNA precursors allowing full activation of the DDR (Francia et al., 2012) ultimately leading to DNA damage-induced transcriptional silencing.

Regarding DDRNA processing by DICER, in the recent years there has been increasing evidence of DICER nuclear localization (Ando et al., 2011, Ohrt et al., 2012, Gullerova and Proudfoot, 2012, Doyle et al., 2013), opposing the previous notion in which DICER was considered exclusively cytosolic (Billy et al., 2001, Provost et al., 2002), leaving open the possibility of a nuclear DICER DDRNA processing. Strongly supporting this hypothesis, a recent report has demonstrated that nuclear accumulation of a phosphorilated form of DICER localizes at DSBs in response to DNA damage (Burger et al., 2017).

Lastly, upon DSB generation, proteins of the NHEJ pathway, such as Lig IV, XRCC4, KU-70, Pol μ and DNA-PK, have been reported to interact at DSBs with nascent RNAs located in actively transcribed genes (Chakraborty et al., 2016) a potential role of ncRNAs in favouring the recruitment of DDR factors.

1.3 Telomeres: structures and functions

1.3.1 The telomeric nucleoprotein structure and function

Telomeres are nucleoprotein structures at the ends of linear chromosomes (**Figure 4**). In humans and other vertebrates, telomeres are composed of a long DNA array of double-stranded *tandem* TTAGGG repeats and associated telomeric DNA-binding proteins, the so-called shelterin complex (de Lange, 2005).

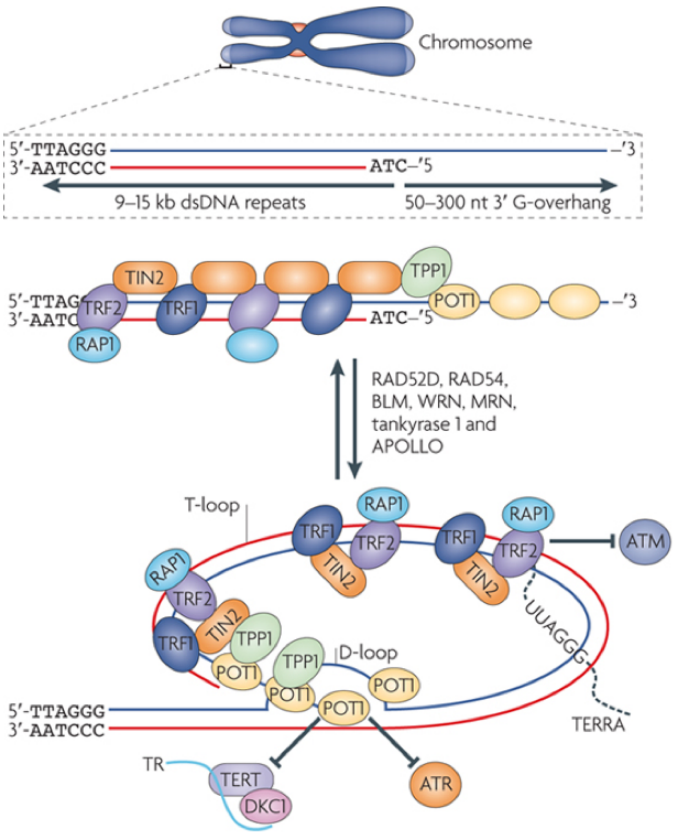

Adapted from (O'Sullivan and Karlseder, 2010)

Figure 4. The telomere structure: Shelterin complex and T-loop scheme.

Telomeres are nucleoprotein complexes composed of double-stranded TTAGGG DNA repeats (which extend for 5-10 kb in humans and up to 100 kb in rodents) and the shelterin proteins TRF1, TRF2, RAP1, TIN2, TPP1 and POT1. Telomeres contain a G-rich 3' overhang which allows the formation of a t-loop structure by invading the upstream double-stranded TTAGGG repeats. This structure protects telomeres from being recognised as DSBs.

Telomeres range from approximately 5-10 kb in human cells to 20-50 kb in mice, which can be synthesized by telomerase, a specialized reverse transcriptase (Greider, 1993).

Telomeres end with a single-stranded G-rich overhang, typically 50-300 nt long (Makarov et al., 1997, O'Sullivan and Karlseder, 2010). Apollo and Exo1 nucleases resect telomeric DNA in the 5'-3' direction in order to generate the G-rich overhang (Wu et al., 2012), which is needed for the invasion of the double-stranded telomeric DNA leading to the formation of a specialized lasso-like structure called the telomere loop or t-loop (Griffith et al., 1999, Doksani et al., 2013).

Telomeric DNA is associated with the shelterin complex (de Lange, 2005), a group of six proteins composed by: telomeric-repeat-binding factor 1 and 2 (TRF1 and TRF2), repressor/activator protein 1 (RAP1), TRF1-interacting nuclear factor 2 (TIN2), protection of telomeres 1 (POT1), and TPP1 (named after combining the first letter of each name, TINT1, PTOP and PIP1, given by the three laboratories that initially characterized it).

TRF1 and TRF2 directly bind telomeric double-stranded DNA as homodimers through their MYB domain (Broccoli et al., 1997) and play a fundamental role in telomere protection and length regulation.

TRF1 overexpression causes telomere shortening, while the expression of a dominant-negative TRF1 leads to telomere lengthening (van Steensel and de Lange, 1997, Munoz et al., 2009). In mouse embryonic fibroblasts (MEFs), Trf1 deletion results in DNA replication fork stalling at telomeres leading to the formation of so-called fragile telomeres, which in turn cause DDR activation at the telomeres -involving ATR, and p53- ultimately leading to cellular senescence (Martinez et al., 2009, Sfeir et al., 2009).

TRF2, structurally similar to TRF1, specifically prevents the activation of ATM at telomere ends (Denchi and de Lange, 2007, Dimitrova and de Lange, 2009, Okamoto et al., 2013), is involved in telomere heterochromatin maintenance (Benetti et al., 2008) and helps the formation of the above-mentioned t-loop structures, whose recent evidence strongly suggests to be required for TRF2 functions (Doksani et al., 2013). Trf2 deletion in mouse cells leads to NHEJ-mediated telomeric fusion events independent of replication

fork stalling (Celli et al., 2006). In addition, constitutive Trf2 deficiency in mice leads to embryonic lethality in a p53-independent manner (Celli and de Lange, 2005).

RAP1 is localized to telomeres through its protein interaction with TRF2 (Chen et al., 2011). RAP1 is the only shelterin protein whose depletion does not lead to embryonic lethality in mice (Martinez et al., 2010), nonetheless resulting in adult mice undergoing increased telomere shortening and DDR activation, therefore suggesting a role in telomere homeostasis.

POT1 directly binds to the 3' single-stranded G-overhang of telomeres (Baumann and Cech, 2001, Lei et al., 2004) favoured by the formation a stable heterodimer with TPP1 *in vivo* (Hockemeyer et al., 2007, Chen et al., 2017). POT1 prevents ATR-mediated DDR activation at telomeres and regulates the length of the 3′ G-strand overhang (Palm et al., 2009); its loss leads to senescence induction in a p53-dependent manner (Wu et al., 2006) with telomere shortening and increased chromosomal fusions (Hockemeyer et al., 2008).

TPP1 functions as a protein hub that coordinates the end-protection functions of the shelterin complex. Apart from the above-mentioned function of favouring the binding of POT1 to telomeric ssDNA, TPP1 plays a fundamental role in regulating telomerase activity through its oligonucleotide/oligosaccharide binding (OB) fold domain (Zhong et al., 2012).

Similar to TPP1, TIN2 is an important protein for the maintenance of the shelterin complex stability. TIN2 binds both to TRF1 and TRF2, stabilizing them at telomeres (Ye et al., 2004). In addition, TIN2 also binds TPP1 and is required for the recruitment of TPP1/POT1 to the shelterin complex (Takai et al., 2011). As a consequence, when TIN2 is depleted, ATR is activated and excessive 3′ overhang is generated (caused by TPP1/POT1 loss) while in parallel TRF2 destabilization also induces ATM activation (Frescas and de Lange, 2014).

Interestingly, a very recent report has described a new specific telomere-associated protein named telomeric zinc finger-associated protein (TZAP), which directly binds double-

stranded telomeric DNA via zinc finger domains (Li et al., 2017). It preferentially binds long telomeres – thus competing with TRF1 and TRF2 for the binding to dsTTAGGG repeats – as they show a lower density of shelterin components compared to short telomeres. When localized at the telomeres, TZAP triggers a telomere trimming mechanism, generating a rapid deletion of TTAGGG repeats thus regulating telomere length by setting an upper length limit when the shelterin complex is not sufficient to prevent TZAP from binding to telomeres (Li et al., 2017).

1.3.2 Telomere length maintenance mechanisms

Every cell division causes a decrease of telomere length as a result of the DNA replication machinery inability to copy the lagging-strand of the most distal telomeric sequences of each chromosome (Harley et al., 1990), a circumstance known as the end replication problem (Watson, 1972). This biological phenomenon, common to most somatic cells in the human body, in the absence of a telomere-elongating mechanism, causes telomeres to shrink to a critical length that may ultimately lead to a telomere dysfunction-induced senescence (d'Adda di Fagagna et al., 2003) also known as replicative senescence (further explained in section 1.4.1.).

Telomere elongation by telomerase is likely the most studied telomere maintenance mechanism (TMM). Human telomerase is an RNA-containing reverse transcriptase that consists of an RNA component (hTR, 451 nt long), a reverse transcriptase catalytic subunit (hTERT) and the accessory proteins dyskerin, NOP10, NHP2, and GAR. In normal conditions, human telomerase activity is restricted to embryogenesis and its expression is switched off in most cells, with the exception of activated lymphocytes, adult stem cells and germ line (Wright et al., 1996). Nonetheless, in human cancer, 80-85% of tumours rely on telomerase for their TMM.

Most enzymes find their substrates by simple diffusion throughout the cell, however, a normal human cell in late S phase accounts for approximately 250 telomerases and 184 telomeres (Xi and Cech, 2014); which suggests telomerase being actively recruited to

telomeres rather than stochastically encountering them. As mentioned above (section 1.3.1), TPP1 is the key shelterin component necessary for telomerase recruitment to telomeres (Xin et al., 2007, Zhong et al., 2012). Telomerase is known to exhibit a preference for short telomeres, indicating a switch between non-extendible to extendible telomere states. The hexameric repeat addition processivity of telomerase is thought to add 50–60 nt to most telomeres after a single initiation event, and it is accelerated at extremely short telomeres, which allows cells to rapidly elongate them (Teixeira et al., 2004). The CTC1-STN1-TEN1 (CST) complex, through the binding of telomeric ssDNA, has been proposed as one mechanism by which an upper limit of telomere synthesis is set, allowing the displacement of telomerase once the overhang has reached a critical length (Chen et al., 2012). A second negative regulator of telomere length in human cells is TERRA RNA (discussed in section 1.3.4), which by directly binding telomerase, has been proposed to inhibit telomerase activity *in cis* (Schoeftner and Blasco, 2008, Redon et al., 2010). Lastly, telomere structures like t-loops and G quadruplexes have also been recently reported to prevent telomerase from accessing the telomeres (Jun et al., 2013, Doksani et al., 2013).

10-15% of human cancers achieve replicative immortality by relying on a telomerase-independent TMM. This mechanism, named alternative lengthening of telomeres (ALT), is an HR-driven pathway where telomeric overhangs invade another telomeric DNA, and use it as a template for DNA synthesis (Cho et al., 2014). Relatively little is known about the mechanism of ALT-mediated telomere synthesis. ALT activity is associated with a set of molecular markers: ALT-Associated PML Bodies (APBs), which are nuclear hubs detectable by fluorescence microscopy hypothesized to enable ALT-mediated HR and telomere extension; extrachromosomal telomeric repeats (ECTRs), among them, C- circles (circular partially single-stranded [CCCTAA]n DNA sequences) are the most commonly assayed ECTR and are detectable by rolling circle amplification assays using a Φ29 DNA polymerase (Henson et al., 2009); Telomere-Sister Chromatid Exchange (T-SCE), which are telomeric crossover events (Londono-Vallejo et al., 2004) detectable by chromosome

orientation fluorescence *in situ* hybridization (CO-FISH); and Telomere Dysfunction-Induced Foci, which are telomeric DDR foci, in ALT likely caused by telomere replication stress (Dilley et al., 2016). Chromatin compaction is decreased at ALT telomeres, and this has been associated with an upregulation of telomere transcription (Episkopou et al., 2014). Furthermore, ALT cancers are highly correlated with mutations in the ATRX/DAXX complex (a chromatin-remodeling complex known to aid deposition of H3K9me3 at telomeres) and histone variant H3.3 (Lovejoy et al., 2012, Heaphy et al., 2011), whose telomeres tend to be heterogeneous in length; some of them are very short, but others can reach up to 100 Kb. Importantly, reintroduction of ATRX into ATRX-mutated ALT cancer cell lines represses the formation of ALT molecular markers (Napier et al., 2015, Clynes et al., 2015), indicating an important role of ATRX in repressing ALT.

1.3.3 The role of telomeres in immortality and cancer

Very recent data are opposing the idea that replicative immortality, relying on either telomerase expression or ALT activity TMMs, is a hallmark of cancer cells. Several independent laboratories have reported that a set of metastatic and cancer-derived cell lines do not exert a TMM, supporting the idea that long telomeres *per se* are sufficient for tumour formation and maintenance (Viceconte et al., 2017, Dagg et al., 2017). In support of this idea, bioinformatics analysis of a large cohort of human tumours (18,430 samples) has recently reported that approximately a fifth of the samples analysed neither expressed telomerase (as shown by the absence of hTERT mutations) nor harboured alterations in ATRX or DAXX genes (Barthel et al., 2017). These new findings add an additional layer of complexity for cancer treatment as in some cases prevention of telomere shortening is not required for oncogenesis neither for cancer progression.

1.3.4 Transcription at telomeres

Telomeres from yeast to humans are transcribed into telomeric repeat-containing RNA (TERRA), which is an RNA transcript originated from several subtelomeric regions located close to chromosome ends and is composed of *tandem* UUAGGG repeat sequences

ranging in size from 100 bases to over 9 Kb in mammals (Azzalin et al., 2007, Porro et al., 2014). Approximately 7% of human TERRA transcripts are polyadenylated (Azzalin and Lingner, 2008) whereas the majority of yeast TERRA molecules carry a 3' poly(A) tail (Luke et al., 2008), and most human and yeast TERRA transcripts carry a 7-methylguanosine (m7G) cap structure in their 5' end (Feuerhahn et al., 2010); all these features stabilise TERRA molecules. By interacting with RNA Pol II, TRF1 positively regulates TERRA expression levels, while heterochromatin represses TERRA transcription (Schoeftner and Blasco, 2008).

Importantly, in human cells, telomere dysfunction induced by removal of TRF2 leads to increased TERRA levels at all transcribed telomeres (Feretzaki and Lingner, 2017, Porro et al., 2014). Furthermore, the TRF2 homodimerization domain, which induces chromatin compaction and prevents DDR activation (Denchi and de Lange, 2007), represses TERRA transcription independently of p53 and does not rely on ATM-dependent DDR signalling (Porro et al., 2014). The UUAGGG-repeat array of TERRA transcripts binds directly to SUV39H1 H3K9 histone methyltransferase, sustaining the accumulation of H3K9me3 at dysfunctional telomeres (Porro et al., 2014). Moreover, TERRA has been reported to accumulate H3K9me3 at functional telomeres (Arnoult et al., 2012), indicating a role of TERRA in heterochromatin reorganization at telomeres.

Recently, gapmer-Locked Nucleic Acid (LNAs) with a telomere sequence have been used to fully deplete TERRA in mouse cells (Chu et al., 2017); this leads to an increase of telomere dysfunction as well as a greater occurrence of other multiple telomeric pathologies such as loss of the telomeric repeat sequences, duplications of telomeric repeats at chromosomal ends and fusions between sister chromatid telomeres. These findings altogether indicate a functional role of TERRA transcripts for the maintenance of telomere integrity.

In addition, full depletion of TERRA has been reported to downregulate subtelomeric genes and internal chromosome target genes, indicating a role for TERRA to modulate

transcription (Chu et al., 2017). TERRA has been shown to associate with proteins belonging to epigenetic complexes, telomeric factors, DNA replication complexes and cell cycle regulators. In mouse stem cells, ATRX stands out as a major TERRA-interacting protein partner. TERRA regulates ATRX association with telomeric chromatin as depletion of TERRA causes increased ATRX localization to telomeres (Chu et al., 2017), suggesting functionally antagonistic roles of TERRA and ATRX at telomeres. Thus, in addition to maintaining telomere integrity in normal cells, TERRA expression, by specifically suppressing ATRX, may promote ALT in cancer cells, a hypothesis supported by the fact that cells harbouring ALT activity accumulate higher TERRA levels (Arora et al., 2014).

1.4 Cellular senescence and Hutchinson-Gilford progeria syndrome

1.4.1 Cellular senescence and aging

Strong evidence indicates the presence of senescent cells *in vivo* and their contribution to organismal aging and pathological conditions like cancer or chronic diseases (Kirkland, 2016, Goldman et al., 2013), and also in normal and tumour tissues following DNA-damaging chemotherapy (Collado and Serrano, 2010). Cellular senescence was originally described by Leonard Hayflick and collaborators as the limited proliferative potential shown by normal cultured cells (Hayflick, 1965). Mortal cells in fact undergo cellular senescence (often accompanied by an enlarged and flattened morphology) in response to a wide range of different types of stresses, such as dysfunctional telomeres, DNA damage and oncogene expression. The hallmark of cellular senescence is the inability of cells to progress through the cell cycle, which leads to a permanent growth arrest that can be monitored by 5-bromodeoxyuridine (BrdU) or H-thymidine incorporation (which indicates the extent of *de novo* DNA synthesis) or by the expression levels of proliferation markers like PCNA or Ki-67. The expression of senescence-associated-β-galactosidase (SA-β-gal), a lysosomal β-galactosidase whose activity (increased in senescent cells and detectable at pH 6) can be measured by histochemical staining, is the first marker ever used to specifically detect senescent cells (Dimri et al., 1995). In addition, the cell cycle inhibitor p16 - a known regulator of senescence encoded by the CDKN2/INK4a locus - is currently used to identify senescent cells (Krishnamurthy et al., 2004). p21, another cell cycle regulator (encoded by CDKN1A gene), is also often expressed in senescence (Campisi, 2001).

Importantly, senescence is associated with the acquisition of a senescence-associated secretory phenotype (SASP), which entails the secretion of cytokines, bradykines, miRNAs, prostenoids, chemokines that attract immune cells and extracellular matrix-damaging molecules, including proteases (Campisi and d'Adda di Fagagna, 2007, Xu et al., 2015a, Xu et al., 2015b, Coppe et al., 2006, Tchkonia et al., 2013). Furthermore, senescent

cells display a cytologically detectable chromatin reorganization phenomenon known as senescence-associated heterochromatin foci (SAHF) (Narita et al., 2003), which in some senescent cells relies on a maintained p21 and p16-dependent activation of the retinoblastoma (pRB) protein.

Senescent cells also exert large and persistent DDR foci, so-called senescence-associated DNA-damage foci (SDF), which are known to play an essential role both in senescence initiation and maintenance (d'Adda di Fagagna et al., 2003, Herbig et al., 2004, Galbiati et al., 2017, Sedelnikova et al., 2004, Fumagalli et al., 2012, von Zglinicki et al., 2005).

In proliferating human cells, progressive telomere attrition ultimately leads to exposed free double-stranded chromosome ends (d'Adda di Fagagna et al., 2003), triggering a persistent and irreparable telomeric DDR (Fumagalli et al., 2012); the so-called replicative senescence. In fact, replicative senescence is not caused by the telomere length average of a cell but by the presence of a small number of telomeres sufficiently short to trigger a DDR that activates a senescent signal (Hemann et al., 2001, Herbig et al., 2004).

In cellular senescence induced by IR, in which multiple random DSBs are generated activating the ATM-p53-p21 pathway, most DSBs are repaired hours after irradiation. However, a subset of damaged sites, mostly telomeres, result in persistent DDR signalling as they are hard to repair (Fumagalli et al., 2012), and this impedes cell cycle progression ultimately leaving cells in a permanent growth arrest.

In recent years, new strategies for targeting senescent cells (named senotherapies) have been developed to directly kill them, either by apoptotic (senoptosis) or by non-apoptotic (senolysis) means (Zhu et al., 2015). Senotherapies, for instance, have been used to eliminate senescent cells that may be preneoplastic, reducing cancer risk from senescence escape (Liu and Sharpless, 2012). On the other hand, senescence is beneficial in some contexts, such as wound repair (Demaria et al., 2014) and in embryogenesis (Munoz-Espin et al., 2013, Storer et al., 2013), therefore these cells should be exempted from been

targeted by senotherapies, one way, for instance, by delivering drugs directly to the sites of pathology.

1.4.2 Hutchinson-Gilford progeria syndrome

Hutchinson–Gilford Progeria Syndrome (HGPS) is a rare premature aging disorder, which affects 1 in 4-8 million new-borns. Within the first year of life, children start to exhibit distinctive clinical pathological features such as, partial alopecia progressing towards total alopecia, loss of subcutaneous fat, progressive joint contractures and nail dystrophy, while displaying a normal motor and mental development (Hennekam, 2006). Eventually, HGPS patients die at an average age of 14 years due to myocardial infarction, heart failure or progressive atherosclerosis (Hennekam, 2006). HGPS is a human genetic disease caused by heterozygous mutations of the LMNA gene encoding lamin A and lamin C resulting in aberrant splicing which leads to the expression of a truncated form of Lamin A protein called progerin (**Figure 5**).

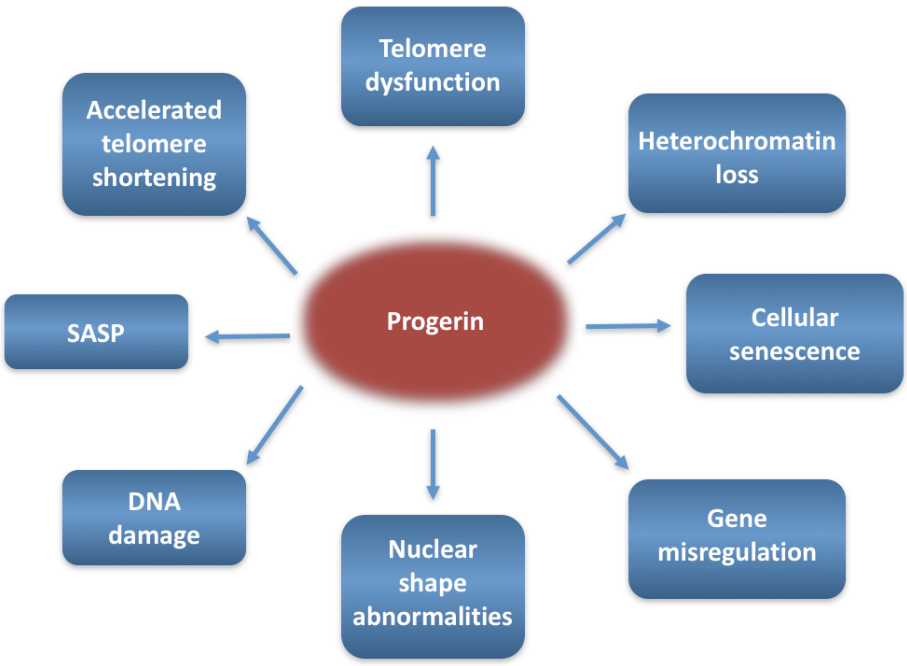

Figure 5. Consequences of progerin expression.

Progerin accumulation leads to nuclear envelope morphological abnormalities, misregulated gene expression, altered DNA repair, DNA damage accumulation, genomic instability and telomere shortening and dysfunction. These progerin-driven defects ultimately end up limiting the cellular proliferative capacity of the cell.

A de novo single-base mutation within exon 11 of LMNA (c.1824C > T) was the first HGPS driver mutation ever reported (De Sandre-Giovannoli et al., 2003, Eriksson et al., 2003) activating a cryptic splice site and resulting in a deletion of 50 amino acids near the C-terminus of Prelamin A (a 664-residue precursor of Lamin A). To date c.1824C > T remains the most common mutation, with also other driver mutations in LMNA gene reported in HGPS patients (Moulson et al., 2007, Reunert et al., 2012, Bar et al., 2017, DeBoy et al., 2017).

Compared to normal fibroblasts, HGPS fibroblasts exhibit nuclear shape abnormalities and severe loss of heterochromatin (Goldman et al., 2004) caused by reduced levels of Heterochromatin Protein 1 alpha (HP1α), decreased marks of histone H3 trimethylated at lysine 27 (H3K27me3) due to downregulation of histone methyltransferase Enhancer of Zeste Homolog 2 (EZH2) and low levels of histone H3 trimethylated at lysine 9 (H3K9me3). Notably, progerin expression also causes aberrant activation of the nuclear factor kappa-light-chain-enhancer of activated B cells (NF-κB) and Notch signaling pathways (Prokocimer et al., 2013), premature senescence (Cao et al., 2007, Gonzalo and Kreienkamp, 2015) and mitochondrial dysfunction (Rivera-Torres et al., 2013). Progerin accumulation is known to affect stem cell dysfunction both *in vitro* (Zhang et al., 2011, Pacheco et al., 2014, Scaffidi and Misteli, 2008) and in the skin of mouse models of progeroid laminopathies (Rosengardten et al., 2011, Espada et al., 2008, Lavasani et al., 2012).

Importantly, HGPS nuclei accumulate DNA damage and exhibit chromosomal instability caused by deficiencies in the DDR and in the mechanisms of DSB repair (Liu et al., 2005) and by accelerated telomere shortening (Decker et al., 2009) and dysfunction (Benson et al., 2010). Telomerase expression or p53 inactivation upon progerin expression reduces DNA damage and increases cell proliferation rates (Kudlow et al., 2008), suggesting that telomere dysfunction and checkpoint activation play important roles in HGPS. Indeed, telomerase expression restores senescence-associated misregulated genes (Kudlow et al.,

2008), the proliferative defect associated with progerin expression (Chojnowski et al., 2015) and prevents progerin-driven heterochromatin loss (Kudlow et al., 2008). In addition, progerin reduces the cellular expression of Lamina-associated polypeptide-α (LAP2α) and its association with telomeres (Chojnowski et al., 2015) and ectopic expression of LAP2α rescues progerin-driven proliferation defects and H3K27me3 loss (Chojnowski et al., 2015).

Thus, telomere dysfunction and its consequences is emerging as a key feature in HGPS. New strategies to control telomere dysfunction, other than telomerase expression (hard to achieve and with potential extra-telomeric effects such as its impact on WNT/β-catenin pathway; (Saretzki, 2014)), are fundamental to understand the true contribution of telomere dysfunction in the pathogenesis of the disease and design efficacious potential therapeutic approaches.

2 Materials and methods

2.1 Cell culture

Mouse embryonic fibroblast (MEF) cell lines ($Trf2^{F/+}$ and $Trf2^{F/F}$ MEFs), which carry a Cre recombinase (Rosa26-CreERT2), a gift from Eros Lazzerini Denchi, SCRIPPS, La Jolla, California, USA (Okamoto et al., 2013), were grown in DMEM without phenol red (as it has weak estrogenic activity and bears a structural resemblance to 4-hydroxytamoxifen) supplemented with 10% fetal bovine serum (FBS) and 1% glutamine. They are MEF-derived cell lines in which either one or both Trf2 alleles are loxP-flanked, and that constitutively express a CRE recombinase fused to the ligand binding domain of the estrogen receptor (ER). For the induction of Trf2 knock out, cells were grown in the presence of 4-hydroxytamoxifen (600 nM) for 48 hours, to allow CRE-ER to translocate into the nucleus and to generate the $Trf2^{+/-}$ and $Trf2^{-/-}$ cell lines.

T19 cells, a gift from Titia de Lange, Rockfeller University, New York, NY, USA (van Steensel et al., 1998), were grown in DMEM supplemented with 10% TET-system approved FBS, 1% L-glutamine, G418 (150 μg/ml) or hygromycin (90 μg/ml), alternatively. They are a HT1080-derived clonal fibrosarcoma cell line with a Tet-OFF system, which express the tetracyclin-controlled transactivator (tTA) and the dominant negative allele of TRF2 (TRF2 ΔBΔM, a mutant allele lacking the basic and myb domains of TRF2) under the tetracycline-controlled promoter. T19 cells were grown in the presence of doxycycline (100 ng/ml), which impedes the binding of the tTA to the promoter. In order to express TRF2 ΔBΔM, T19 cells were grown in the absence doxycyclin, and telomere uncapping was achieved 7-8 days after doxycyclin removal.

BJ cells (The American Type Culture Collection, ATCC) were grown in MEM supplemented with 10% FBS, 1% L-glutamine, 1% non-essential amino acids (NEAA), sodium pyruvate ($C_3H_3NaO_3$) 1mM. Phoenix amphotropic (ATCC) cells were grown in DMEM, supplemented with 10% FBS and 1% L-glutamine.

HGPS patient-derived human primary fibroblasts, a gift from Giovanna Lattanzi, Istituto di Genetica Molecolare, Consiglio Nazionale delle Ricerche, Bologna, Italy, were grown in DMEM supplemented with 20% FBS and 1% L-glutamine.

All cells were grown at 37°C, 5% CO_2.

2.2 RNA isolation

Total RNA from cultured cells was extracted with RNeasy Mini Kit (Qiagen) or with Maxwell® RSC miRNA Tissue Kit (Promega) for messenger RNA detection. mirVana miRNA Isolation kit (Life Technologies) or Maxwell® RSC miRNA Tissue Kit (Promega) was used for DDRNA and dilncRNA detection, according to the manufacturer's instructions. RNA extracted with mirVana miRNA Isolation kit using the Enrichment Procedure for Small RNAs was used as starting material for Target-Enrichment of small RNAs (TEsR). RNA was quantified with a NanoDrop spectrophotometer (Thermo Scientific). An Agilent 2100 Bioanalyzer instrument, which is a micro-capillary based electrophoretic cell, was used to assess the quality of RNA.

2.3 Real-time quantitative PCR for gene expression

1 μg of total cell RNA was reverse transcribed using SuperScript VILO cDNA Synthesis Kit. A volume corresponding to 10 ng of initial RNA was used for each qPCR reaction using GoTaq qPCR Master Mix (Promega) or LightCycler® 480 SYBR Green I Master (Roche) on a Roche LightCycler 480 detection instrument. Each reaction was performed in three technical replicates. Human ribosomal protein large P0 (Rplp0) and mouse beta-2 microglobulin (B2M) were used as control transcripts for normalization. Primers sequences (5'-3' orientation) were:

Mouse Dicer Fw: GCAAGGAATGGACTCTGAGC

Mouse Dicer Rv: GGGGACTTCGATATCCTCTTC

Mouse Drosha Fw: CGTCTCTAGAAAGGTCCTACAAGAA

Mouse Drosha Rv: GGCTCAGGAGCAACTGGTAA

Mouse B2M Fw: CTGCAGAGTTAAGCATGCCAGTA

Mouse B2M Rv: TCACATGTCTCGATCCCAGTAGA

Human Dicer Fw: GCAAAGCAGGGCTTTTCAT

Human Dicer Rv: AGCAACACAGAGATCTCAAACATT

Human Drosha Fw: TGCACACGTCTAACTCTTCCAC

Human Drosha Rv: GGCCCGAGAGCCTTTTATAG

Human Rplp0 Fw: TTCATTGTGGGAGCAGAC

Human Rplp0 Rv: CAGCAGTTTCTCCAGAGC

Human Progerin Fw: ACTGCAGCAGCTCGGGG

Human Progerin Rv: TCTGGGGGCTCTGGGC

Human p21 Fw: TCACTGTCTTGTACCCTTGTGC

Human p21 Rv: GGCGTTTGGAGTGGTAGAAAT

Human p16 Fw: CTTTCAATCGGGGATGTCTG

Human p16 Rv: GTGGACCTGGCTGAGGAG

Human IL-1A Fw: GGTTGAGTTTAAGCCAATCCA

Human IL-1A Rv: TGCTGACCTAGGCTTGATGA

Human IL-6 Fw: CCAGGAGCCCAGCTATGAAC

Human IL-6 Rv: CCCAGGGAGAAGGCAACTG

Human IL-8 Fw: TTGGCAGCCTTCCTGATTTC

Human IL-8 Rv: TCTTTAGCACTCCTTGGCAAAAC

2.4 Real-time quantitative PCR for small RNAs

5 µg of total cellular RNA were run and fractionated on a 10% polyacrylamide, 7 M Urea gel to allow small RNA separation under denaturing conditions and RNA species shorter than 40 nucleotides were gel-extracted by incubating the gel fraction overnight in an Elution Buffer (0.3 M $NaCH_3CO_2$ pH 5.5, 0.1 mM EDTA, 0.2% sodium dodecyl sulphate (SDS)) followed by ethanol precipitation. 10 pg of an RNA spike-in was added to all samples before cellular RNA was loaded on the gel in order to normalize for the efficiency

of RNA extraction from gel. cDNA was synthesized using the miScript II RT kit (Qiagen) with HiSpec buffer. PCR was performed using the miScript PCR system (Qiagen) accordingly to the manufacturer's instructions. Each reaction was performed in three technical replicates. mir29b or mir17 was used as a control gene for normalization. Primers sequences (5'-3' orientation) were as follows:

mir29b Fw: TAGCACCATTTGAAATCAGTGTT

mir17 Fw: CAAAGTGCTTACAGTGCAGGTAG

spike-in Fw: CGAATTCCACAAATTGTTATCC

teloG Fw: TAGGGTTAGGGTTAGGGT

teloC Fw: CCCTAACCCTAACCCTAA

2.5 Strand-specific real-time quantitative PCR

Total cellular RNA extracted from mirVana miRNA Isolation kit (Life Technologies) or Maxwell® RSC miRNA Tissue Kit (Promega) was used for dilncRNA detection. Samples were treated with DNase I (Thermo Scientific) at 37°C for 1 hour to remove any potential residual genomic DNA contamination (1 unit of DNase I per 1 μg of RNA). 1 μg of total RNA was reverse-transcribed using the Superscript First Strand cDNA synthesis kit (Invitrogen) with strand-specific primers. To amplify telomeric repeats I adapted a technique described in (Cawthon, 2002), which allows the generation of a fixed-length telomeric amplification product. For reverse-transcription the following primers were used: Rplp0 Rv for the detection PCR of Rplp0 mRNA; teloC Rv for the detection of the G-rich telomeric dilncRNA; teloG Rv for the detection of C-rich telomeric dilncRNA. Reverse transcription reactions must be performed in separate tubes to detect each telomere strand, as the addition of both teloC Rv and teloG Rv in a single reaction does not allow to distinguish between strands at the qPCR level. Quantitative PCR was performed using LightCycler® 480 SYBR Green I Master (Roche). For each reaction, 50 ng of cDNA were used. Each reaction was performed in triplicate. Rplp0 was used as a control gene for normalization. Primer sequences (5'-3' orientation) were as follows:

Rplp0 Fw: TTCATTGTGGGAGCAGAC

Rplp0 Rv: CAGCAGTTTCTCCAGAGC

teloC Rv: CCCTAACCCTAACCCTAA

teloG Rv: TAGGGTTAGGGTTAGGG

telo Fw: CGGTTTGTTTGGGTTTGGGTTTGGGTTTGGGTTTGGGTT

telo Rv: GGCTTGCCTTACCCTTACCCTTACCC TTACCCTTACCCT

2.6 Target-Enrichment of small RNAs (TEsR)

Two linkers were ligated to the two ends of the RNA molecules in the MEFs RNA samples extracted with mirVana miRNA Isolation kit using the Enrichment Procedure for Small RNAs. The 3' end of the starting RNA was ligated to a monoadenylated DNA linker by a T4 RNA ligase 2 truncated enzyme (NEB) by incubating for 1 hour at 25°C. The 5' RNA linker was then ligated by the use of a T4 RNA ligase 1 (NEB) to the target RNA at 20°C for 1 hour, after the removal of the 5' cap structure by a Tobacco Acid Pyrophosphatase (Epicentre), incubated at 37°C for 1 hour. The 3' linkers allowed for cDNA synthesis using PrimeScript RT-PCR Kit (Takara) and reverse transcription reaction was incubated at 44°C for 1 hour. Subsequent PCR amplification using Phusion® High-Fidelity DNA Polymerase (NEB) was peformed using the following cycling conditions: 98°C 2 minutes; 22 cycles of: 98°C for 30 seconds, 55°C for 30 seconds, 72°C for 30 seconds; 72°C for 5 minutes; hold at 4°C. To capture the amplified cDNA targets, I produced and used complementary RNA baits containing biotin-labeled nucleotides. The RNA baits were produced by using AMbion MAXIscript T7 In Vitro Transcription kit (Life Technologies) and Biotin RNA labelling Mix (Roche). A T7-promoter-containing dsDNA was used as template for *in vitro* transcription by incubating at 37°C for 1 hour. RNA baits and cDNA targets were incubated at 37°C for 48 hours in the presence of SUPERase-inhibitor (Life Technologies) and of the following blocking agents: Human Cot-1 (Life Technologies), UltraPure™ Salmon Sperm DNA Solution (Thermo Scientific) and a 200 μM Customized Block. The hybrid RNA-cDNA molecules were captured by Dynabeads® MyOne™ Streptavidin C1

(Life Technologies) beads, while non-targeted cDNAs were washed away. Captured cDNAs were then indexed by PCR with Script Index PCR primers (Illumina) and sequenced by a MiSeq (Illumina) sequencer. Oligonucleotide sequences (5'-3' orientation) were:

3' DNA linker: AGATCGGAAGAGCACACGTCTGAACTCCAGTCAC-Amine

5' RNA linker: ACACUCUUUCCCUACACGACGCUCUUCCGAUCU

RT primer: GTGACTGGAGTTCAGACGTGTGCTCTTCCGATCT

PCR Fw: AATGATACGGCGACCACCGAGATCTACACTCTTTCCCTACACGACGCT CTTCCGATCT

PCR Rv: CAAGCAGAAGACGGCATACGAGATCGGTCTCGGCATTCCTGCTGAAC CGCTCTTCCGATCT

Customized Block Fw: AATGATACGGCGACCACCGAGATCTACACTCTTTCCCTAC ACGACGCTCTTCCGATCT

Customized Block Rv: CAAGCAGAAGACGGCATACGAGATCGTGATGTGACTGGA GTTCAGACGTGTGCTCTTCCGATCT

RNA bait*: CAUGAGCAUGAGUAG**NNNNNNNNNNNNNNNNNNNNNNNN**GUA GCUUGGCAUACC

ScriptSeq reverse index adapter primer*: CAAGCAGAAGACGGCATACGAGA**TXXX XXX**GTGACTGGAGTTCAGACGTGTGCTCTTCCGATCT

***** Customisable RNA bait sequences and sample index sequences are shown in bold font. N represents a given nucleotide according to the sequence of the transcriptome aiming to enrich. X represents a given nucleotide according to the complete list of index sequences provided by ScriptSeq™ Index PCR Primers.

2.7 Short interfering RNA transfection

The RNA interference (RNAi) is composed of several categories of RNA, such as miRNA, siRNA and piRNA (He and Hannon, 2004). In cultured cells, short synthetic siRNAs are typically used for downregulation of endogenous mRNA. For siRNA transfection, I plated cells so that at the day of transfection they are at an approximate confluency of 30-40%. At

day of transfection, growth medium was removed from the cells and substituted with 0.75 volumes of fresh culture medium. For each transfection reaction, I mixed 0.125 volumes of Opti-MEM with siRNA oligos (5 or 20 nM final concentration) and 0.125 volumes of Opti-MEM with Lipofectamine RNAiMAX transfection reagent (Life technologies). The mix was incubated for 20 minutes at room temperature (RT) to allow the formation of siRNA-containing lipid particules and subsequently added to the cells were the fresh medium was previously added. I used ON-TARTGETplus SMARTpool siRNA oligonucleotides (Dharmacon), which for each mRNA, a set of four siRNAs are used. Sequences were as follows (5'-3' orientation):

siDicer human UAAAGUAGCUGGAAUGAUG;

GGAAGAGGCUGACUAUGAA; GAAUAUCGAUCCUAUGUUC;

GAUCCUAUGUUCAAUCUAA

siDrosha human CAACAUAGACUACACGAUU;

CCAACUCCCUCGAGGAUUA; GGCCAACUGUUAUAGAAUA;

GAGUAGGCUUCGUGACUUA

siDicer1 mouse GGUAGACUGUGGACCGUUU;

GGAAAUACCUGUACAACCA; GCAAUUUGGUGGUUCGUUU;

ACAGGAAUCAGGAUAAUUA

siDrosha mouse UGGAAGGAGUUACGCUUUA;

GGAAUCCGCCACAGCAUUU; GUGAUCACUUUCCCGAUUA;

UAAUGCACCUGGACAAGUU

siControl (siGFP) GCAAGCUGACCCUGAAGUUCAU

2.8 Transfection of Antisense oligonucleotides (ASOs)

Locked Nucleic Acid (LNA) are nucleic acids analogues which contain a bridge between the 2' oxygen and 4' carbon that "lock" the ribose in a Watson-Crick-binding optimal conformation. This structure confers LNA high thermal stability and increases their melting temperature allowing a higher binding affinity for a complementary target

sequence. For these reasons, LNAs are used as Antisense Oligonucleotides (ASOs), which by binding the target nucleic acid sequence, inhibit their further processing and/or function. LNA ASOs were transfected as reported for siRNAs (see the "Short interfering RNA transfection" section). As for siRNA transfections, for each transfection reaction, I used 20 nM of LNA ASOs. In order to prevent the formation of secondary structures of the oligos, Opti-MEM with ASOs was incubated at 95°C for 5 minutes and immediately placed on ice for 5 minutes. The sequences for the LNA ASOs were as follows (5'-3' orientation):

Control: TTATCCGCTCACAATTCCACAT

Telo C: CCCTAACCCTAACCCTAACCC

Telo G: GGGTTAGGGTTAGGGTTAGGG

2.9 Retroviral transduction

Phoenix amphotropic cells were used as a retrovirus producer cell line, which is based on the HEK 293T cell line that produces the gag, pol and envelope proteins which allow the formation of the retrovirus. The retroviral expression vectors used (pLPC-LaminA and pLPC-Progerin, Addgene plasmids numbers 69059 and 69061 respectively) included the viral packaging signal, the Lamin A or Progerin genes under the LTR promoter and a puromycin resistance marker. Phoenix amphotropic cells were plated so that at time of transfection they were approximately 60% confluent. I used the calcium phosphate ($Ca_3(PO_4)_2$) method to transfect Phoenix amphotropic cells, which is based on the formation of a precipitate containing $Ca_3(PO_4)_2$ and DNA that adheres to the cell surface facilitating its internalization through endocytosis. The precipitate is obtained by slowly dropping a solution containing calcium chloride ($CaCl_2$) and plasmidic DNA (10 μg for each 10-cm plate of Phoenix amphotropic cells) in a HEPES-buffered saline (HBS) solution containing sodium phosphate (Na_2PO_4). In order to increase the virus yield by affecting the intracellular exocytic pathways caused by an increase of endosomal pH, chloroquine was added to the medium at a final concentration of 40 μM. The

HBS/DNA/$CaCl_2$ solution was added to the Phoenix amphotropic cells within 5 minutes of preparation. The day after transfection, growth medium was replaced with 5 ml of fresh medium per 10-cm dish of Phoenix amphotropic cells to concentrate viral particles in the supernatant. 48 hours post-transfection, the concentrated viral supernatants were collected and filtered with a 0.45 μm filter to remove all potential Phoenix amphotropic cells present in the supernatant. Polybrene at a final concentration of 8 μg/ml was added to the filtered supernatant to increase the infection efficiency by allowing the viral glycoproteins to bind more efficiently to their receptors. These supernatants were used to perform four rounds of infections in BJ human fibroblasts for a period of 2 days. After infection, BJ cells were grown for two days in the presence of puromycin at a concentration of 2 μg/ml to select for the successfully infected cells.

2.10 Protein immunoblotting

Cells were lysed in Laemmli buffer, an aqueous solution containing 2% SDS, 10% glycerol and 60 mM Tris HCl pH 6.8. SDS allows the denaturation of proteins leaving a uniform negative charge throughout the length of the polypeptide, which helps the separation of proteins by electrophoresis based on their molecular weight. To measure the concentration of proteins in the samples, I used the biochemical Lowry protein assay in which the total protein concentration is exhibited by a color change of the sample solution in proportion to protein concentration. 30 μg of whole cell extracts were run in running buffer (25 mM Tris HCl, 0.2 M glycine, 0.1% SDS, pH 8.3) on a 7.5%, 12% or 4-20% Mini-PROTEAN® TGX™ Precast Protein Gels (Bio-Rad), which allowed the resolution of proteins of 40-200 kDa, 20-120 kDa or 10-200 kDa respectively. After running, the proteins were transferred to a nitrocellulose membrane in a wet electroblotting instrument using an aqueous transfer buffer containing 25 mM Tris HCl, 0.2 M Glycine and 20% methanol. Transferred membranes were temporarily stained with Ponceau to evaluate the efficiency of transfer. Membrane blocking of unspecific sites and primary and secondary antibody incubations were carried out in 5% milk in TBST (0.1% Tween in Tris-Buffered

Saline). All the washes between incubations were performed in TBST. The primary antibody was used to specifically detect the protein of interest, whereas the secondary antibody, linked to a horseradish peroxidase, was used to detect a species-specific antigen of the primary antibody. The localized light produced by the peroxidase in the presence of the acridan-based substrate, was detected by a ChemiDoc Imager (Bio-Rad).

2.11 Indirect immunofluorescence

Cells were grown on coverslips and washed twice for 5 minutes with Phosphate Buffered Saline (PBS) prior to being fixed with either 1:1 methanol/acetone solution for 2 minutes at RT or with 4% Paraformaldehyde (PFA) for 10 minutes at RT. In case of PFA fixation, cells were permeabilized with 0.2% Triton X-100 for 10 minutes at RT. Coverslips were incubated for 1 hour in blocking solution (PBG; 0.5% BSA, 0.2% gelatin from cold water fish skin) and subsequently incubated with a mix of primary antibody(s) and PBG for 1 hour at RT in a humidified chamber. Cells were washed 3 times for 5 minutes with PBG and later incubated with second solution containing secondary antibody(s) and PBG for 1 hour at RT in a dark chamber to avoid the fading of the fluorochrome conjugated to the secondary antibody. Cells were washed twice for 5 minutes with PBG, twice for 5 minutes with PBS and incubated with 4'-6-Diamidino-2-phenylindole (DAPI, 1µg/ml, Sigma-Aldrich) for 2 minutes at RT. Cells were sequentially washed with PBS and water and coverslips were then mounted with mowiol mounting medium (Calbiochem), which acts as an anti-fade agent which is capable of partially avoiding light-induced fading of the fluorophore.

2.12 BrdU incorporation assay followed by immunofluorescence.

To study DNA replication at a single cell level, cells were incubated with 5-bromodeoxyuridine (BrdU, Sigma-Aldrich, 10 µg/ml) for 8-24 hours. BrdU is a synthetic thymidine nucleoside analogue, which is incorporated into replicating DNA and can be detected by immunofluorescence. BrdU-pulsed cells plated on coverslips were fixed with

4% PFA for 10 minutes and permeabilized with 0.2% Triton X-100 for 10 minutes at RT. Cells were subsequently blocked with PBG for 1 hour and later incubated for 45 minutes at RT with a mixture containing anti-BrdU primary antibody (diluted 1:20), DNase (Promega, 0.1 U/µl,) and DNase buffer. Cells were then washed 3 times for 5 minutes with PBG and later incubated with a solution containing a secondary antibody, capable of recognising the anti-BrdU primary antibody, and PBG for 1 hour at RT in a dark chamber to avoid the fading of the fluorochrome conjugated to the secondary antibody. Cells were later washed twice with PBG and twice with PBS. DAPI staining was used to detect each nucleus and mowiol (Sigma-Aldrich) solution was used to mount coverslips.

2.13 Resazurin cell proliferation assay

Cultured cells with active metabolism can reduce a blue compound called resazurin (7-hydroxy-3H-phenoxazin-3-one-10-oxide, Sigma-Aldrich), to generate a pink molecule named resorufin (7-Hydroxy-3H-phenoxazin-3-one), with absorbance at 570 nm. Resazurin reduction may originate via different oxidase enzyme systems, using NAD(P)H as the major electron donor. The metabolic activity of cultured cells directly correlates to the production of resorufin, which was quantified by absorbance spectroscopy in a Perkin Elmer EnVision™ 2104 Microplate Reader. Prior to absorbance reading, cultured cells plated in a 96-well plate were incubated for 2 hours with resazurin (1:10).

2.14 Ionizing radiation

Ionizing radiation (IR) at 20 Grays (Gy, the International System of Units of absorbed radiation dose, where 1 Gy is the absorption of a joule of radiation energy per kilogram of matter) was used to generate acute exogenous DNA damage to induce IR-dependent cellular senescence. IR-induces lesions including base damage, SSBs, DSBs and DNA cross-links. A radiation-generating machine (Faxitron X-Ray Corporation), based on a high-voltage X-rays generator tube, was used for cell irradiation.

2.15 Imaging

Immunofluorescence images were acquired using a wide field Olympus Biosystems Microscope BX61 or a GE Healthcare DeltaVision Elite high-resolution fluorescence microscope. To allow a more accurate and high throughput signal discrimination and detection of co-localization events, software-based image deconvolution of DeltaVision acquisitions was performed in order to generate optical sections at different levels along the z axis of the cell. Co-localization between DDR markers and telomeres was assessed by ImageJ software with a customized ImageJ macro to allow 3D stack analysis. Two points were considered co-localizing if their respective intensities were higher than the threshold of their channels and if 5 pixels or more overlapped between both channels within the same section of the stack. Olympus wide field microscopes were used for the remaining imaging experiments (BrdU, Ki67 and DDR markers). Comparative immunofluorescence analyses were performed in parallel with identical acquisition parameters.

2.16 Antibodies

As primary antibodies, I used anti-Lamin A/C (goat, Santa Cruz sc6215, 1:1000); anti-γH2AX (mouse, Millipore 05-636, 1:200); anti-ATM pS1981 (mouse, Rockland 200-301-400, 1:1000; rabbit, Abcam ab2888, 1:500); anti-pS/TQ (rabbit, Cell Signalling 2851, 1:200); anti-53BP1 (rabbit, Novus NB100-304, 1:1000; goat, Novus AF1877, 1:1000); anti-BrdU (mouse, Becton Dickinson 347580, 1:20), anti-Ki67 (rabbit, Abcam ab16667, 1:50); anti-TRF2 (mouse, Millipore 05-521, 1:200); anti-FLAG (mouse, Sigma-Aldrich F3165, 1:500); anti-Vinculin (mouse, Sigma-Aldrich V9131, 1:2000); anti-Tubulin (mouse, Sigma-Aldrich T5168, 1:2000). As secondary antibodies, I used anti-Mouse or anti-Rabbit Alexa 488 IgG (donkey, Life Technologies, 1:400); anti-Mouse or anti-Rabbit Cy3 IgG (donkey, Jackson Immuno Research, 1:400), anti-Mouse, anti-Goat or anti-Rabbit Alexa 647 IgG (donkey, Life Technologies, 1:400).

2.17 Statistical analyses

p-values below 0.05 were considered as statistically significant. T-Student's two-tailed t-test was used for means comparisons of two independent samples whereas one-way ANOVA followed by the indicated post hoc test was used to compare the means of multiple independent samples. Chi-squared test was used for qualitative data where expected frequencies were compared to the observed frequencies.

3 RESULTS

3.1 Development of Target-Enrichment of small RNAs (TEsR).

3.1.1 Overview and introduction of the method.

In collaboration with the laboratory of Piero Carninci at the RIKEN Center for Life Science Technologies (Yokohama, Japan), we have developed a method that we named Target-Enrichment of small RNAs (TEsR), which allows the targeted sequencing of rare small RNAs (sRNAs) and diverse precursor and mature forms of sRNAs not easily detectable by current state-of-the-art sRNA sequencing methods (Nguyen et al. in press, 2017). In order to set up this method, Quan Nguyen, a postdoctoral fellow at RIKEN, visited our laboratory in Milan to develop the workflow of TEsR. Later on, I visited myself the RIKEN laboratory in Japan to continue this collaboration and I spent there 5 weeks to finalize the project.

In brief, TEsR allows the enrichment of the sRNAs of interest by generating RNA libraries that are hybridized to one or multiple sequence-specific biotin-labeled RNA bait(s). Non-hybridized RNAs are washed away, while bait-hybridized RNA molecules are retained and sequenced.

Compared to the current sequencing approaches, the main advantages of TEsR are: (i) it generates 400-30,000 fold deeper sequencing data; (ii) it allows inexpensive sequencing of multiple samples and target RNAs in a single run with a small sequencer such as Illumina MiSeq; (iii) it captures RNA lengths ranging from microRNA size to long RNA transcripts (shorter than 1 Kb to be suitable for Illumina sequencing); (iv) it enriches for mature sRNAs and their precursors and generates strand-specific sequencing reads, therefore, being capable of differentiating both sense and antisense RNAs; (v) it works robustly with small RNA inputs (as little as 10ng of RNA is enough to generate a TEsR library).

In TEsR, linkers are ligated to each of the two ends of the full-length sRNA molecules (**Figure 6a**). In order to minimize undesired ligations, amine-blocked linkers are used to block 3'-ends and pre-adenylated DNA linkers to increase reactivity with 3'-end of RNA (**Figure 7a**). Moreover, to capture also the significant proportion of sRNAs that are

capped, as this is the case for many small nuclear RNA (snRNA), small nucleolar RNA (snoRNA), tRNA, and miRNA, a 5'-cap removal step before ligating the 5'-RNA linker to the 3' end of sRNA is applied. In TEsR, after linkers' ligation, all ligated sRNAs are amplified by PCR (**Figure 7b**), targeted molecules are specifically enriched by hybridizing with biotinylated RNA baits generated in the lab (**Figure 6b, c and Figure 7c**), and PCR products are then wash-removed from abundant and/or irrelevant RNA species. Finally, by the use of sequencing primers, the enriched bait-captured products are PCR-amplified and the final sequencing libraries are generated (**Figure 6c and Figure 8**).

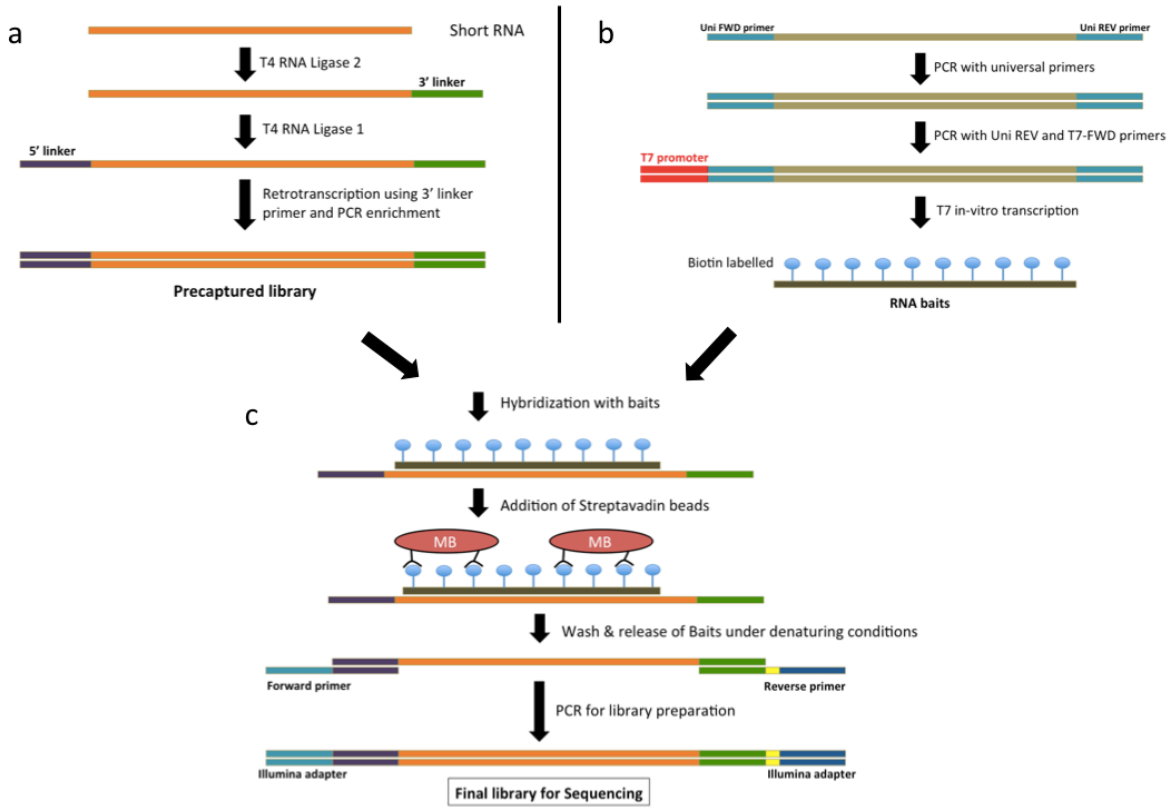

Figure 6. Overview of the Targeted Enrichment of RNAs (TEsR) method.

(a) Small RNA ends are ligated to a RNA and a DNA linker in the 5' and 3' end respectively, followed by retrotranscription of RNAs and PCR amplification using primers on both attached linkers. **(b)** A starting DNA oligo containing the target sequence to enrich for is PCR-amplified and a T7 promoter sequence is incorporated. *In vitro* transcription using Biotin-16-dUTP allows the synthesis of biotinilated RNA baits. **(c)** Capturing of target RNAs is performed through binding of the precaptured denatured libraries to RNA baits. Streptavidin magnetic beads (MB) are used to trap the RNA baits. After release of libraries, targeted sequences are indexed by PCR with sequencing primers for final library preparation.

Importantly, so far, no method for targeted sequencing of sRNA was available. To address this need, we have developed a complete protocol (Nguyen et al. in press, 2017) and optimized conditions compatible for capturing and deep-sequencing a wide range of sRNA transcripts. We thus carefully calibrated the key capture parameters like probe concentration and ratios, hybridization time and temperature, and wash removal post hybridization.

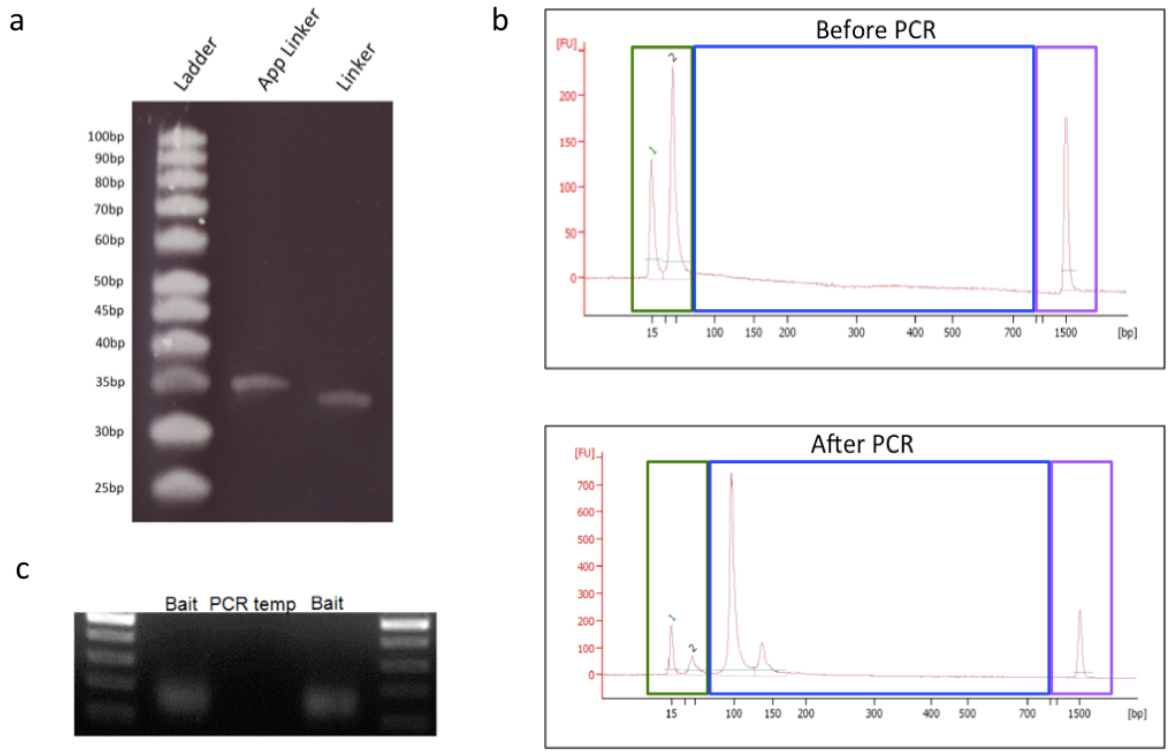

Figure 7. Profiles exemplifications for the monoadenylation of 3' DNA linker and library and RNA bait generations.

(a) Testing the production of adenylated 3' adapter on a denaturing 20% polyacrylamide gel. 'Linker' lane is the control with template only, without adenylation; the 'App Linker' indicates the adenylated adapter. The quality of adenylated adapter product can be judged based on the percent of adenylated vs not adenylated. **(b)** The top and low panels show the bionanalyzer profiles of precaptured libraries before and after the PCR step, respectively. Green boxes indicate the lower Bioanalyzer marker (1) and other pre-PCR oligos (2). In particular, (2) -in the upper panel- shows the oligos used for ligation to RNA as well as those used for reverse transcription, however the contamination of undesired oligos (like adapter dimers) after PCR amplification of cDNA is markedly reduced as seen in (2) of the lower panel. Blue boxes show library size distributions and Purple boxes show the upper Bioanalyzer marker. **(c)** Validation of RNA products after T7 *in vitro*

transcription. RNA baits were run on a 1% agarose gel. RNase-treated baits (PCR temp) were used as a control, proving that the signal obtained was mainly from RNA molecules.

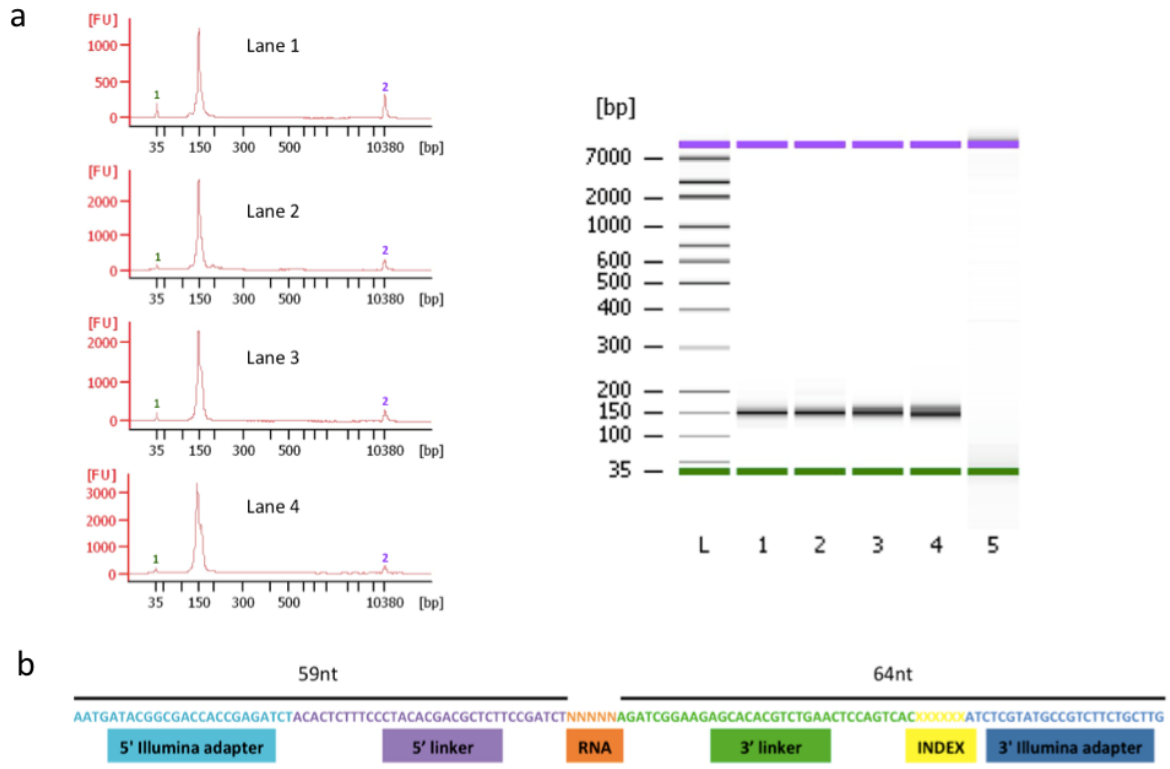

Figure 8. Bioanalyzer profiles and schematic overview of representative final TEsR libraries.

(**a**) Representative High Sensitivity Bioanalyzer profiles of final libraries of 4 different biological replicates (lanes 1-4). On the left, 1 -in green- represents the lower Bioanalyzer marker and 2 -in purple- shows the upper Bioanalyzer marker. On the right, lane number 5 shows the negative control PCR, where no template was used. L represents the dsDNA ladder used. (**b**) Single nucleotide resolution scheme of final libraries. N represents a given nucleotide according to the sequence of the transcriptome enriched for. X represents a given nucleotide according to the complete list of index sequences provided by ScriptSeq™ Index PCR Primers.

3.1.2 Validation of the TEsR method.

In order to validate TEsR, three different sRNAs were captured: miR29b1, Snord68 (small nucleolar RNA, C/D box 68) and Snord70 (small nucleolar RNA, C/D box 70) in four independent biological replicates (**Figure 9**) where total RNA samples from mouse embryonic fibroblasts (MEF) were used. For each TEsR experiment, simultaneous hybridization of three sRNA targets was carried out by simply pooling different RNA baits

containing the sequences of the three targets at equimolar concentrations into one hybridization reaction tube. For all four experiments, the enrichment obtained of the three sRNA targets was approximately 4 times higher than the total remaining 5,515 annotated mouse sRNAs, including all miRNAs, small ribosomal RNAs, snoRNAs, and snRNAs (**Figure 9a**). Importantly, a pooled read coverage of the three sRNA targets of 78% to 83% of the total read counts sequenced from the libraries was obtained. Conversely, in control standard libraries run on a sequencer with higher depth capability (HiSeq), the three sRNAs accounted only for approximately 0.2 % of the total reads counts (**Figure 9b**), thus demonstrating that TEsR generated a 400-fold enrichment of these three sRNA targets compared to standard sequencing. Moreover, we obtained a dramatic shift in detection ranks of the three targeted sRNAs when comparing captured to not-captured libraries (**Figure 9 c, d**), proving a more efficient performance and cost-effective results obtained by TEsR method, even on a Illumina MiSeq sequencer with lower sequencing depth as compared to HiSeq.

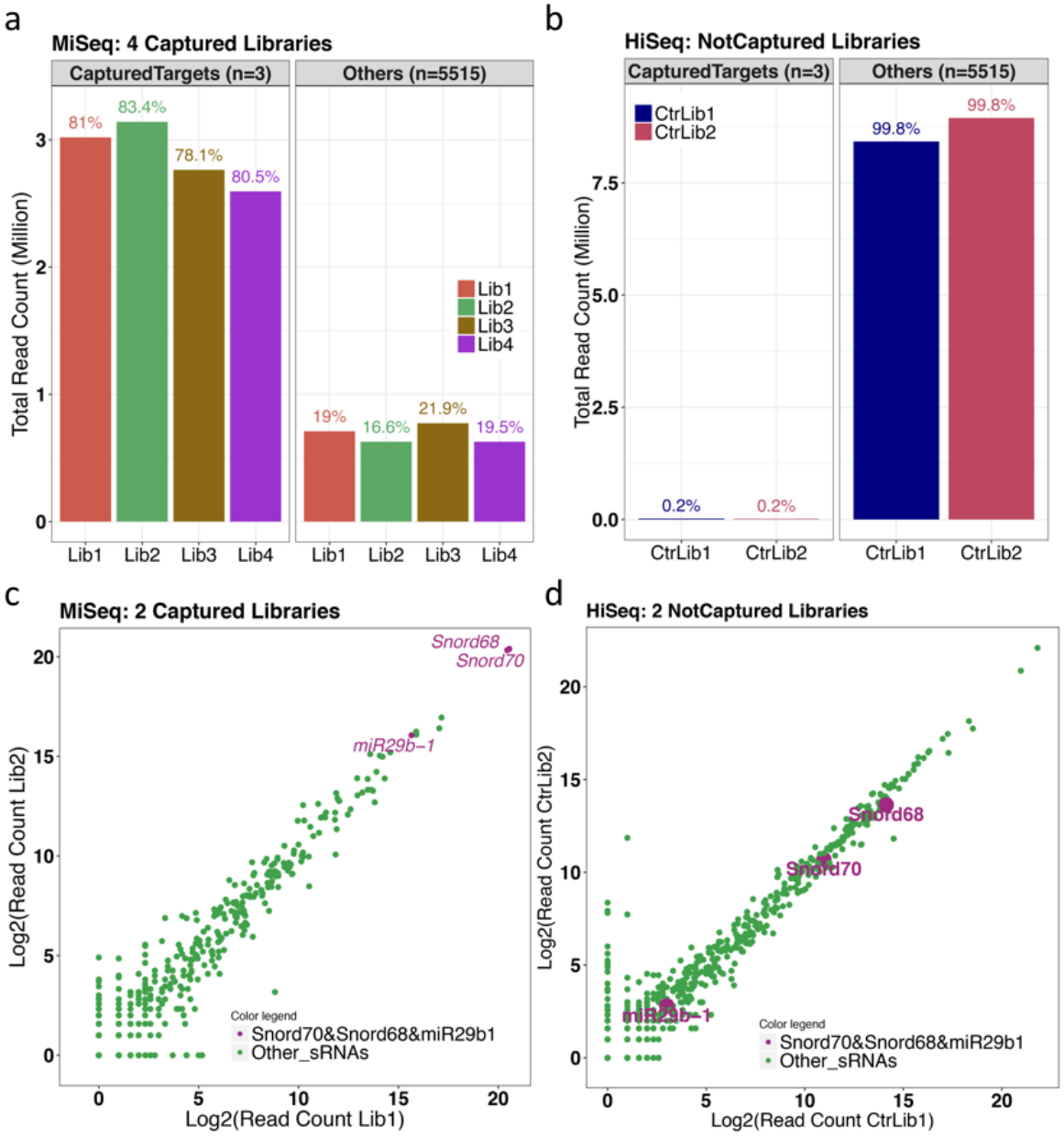

Figure 9. Evaluation of the enrichment of three sRNA targets by TEsR.

Different probes were used for simultaneously capturing three sRNAs: miR29b1, Snord68 and Snord70. (**a**) The relative abundance of captured targets compared to all remaining not-captured sRNA in each of the 4 captured Illumina MiSeq sequencing libraries and (**b**) in not-captured Illumina HiSeq sequencing of standard TruSeq small RNA libraries. The ranks of abundance levels for three captured small RNA targets in captured libraries (**c**) compared to in not-captured libraries (**d**), in two biological replicates are shown for captured and control libraries (CtrLib). Results by Quan Nguyen.

Next, spike-in RNAs and serial dilutions of total RNA samples were used to estimate the correlation between final read counts and initial concentrations of the captured RNA molecules. Two different RNA molecules were targeted separately, each of which had

three different dilutions (**Figure 10a**). The first target was a chemically-synthesized spike-in RNA molecule different in sequence from any well-known endogenous sRNA in mouse and human. The second RNA captured was the human endogenous miR29b-1. Importantly, a strong correlation was observed between concentrations and read count values for both miR29b-1 and spike-in target (R^2 >0.99) demonstrating the linear range of the data (**Figure 10a**). Moreover, the reproducibility of the method was assessed by capturing and sequencing Snord70, Snord68 and miR29b-1 in two distinct replicates (**Figure 10b**). All captured targets were consistently placed on the regression line between the two replicates thus proving the reproducibility of TEsR (**Figure 5b**).

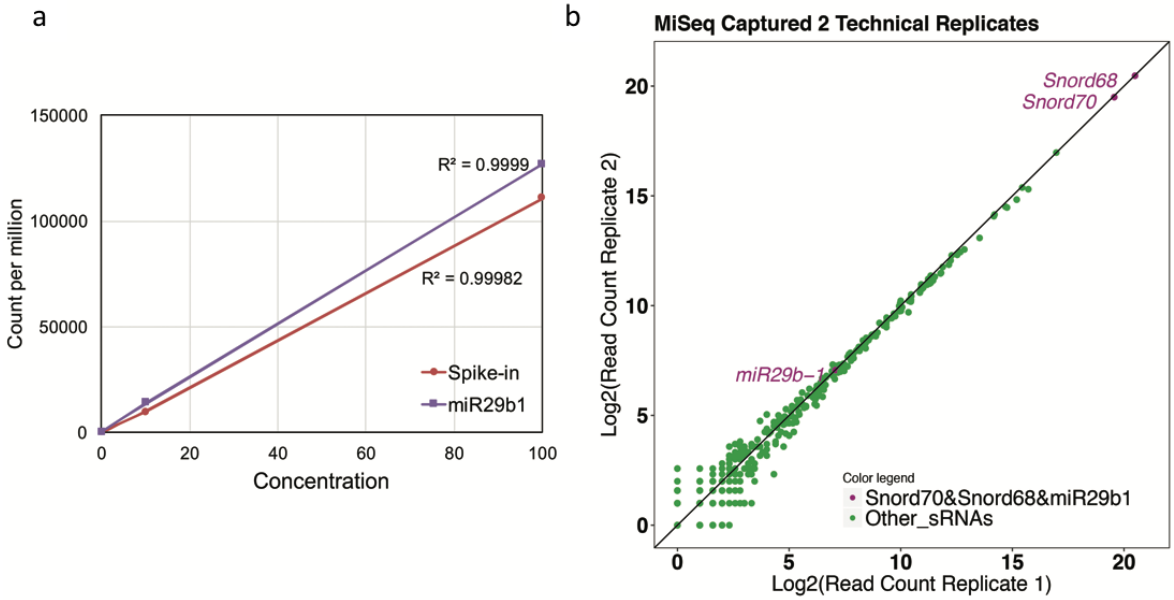

Figure 10. Assessing reproducibility and quantitativeness of the TEsR method.

(**a**) Correlations of read count per million to concentrations of each captured targets, including a spike-in and the endogenous miR29b RNA, each with three dilutions (0.1, 10 and 100). (**b**) Correlation plots of the abundance of small RNA from two independent TEsR experiments. Snord70, Snord68 and miR29b1 were the three captured targets, shown in red. Results by Quan Nguyen.

3.2 DICER and DROSHA-dependent telomeric RNAs are induced at dysfunctional telomeres.

3.2.1 Telomere dysfunction induces the transcription of telomeric DDRNAs and their precursors.

To test the potential generation of DDRNAs at endogenous damaged sites like telomeres, I employed Trf2 conditional knock out mouse embryonic fibroblast (MEF) cell lines ($Trf2^{F/+}$ and $Trf2^{F/F}$ MEFs), which carry a Cre recombinase (Rosa26-CreERT2) inducible by 4-hydroxytomaxifen (4OHT). I treated MEFs with 4OHT for 48 hours in order to induce the translocation of Cre recombinase into the nucleus. Trf2 removal leads to telomere dysfunction, as telomeric DNA ends are recognized as DSBs, which can be detected by immunofluorescence in the form of Telomere Induced Foci (TIFs) (**Figure 11** and (Okamoto et al., 2013)).

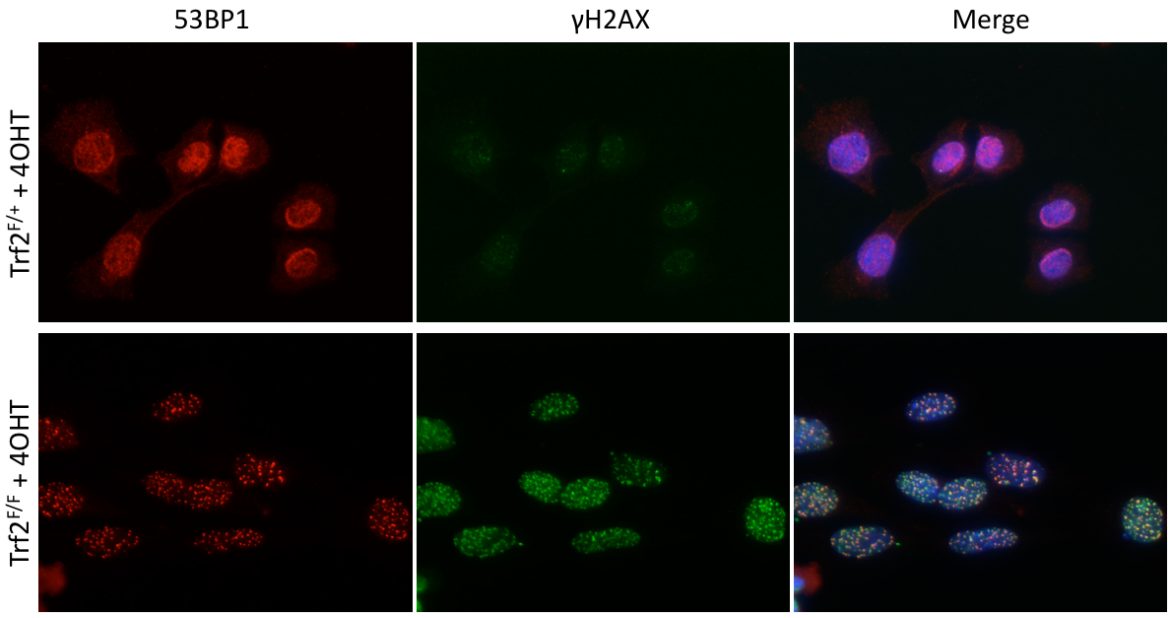

Figure 11. Induction of telomere dysfunction in Mouse Embryonic Fibroblasts (MEFs).

MEFs of the indicated genotype were treated with 4OHT (0.6 μM) for 48 hours and subsequent immunofluorescence experiments were performed to stain for 53BP1 and γH2AX DDR markers.

As DDRNAs are transcribed at DSBs and contain the corresponding sequence of the damaged genomic site, I aimed to study and monitor the expression of telomeric DDRNAs

(tDDRNAs) by using an RT-qPCR-based method developed to detect and quantify small RNAs (**Figure 12**). In brief, this method allows the polyadenylation of RNAs by a poly(A) polymerase followed by reverse transcription using oligo-dT primers. These oligo-dT primers contain a universal tag sequence on the 5' end, allowing amplification of small RNA in the real-time PCR step (**Figure 12**). In order to detect tDDRNAs, I designed primers to selectively amplify either the G-rich strand (teloG) or the C-rich strand (teloC) of potential tDDRNAs generated at dysfunctional telomeres.

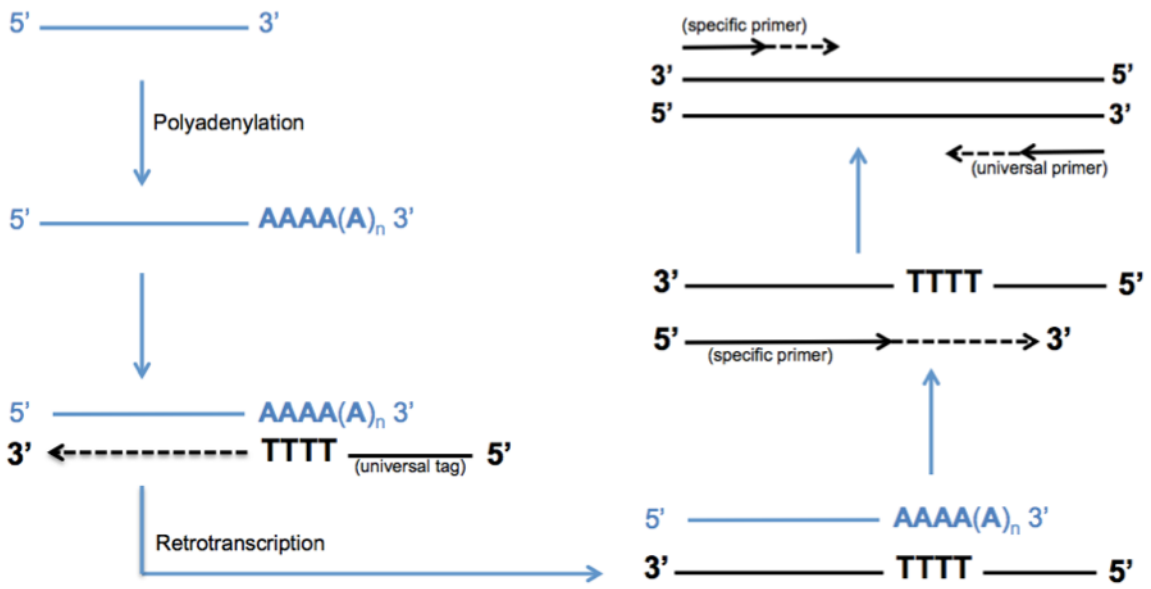

Figure 12. Detection of DDRNAs: schematic description of the amplicon synthesis.

Small RNA is firstly polyadenilated, then retrotranscription is enabled by using a primer containing a polyT tail and a universal tag. Lastly, qPCR is performed using universal and specific primers on the cDNA.

In order to minimize the contribution of longer telomeric RNA species, including TERRA, I employed a gel-extracted fraction of RNAs shorter than 40 nucleotides prior to the polyadenylation step in **Figure 12**. Upon Trf2 knock out I observed an induction of both teloG and teloC DDRNAs (**Figure 13a**), raising the possibility of the *in vivo* formation of double-stranded tDDRNA molecules. The signals detected were not due to genomic DNA contamination as only a low qPCR background signal was detected in the absence of reverse transcriptase (**Figure 13b**).

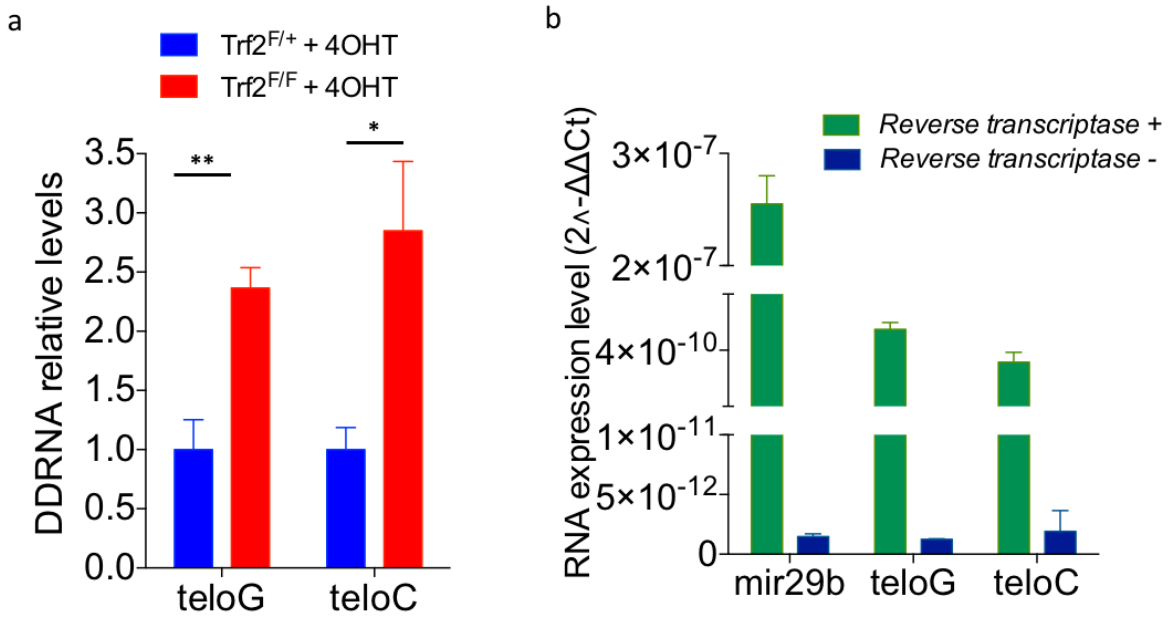

Figure 13. Deprotection of telomeres leads to increased levels of tDDRNAs in MEFs.

(a) MEFs of the indicated genotype were treated with 4OHT (0.6 μM) for 48 hours and collected for total cell RNA extraction. Small RNAs were gel-extracted (< 40 nt) and used for PCR amplification (as described on Figure 12) to detect tDDRNAs. DDRNA levels were normalized to mir29b and $Trf2^{F/+}$ + 4OHT MEFs. Error bars represent the s.e.m. n=3 independent experiments. *p-value<0.05, **p-value<0.01, Student's t-test. **(b)** Gel-extracted small RNA fraction (< 40 nucleotides) was used PCR amplification as in a. Retrotranscription reactions were performed in the presence (Reverse transcriptase +) or absence (Reverse transcriptase -) of the reverse transcriptase enzyme. Error bars represent s.d. of 3 technical replicates.

To extend these observations to human cells, I used T19 cells, a HT1080 fibrosarcoma cell line expressing a doxycycline-induced FLAG-tagged dominant negative form of TRF2 (TRF2 ΔBΔM). TRF2 ΔBΔM binds the endogenous wild type TRF2 and forms an inactive heterodimer, unable to bind DNA, thus blocking the accumulation of TRF2 on chromosome ends ultimately leading to telomere deprotection and DDR activation. The expression of TRF2 ΔBΔM was induced by culturing cells in the absence of doxycycline for 8 days. Cells expressing the TRF2 ΔBΔM mutant stained positive for FLAG-tag and DNA damage response in the form of 53BP1 foci (**Figure 14** and (van Steensel et al., 1998)).

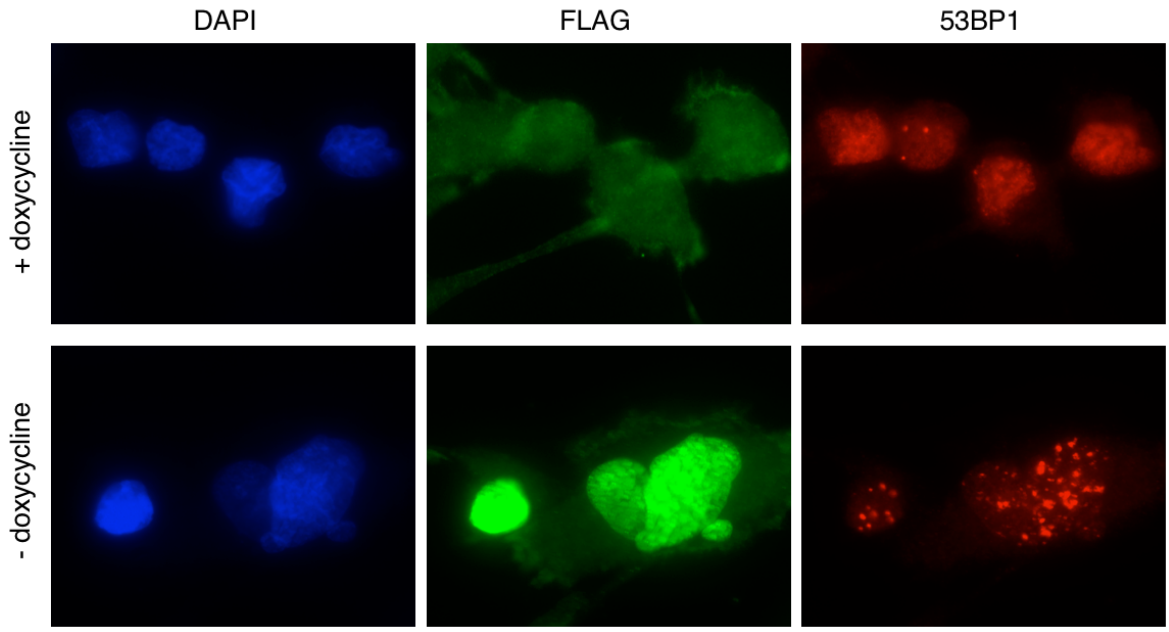

Figure 14. Induction of telomere dysfunction in T19 human cells.

T19 cells were treated, or not, with doxycycline. FLAG-tagged TRF2 ΔBΔM expression was detected by FLAG immunofluorescence staining in cells cultured without doxycycline for 8 days. Cells cultured with and without doxycycline for 8 days were stained for 53BP1. FLAG-tagged TRF2 ΔBΔM-expressing cells elicit telomere DNA damage as indicated by 53BP1 foci accumulation.

Consistent with tDDRNA induction in Trf2-depleted MEFs, I observed in T19 cells both teloG and teloC DDRNA levels increased upon induction of telomere dysfunction (**Figure 15**), suggesting a conserved mechanism for tDDRNA induction across mammalian species.

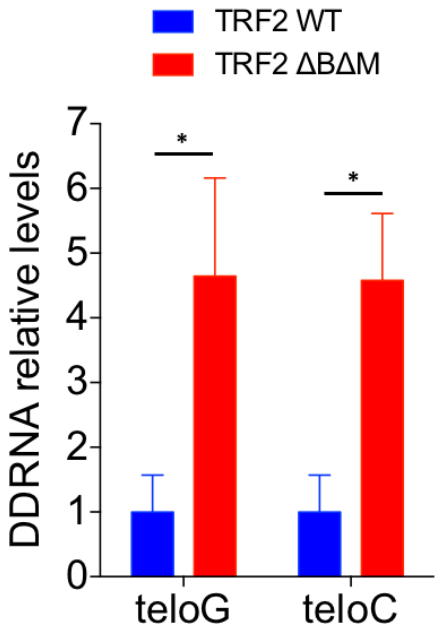

Figure 15. Deprotection of telomeres leads to increased levels of tDDRNAs in T19 cells.

T19 cells were treated, or not, with doxycycline for 8 days and collected for RNA extraction. Small RNAs were gel-extracted (< 40 nt) and used for PCR amplification (as described on Figure 12) to detect tDDRNAs. DDRNA levels were normalized to mir29b and TRF2 WT T19 cells. Error bars represent the s.e.m. n=3 independent experiments. *p-value<0.05, Student's t-test.

To further characterize the length and sequence of tDDRNAs, I treated $Trf2^{F/+}$ and $Trf2^{F/F}$ MEFs with 4OHT for 48 hours and performed TEsR, which captured and enriched for tDDRNAs followed by next generation sequencing as described in section 3.1. By this approach, I observed that telomere dysfunction induced the accumulation of small telomeric transcripts generated from both teloG and teloC strands, including the expected tDDRNA size range products (**Figure 16**).

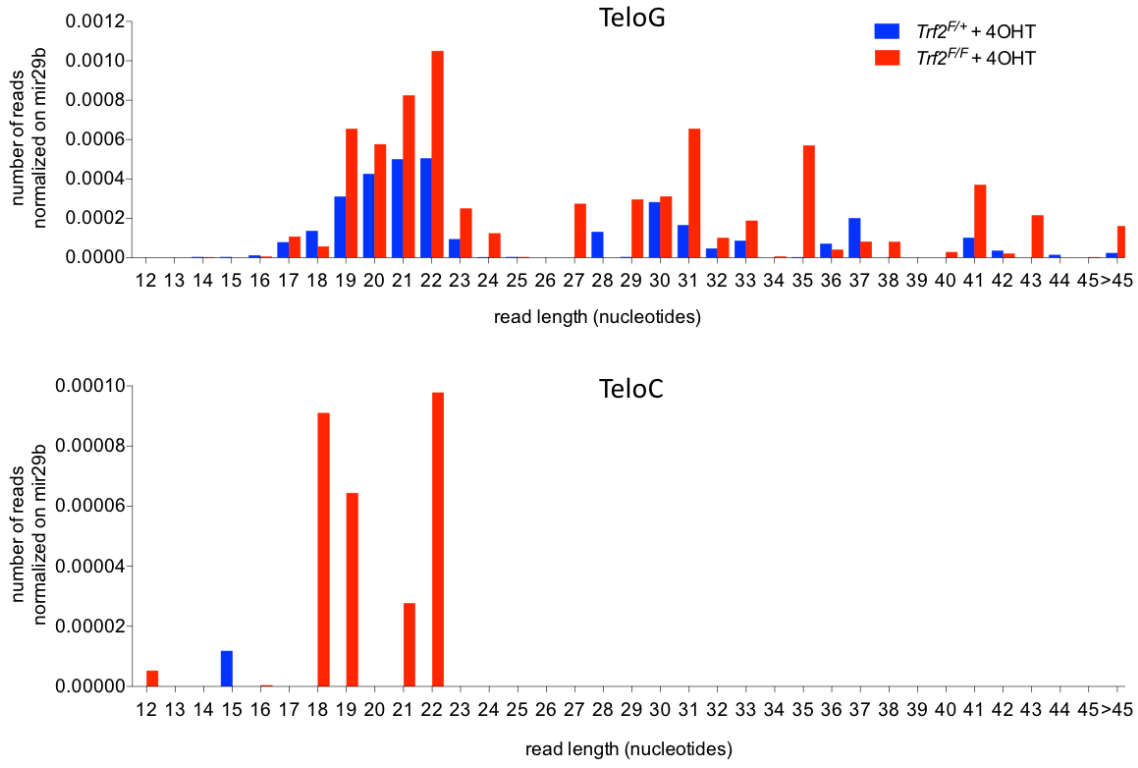

Figure 16. Characterization of tDDRNAs by Targeted Enrichment of RNAs (TEsR) method.

Small RNA (<200 nucleotides) fractions were isolated from MEFs of the indicated genotype treated with 4OHT (0.6 μM) for 48 hours, enriched for species with telomeric sequences using the TEsR method described on Figure 9. Bar graphs show for each read length the number of telomeric reads, either G rich or C rich, normalized on mir29b reads. n=3 independent experiments. Bioinformatics analysis was performed by Fabio Iannelli.

As previous work from our lab has shown DROSHA and DICER involved in DDRNA biogenesis on DSB generation (Francia et al., 2012, Michelini et al., 2017), I next looked for evidence of longer telomeric RNA species – we termed damage-induced long non-coding RNAs (dilncRNAs) – that would serve as RNA substrates of DROSHA and DICER for tDDRNA production. For this purpose, I performed a strand-specific fixed-length RT-qPCR that allows the real-time amplification and quantification of repetitive sequences, such as UUAGGG tandem repeats. PCR on RNA molecules shorter than 40 nucleotides did not generate any amplicon, ruling out the possibility of DDRNA detection by this approach (**Figure 17a**). Upon Trf2 knock out, I observed an increase of 10- to 20-fold telomeric dilncRNAs (tdilncRNAs) compared to control cells (**Figure 17b**), demonstrating a strong induction of telomere transcription on both strands upon telomere dysfunction.

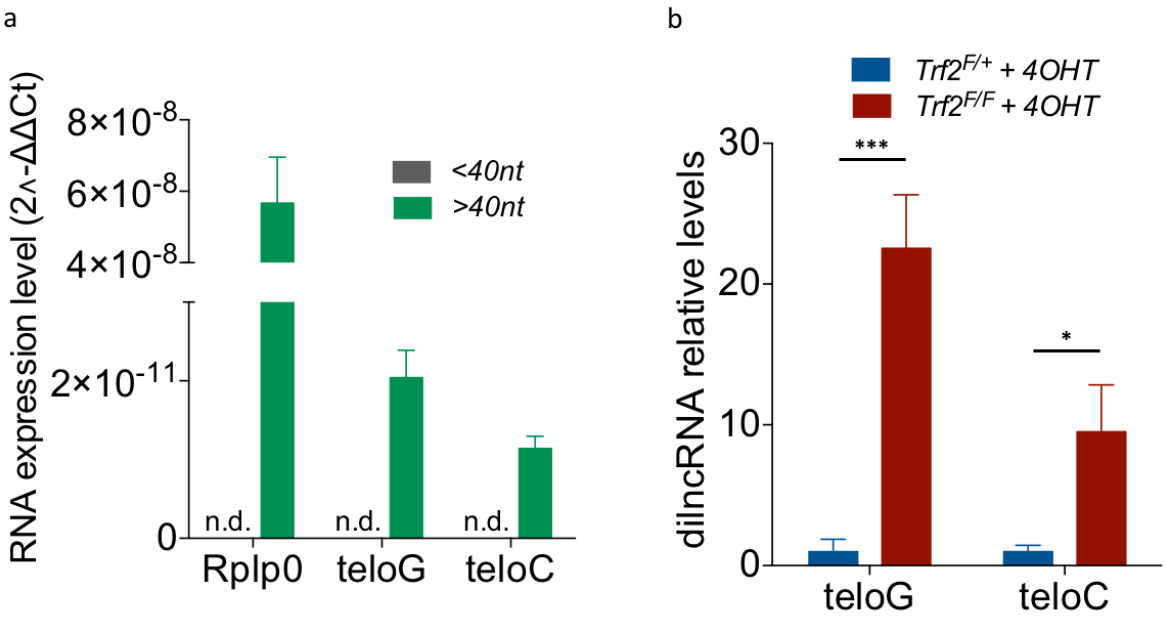

Figure 17. Deprotection of telomeres leads to increased levels of tdilncRNAs in MEFs.

MEFs of the indicated genotype were treated with 4OHT (0.6 μM) for 48 hours and collected for total cell RNA extraction. **(a)** Gel-extracted total RNA was separated in less than 40 (<40) and more than 40 (>40) nucleotides. Strand-specific fixed-length RT-qPCR was used (n.d. = not detectable). Error bars represent s.d. of 3 technical replicates. **(b)** MEFs of the indicated genotype were treated with 4OHT (0.6 μM) for 48 hours and total cell RNA was isolated in order to perform strand-specific fixed-length RT–qPCR to detect

tdilncRNAs. tdilncRNA levels were normalized to Rplp0 mRNA and Trf2$^{F/+}$ + 4OHT MEFs. Error bars represent the s.e.m. n=3 independent experiments. *p-value<0.05; ***p-value<0.001, Student's t-test.

3.2.2 DDR at dysfunctional telomeres is DROSHA and DICER dependent.

As DDRNA biogenesis has been shown to be DROSHA and DICER dependent, I investigated their role in telomeric RNA processing by knocking down individually both endoribonucleases in Trf2$^{F/F}$ MEFs. I observed that DICER or DROSHA depletion fully abolished both teloG and teloC tDDRNAs induction upon telomere dysfunction induction (**Figure 18**).

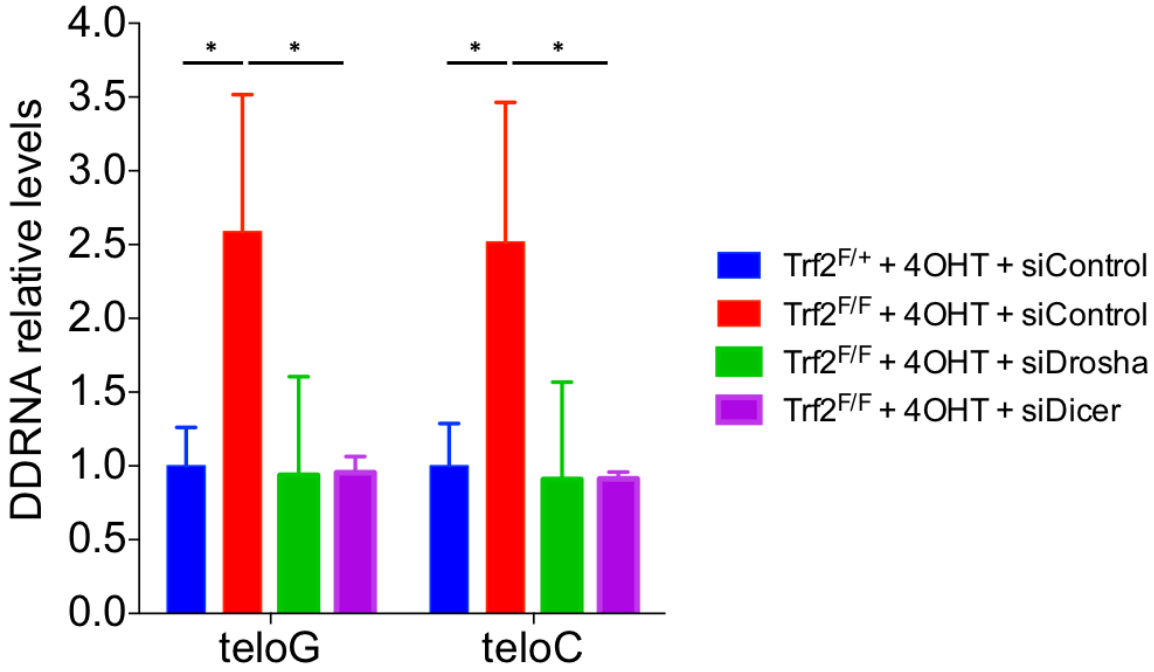

Figure 18. Drosha and Dicer are involved in tDDRNA generation.

MEFs of the indicated genotype were simultaneously treated with 4OHT (0.6 μM) and transfected with the indicated siRNA for 48 hours and collected for total cell RNA extraction. Small RNA was gel-extracted (< 40 nt) and used for PCR amplification (as described on Figure 12) to detect tDDRNAs. Since most microRNAs (included mir29b) are susceptible to Drosha and Dicer knock down, a spike-in RNA introduced in the samples prior to gel loading was used to normalize at the qPCR step. DDRNA levels were normalized to Trf2$^{F/+}$ + 4OHT + siControl. Error bars represent the s.e.m. n=3 independent experiments. *p-value<0.05, Student's t-test.

Furthermore, I monitored tdilncRNAs in Drosha- and Dicer-deficient Trf2$^{F/F}$ MEFs. Upon trf2 knock out, tdilncRNAs increased significantly in Drosha-depleted cells (**Figure 19**). These results are consistent with dilncRNAs being DDRNA precursors, which are processed by DROSHA and DICER to generate functional tDDRNAs. Dicer knockdown did not show a significant increase of tdilncRNA as it likely leads to the accumulation of small RNA intermediates too short to be detected by qPCR in this experimental setting.

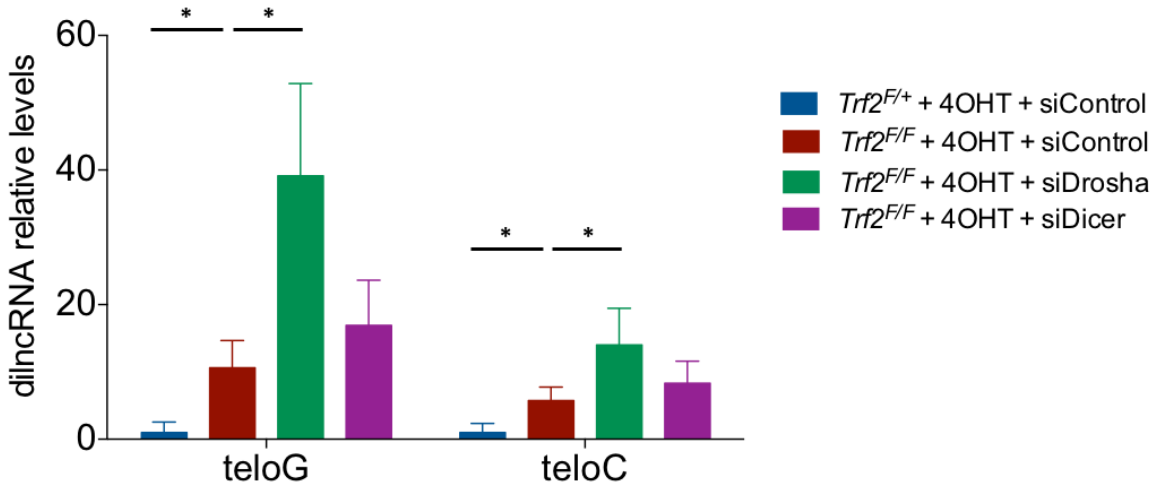

Figure 19. Drosha and Dicer are involved in tdilncRNA processing.

MEFs of the indicated genotype were simultaneously treated with 4OHT (0.6 μM) and transfected with the indicated siRNA for 48 hours and total cell RNA was isolated in order to perform strand-specific RT–qPCR to detect tdilncRNAs. tdilncRNA levels were normalized to Rplp0 mRNA and Trf2$^{F/+}$ + 4OHT + siControl MEFs. Error bars represent the s.e.m. n=3 independent experiments. *p-value<0.05; Student's t-test.

Next, I studied the impact of Drosha or Dicer knockdown in DDRNA biogenesis and its potential inhibition of DDR activation at dysfunctional telomeres. Consistent with the reported unaltered levels of γH2AX in cells exposed to ionizing radiation and depleted of either Drosha or Dicer (Francia et al., 2012), induction of telomere dysfunction in Trf2$^{F/F}$ MEFs followed by Drosha or Dicer depletion lead to unaltered γH2AX foci formation (**Figure 20 b,c**). I studied then the activation of the DDR apical kinase ATM at serine 1981 (ATM pS1981) and observed that the fraction of positive cells for pATM pS1981, as well as the ones positive for the consensus target sequence (pS/TQ) of proteins phosphorylated

by PI3-like kinases including ATM, were strongly decreased upon Drosha or Dicer knockdown (**Figure 20 b,c**).

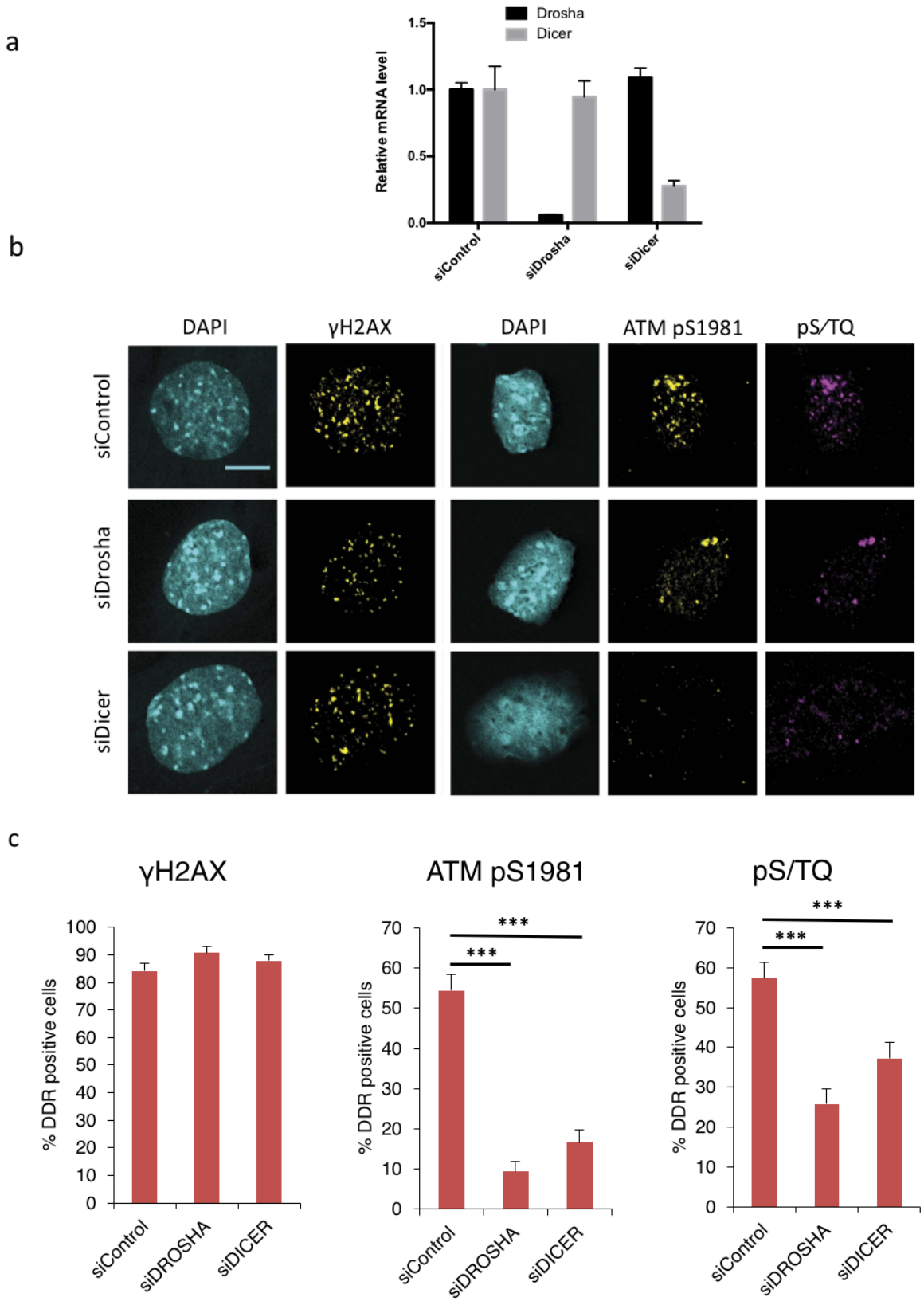

Figure 20. Drosha and Dicer are necessary for full DDR activation at deprotected telomeres.

MEFs Trf2$^{F/F}$ were simultaneously treated with 4OHT (0.6 μM) and transfected with the indicated siRNA. 48 hours later, cells were 4% PFA-fixed or collected for RNA extraction. **(a)** Representative RT-qPCR to detect Drosha and Dicer mRNA levels. Error bars represent the s.e.m. of 3 technical replicates. **(b)** Fixed cells were stained for the indicated DDR markers. Scale bar, 10 μm. **(c)** Quantification of data shown in b. Bar graphs show the percentage of DDR-positive cells±95% confidence interval n=3 independent experiments. ***p-value<0.001, Chi-squared test. A cell was counted as positive if showing >3 foci. Combined results by Julio Aguado and Francesca Rossiello.

Moreover, I observed that also in the T19 human cell system, both Dicer and Drosha knockdown decreased the recruitment of ATM pS1981 and pS/TQ, to dysfunctional telomeres, but not the formation of γH2AX foci (**Figure 21**).

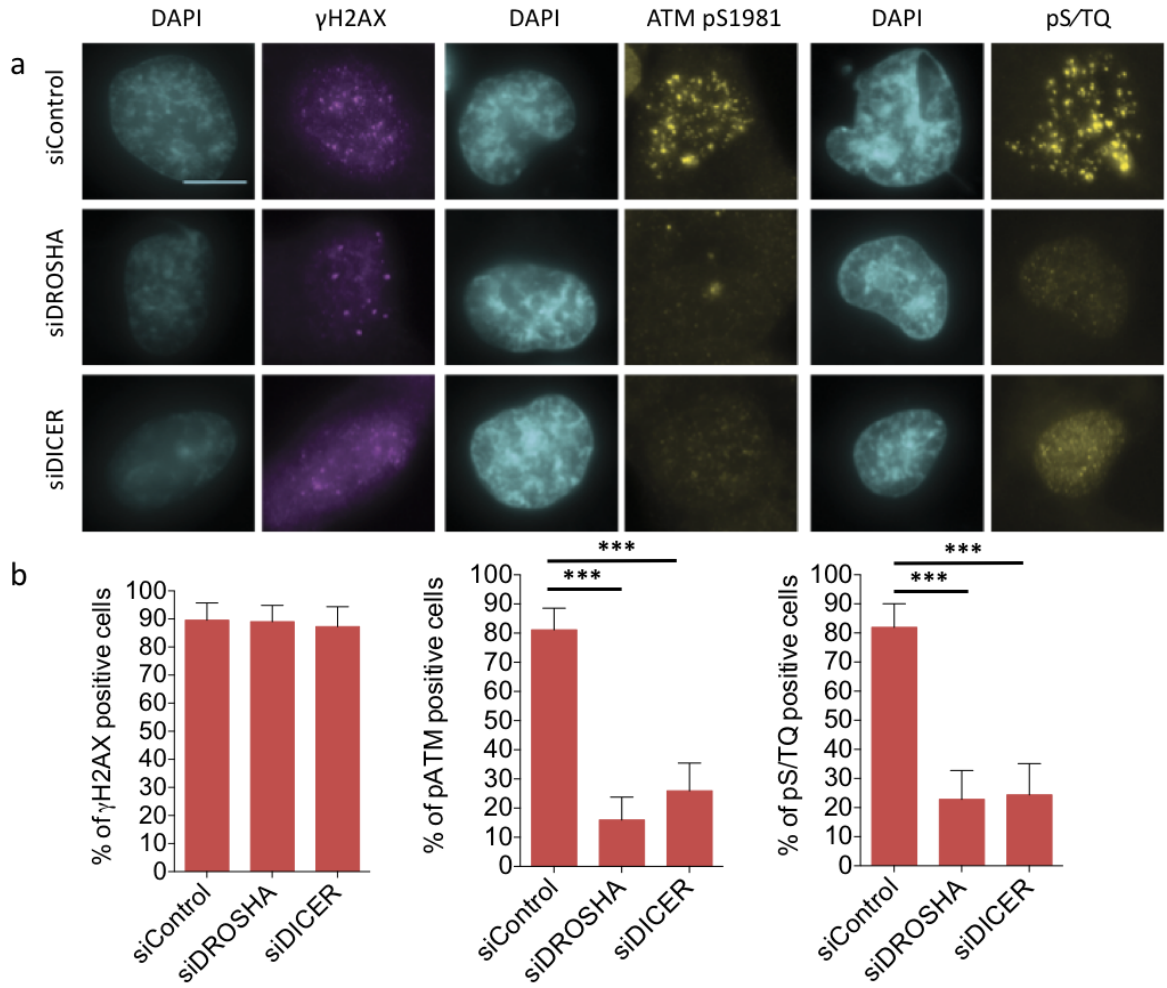

Figure 21. DROSHA and DICER are necessary for full DDR activation at deprotected telomeres in T19 cells.

(a) T19 cells were cultured without doxycycline for 8 days in order to express TRF2 ΔBΔM. Cells were 4% PFA-fixed or collected for total RNA extraction prior to a 48-hour transfection with the indicated siRNAs. Fixed cells were stained for the indicated DDR markers. Scale bar, 5 μm. **(b)** Quantification of data shown in **a**. Bar graphs show the percentage of DDR-positive cells±95% confidence interval n=3 independent experiments. ***p-value<0.001, Chi-squared test. A cell was counted as positive if showing >3 foci.

Thus, the recruitment of DDR factors downstream of γH2AX, including ATM pS1981 and pS/TQ, to dysfunctional telomeres requires Dicer and Drosha endoribonucleases both in human and mouse cells.

3.2.3 Telomeric antisense oligonucleotides prevent DDR activation at dysfunctional telomeres.

As tDDRNAs at dysfunctional telomeres have a crucial role in DDR signalling, we aimed to inhibit them with the use of antisense oligonucleotides (ASOs). Inhibitory ASOs are commonly employed to block the functions of RNA molecules (McClorey and Wood, 2015) by steric hindrance. Thus, we designed ASOs to either bind the G-rich (named anti-teloG) or C-rich (named anti-teloC) strand of tDDRNAs and tdilncRNAs and an ASO with an unrelated control sequence. We then transfected ASOs in $Trf2^{F/F}$ MEFs treated with 4OHT for 48 hours to induce telomere dysfunction. Most importantly, both anti-teloG and anti-teloC ASOs, but not the control one, reduced the number of 53BP1 and pS/TQ foci at dysfunctional telomeres (**Figure 22**). On the contrary, and in agreement with the Dicer and Drosha knockdown experiments, we observed unaltered γH2AX foci formation (**Figure 22**).

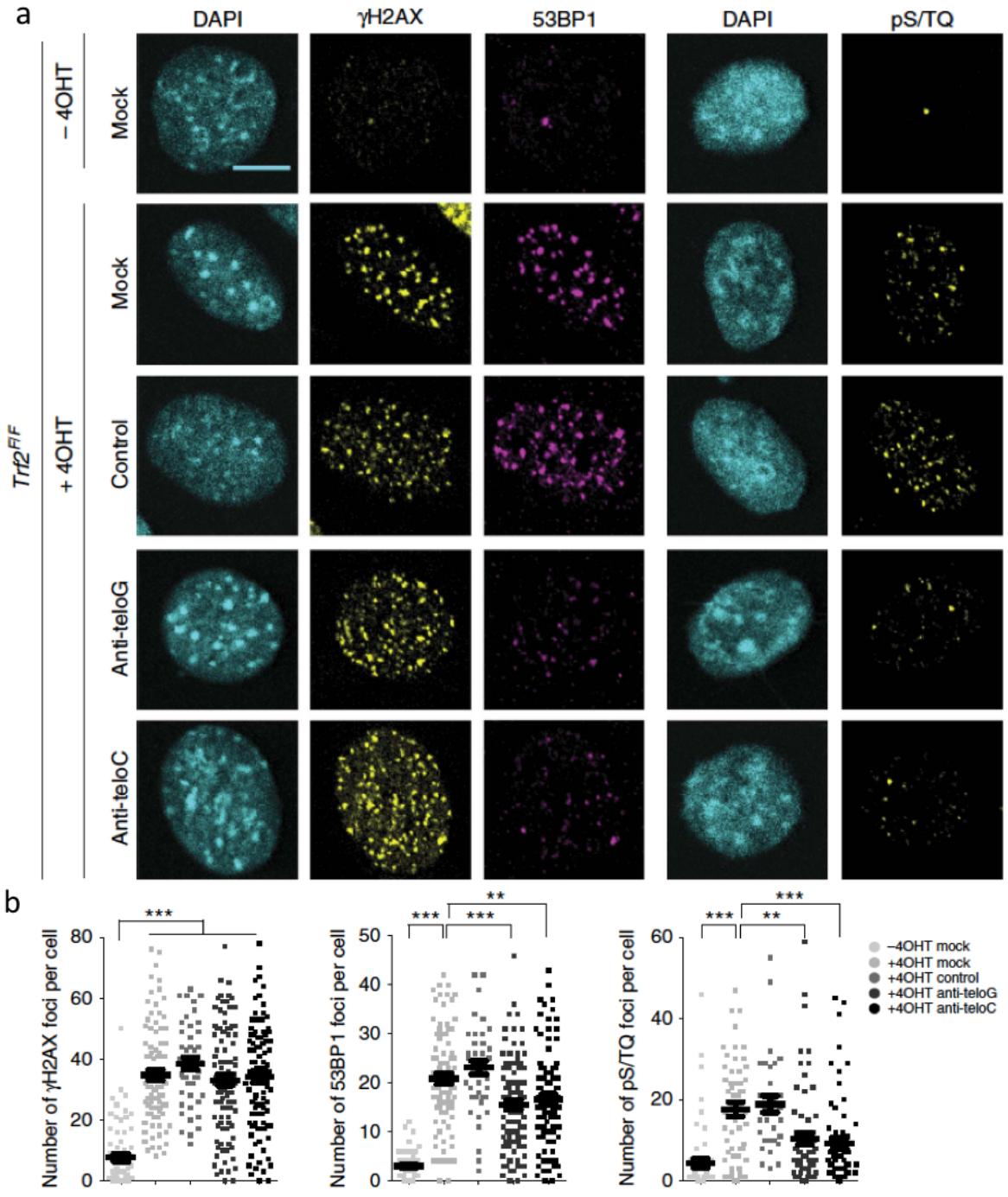

Figure 22. Telomeric ASOs inhibit DDR activation at dysfunctional telomeres.

(a) MEFs Trf2$^{F/F}$ were treated, or not, with 4OHT (0.6 μM) and transfected with the indicated ASO. Fixed cells were stained for the indicated DDR markers. Scale bar, 10 μm. **(b)** Quantification of data shown in **a**. Dot plots show the number of DDR foci per cell. Lines indicate the mean ±s.e.m. n=3 independent experiments. **p-value<0.01; ***p-value<0.001, one-way ANOVA with multiple-comparison post-hoc corrections. Results by Francesca Rossiello.

3.3 A link between tDDRNAs and telomere-driven cellular senescence.

3.3.1 Replicative senescent cells undergo telomeric DDRNA accumulation

Progressive telomere attrition occurs as proliferating mortal human cells undergo population doublings, ultimately leading to exposed free double-stranded chromosome DNA ends (d'Adda di Fagagna et al., 2003). This event, triggers a persistent and irreparable telomeric DDR (Fumagalli et al., 2012), which leads to senescence induction. In order to test whether tDDRNA production indeed triggers replicative senescence, I purified RNA from early passage (population doubling 32) and late passage (population doubling 89) BJ cells and observed an induction of both teloG and teloC DDRNAs (**Figure 23**), consistent with the reported accumulation of DNA damage at the telomeres.

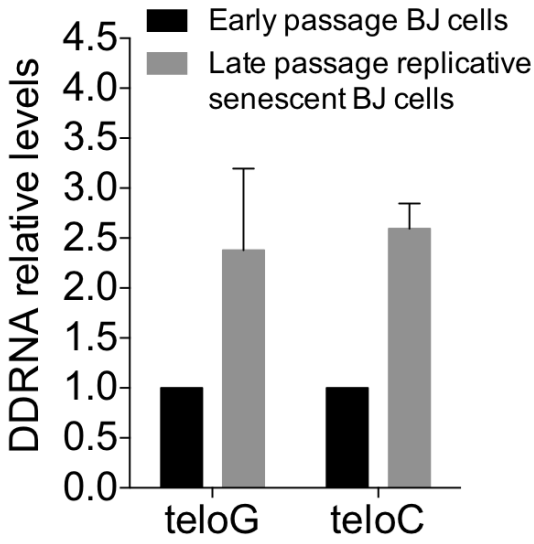

Figure 23. tDDRNAs are induced in replicative senescent cells.

Small RNA was gel-extracted (< 40 nt) and used for PCR amplification (as described on Figure 12) to detect tDDRNAs. Error bars represent the s.e.m. n=3 independent experiments. tDDRNA levels were normalized to mir29b and to Early passage BJ cells.

3.3.2 A role of tDDRNAs in IR-induced senescence

As IR-induced senescence is a result of the inability of cells to repair some genomic sites of the genome, including telomeres (Fumagalli et al., 2012), I aimed to set up an experimental design where quiescent early passage BJ cells were irradiated (20 Gy) and

left to recover for four weeks prior to RNA extraction. Consistent with the reported accumulation of DNA damage at the telomeres, I could detect an induction of DDRNAs upon IR-induced senescent cells as compared to BJ control cells (**Figure 24**).

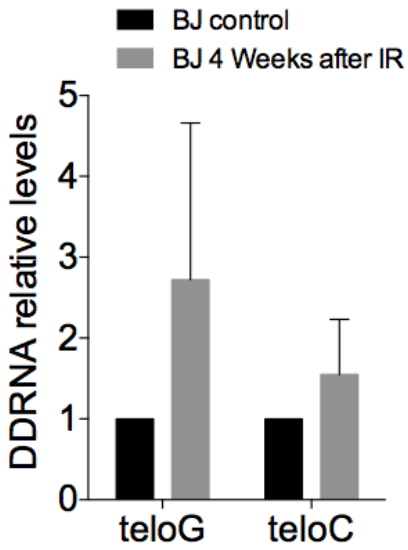

Figure 24. tDDRNAs accumulate in IR-induced senescent cells.

Small RNA was gel-extracted (< 40 nt) and used for PCR amplification (as described on Figure 12) to detect tDDRNAs. Error bars represent the s.e.m. n=3 independent experiments. tDDRNA levels were normalized to mir29b and BJ control non-irradiated cells.

Next, I aimed to monitor senescence markers by directly inhibiting tDDRNA and tdilncRNA functions through ASO delivery. To do so, cells were transfected at 50% confluency and irradiated (at 20 Gy) once they became fully confluent. Four weeks after irradiation I tested for senescence markers.

p21 and p16 mRNA levels, markers often expressed in senescence, and SASP genes IL-6, IL-8 and IL-1A were all induced four weeks after irradiation (**Figure 25**). Interestingly, p16 and p21 mRNA levels decreased upon telomeric ASO treatment (**Figure 25a, b**) whereas SASP genes remained unaltered (**Figure 25c**); suggesting a tDDRNA/tdilncRNA-independent mechanism for SASP production.

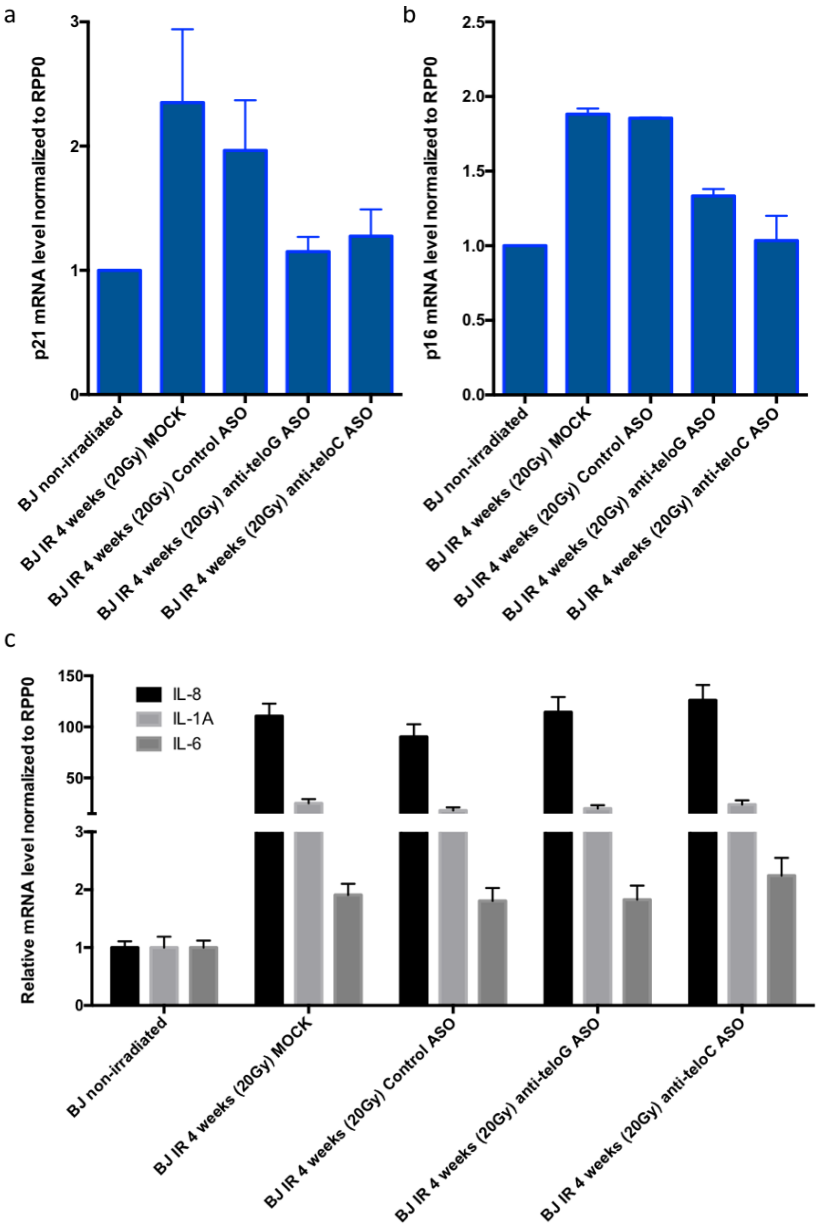

Figure 25. Telomeric ASO treatment suppresses p21 and p16 induction of IR-induced cells while maintaining SASP gene expression levels.

RT-qPCR analysis of p21 **(a)**, p16 **(b)** and SASP (IL-8, IL-1A and IL-6) (**c**) mRNA levels of IR-induced BJ cells. Rplp0 (RPP0) mRNA was used as normalizer. n=2 independent experiments. Error bars represent the s.e.m.

3.4 The role of tDDRNAs at progerin-driven telomere dysfunction in Hutchinson–Gilford Progeria Syndrome.

3.4.1 Progerin expression induces the transcription of telomeric DDRNAs and their precursors.

To investigate the potential generation of tDDRNAs and study their role in an amenable human cell model of HGPS, I expressed wild type or the HGPS mutant form of lamin A gene (known as progerin) through retroviral delivery in normal human skin fibroblasts (BJ; **Figure 26a**) – this is a relevant cell model as skin abnormalities are one of the major HGPS phenotypes. As progerin expression has been reported to induce telomere dysfunction, I monitored tDDRNAs expression and indeed I discovered increased levels of both teloG and teloC DDRNAs upon progerin expression (**Figure 26b**).

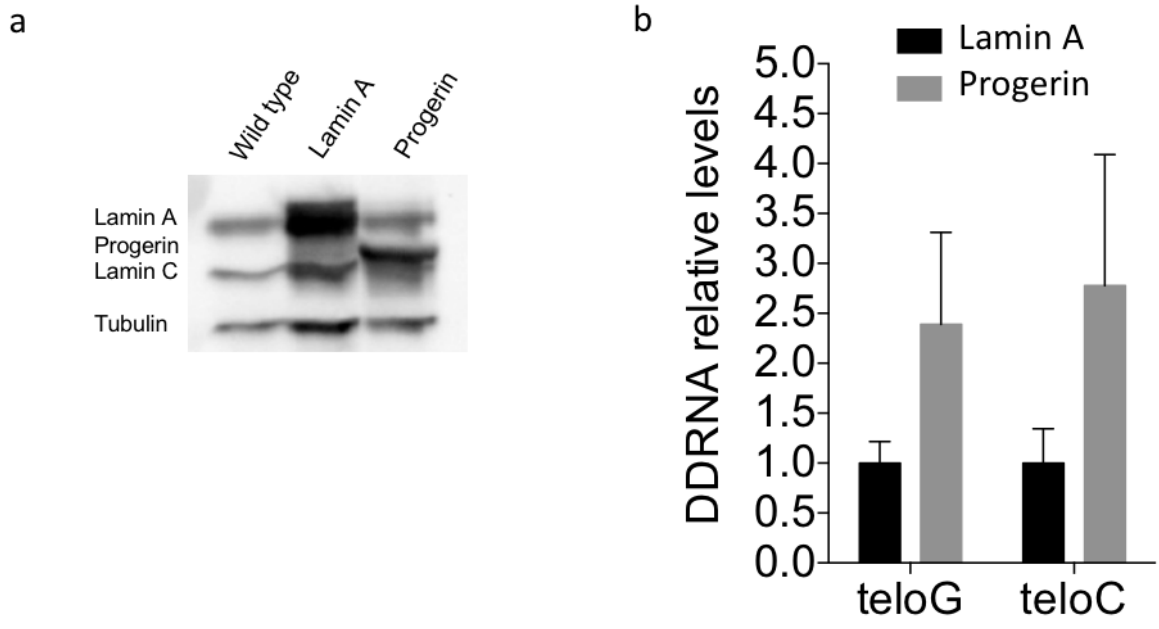

Figure 26. Progerin expression leads to increased levels of tDDRNAs.

(a) Western blot analysis shows lamin A/C and progerin expression in wild type normal human skin fibroblasts and retrovirally-transduced Lamin A-expressing and Progerin-expressing cells. Tubulin was used as loading control. **(b)** Small RNA was gel-extracted (< 40 nt) and used for PCR amplification (as described on Figure 12) to detect tDDRNAs. DDRNA levels were normalized to mir17 and Lamin A control cells.

I next measured tdilncRNAs expression levels upon progerin expression and observed a 3- to 5-fold increase of both telomere strands as compared to control-cells levels (**Figure 27**). Induction of tDDRNAs and their precursors are consistent with increased telomeric DDR activation as previously reported (Benson et al., 2010).

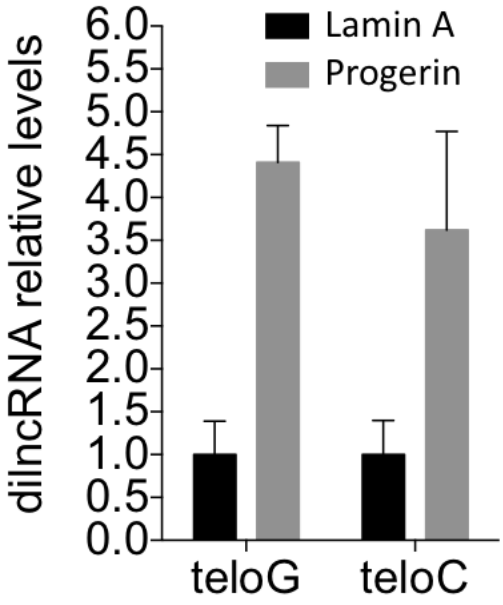

Figure 27. Progerin expression leads to increased levels of tdilncRNAs.

Total cell RNA was isolated and used for strand-specific RT-qPCR to detect tdilncRNAs. tdilncRNA levels were normalized to Rplp0 mRNA and Lamin A control cells. Error bars represent the s.e.m. n=3 independent experiments.

3.4.2 Progerin expression reduces cell proliferation and induces SASP expression.

Furthermore, progerin-expressing cells showed a decrease in BrdU incorporation and in the percentage of Ki67-positive cells, both readouts of cell proliferation (**Figure 28a**) associated with an induction of expression of the senescence-associated secretory phenotype (SASP) genes interleukin-6 (IL-6), interleukin-8 (IL-8) and interleukin-1A (IL-1A) (**Figure 28b**), consistent with the reported senescence induction phenotype.

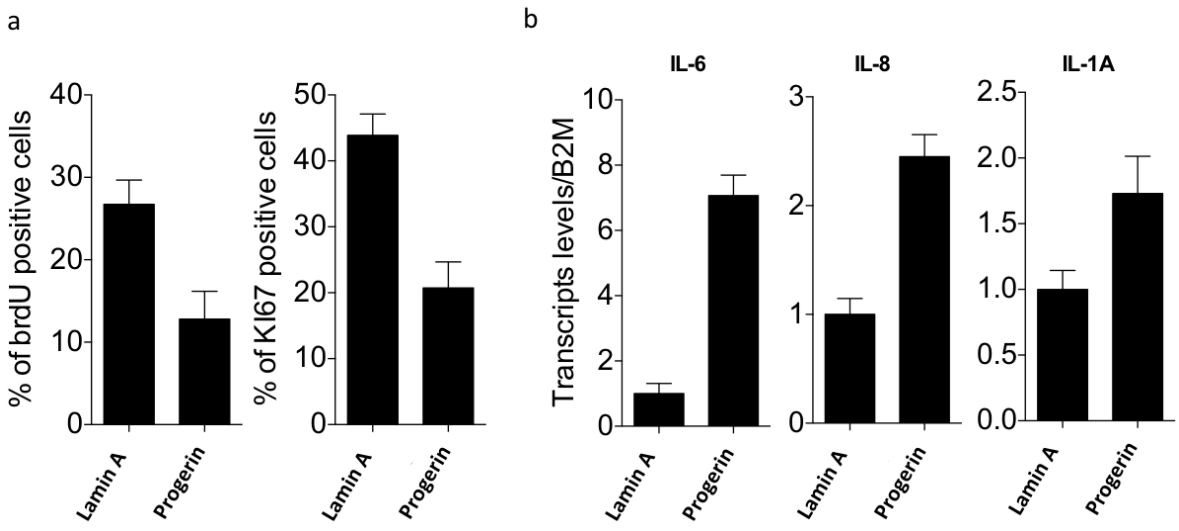

Figure 28. Progerin expression reduces cell proliferation and induces SASP expression.

(a) Bar graphs show the percentage of BrdU and Ki67 positive cells ± 95% confidence interval. At least 100 cells were counted for each condition. n=3 independent experiments. **(b)** RT-qPCR analysis of the senescence-associated secretory phenotype (SASP) genes interleukin-6 (IL-6), interleukin-8 (IL-8) and interleukin-1A (IL-1A) in BJ cells. Values are normalized to 1 on Lamin A overexpressing controls.

3.4.3 Telomeric antisense oligonucleotides reduce progerin-driven telomeric DNA damage and improve the proliferation of progerin-expressing cells.

I next tested whether progerin-induced DDR at telomeres could be modulated by the direct inhibition of tDDRNA and tdilncRNA functions through ASO delivery (as shown in **Figure 22**). I then transfected ASOs in BJ cells and expressed progerin or Lamin A through retroviral delivery. After 8 days, cells were stained for TRF2 and 53BP1 to look for DDR at the telomeres (**Figure 29a**). As expected, progerin expression induced the accumulation of TIFs as compared to Lamin A expressing cells (**Figure 29b** and (Benson et al., 2010)). Most importantly, upon progerin expression, both anti-teloG and anti-teloC, but not the control ASO, significantly reduced the TIFs to the levels of LaminA expressing control cells (**Figure 29b**).

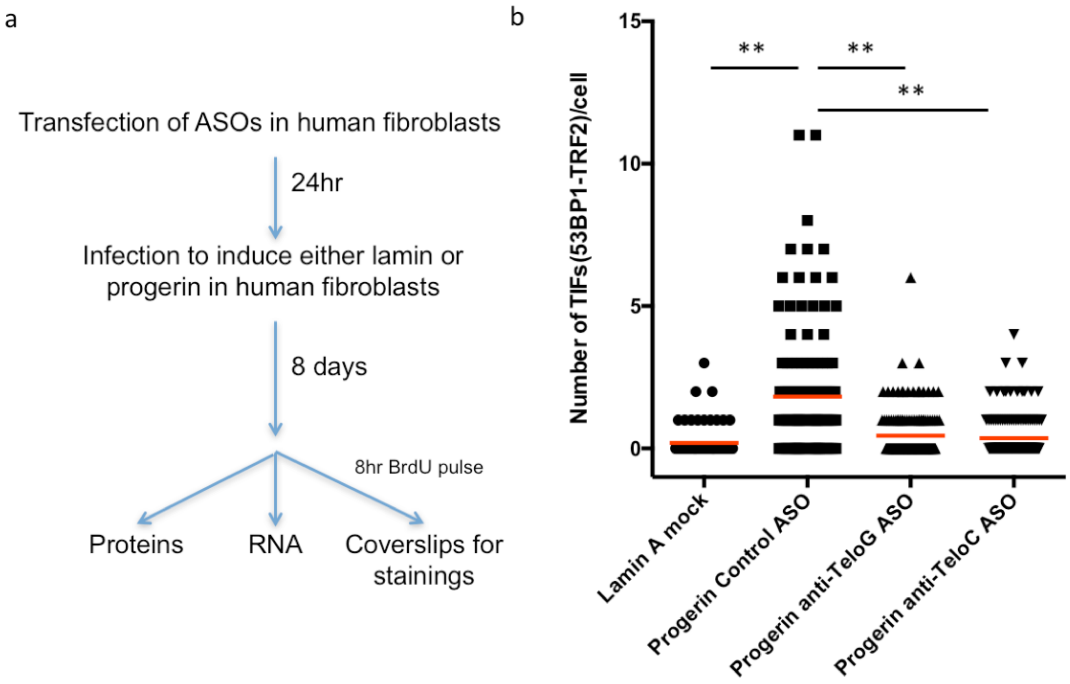

Figure 29. Telomeric ASOs inhibit DDR activation at progerin-driven dysfunctional telomeres.

(a) BJ cells were transfected with telomeric or control ASOs and induced the expression of either progerin or Lamin A through retroviral delivery for 8 days. Cells were thereafter collected for RNA and protein extractions or fixed for staining. **(b)** Cells were stained for 53BP1 and TRF2 and set for quantification of telomere dysfunction-induced foci (TIFs) as determined by the co-localization of 53BP1 and TRF2. Co-localization was assessed by ImageJ software with a customized ImageJ macro to allow 3D stack analysis. As stated in material and methods, two points were considered co-localizing if their respective intensities were higher than the threshold of their channels and if 5 pixels or more overlapped between both channels within the same section of the stack. **p-value<0.01; one-way ANOVA with multiple-comparison post-hoc corrections. n=3 independent experiments.

Importantly, non-telomeric DDR foci remained unaffected upon telomeric or control ASOs (**Figure 30**).

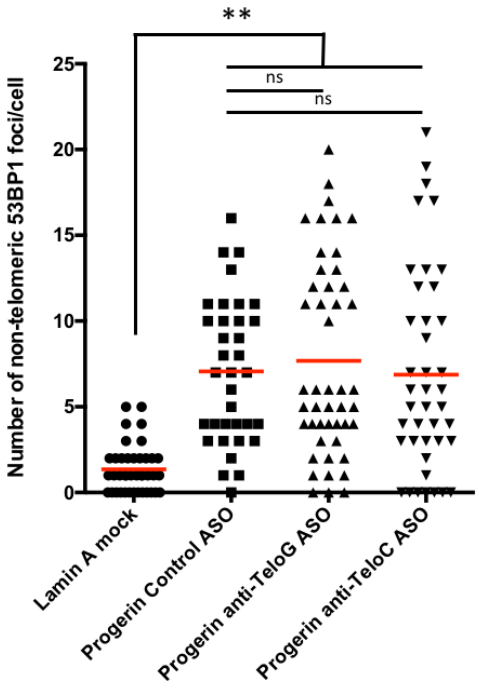

Figure 30. Telomeric ASO treatment has no effect in non-telomeric DDR foci.

BJ cells were transfected with the indicated ASOs and induced the expression of either progerin or Lamin A through retroviral delivery for 8 days. Cells were thereafter stained for 53BP1 and TRF2. Quantification was performed by subtracting the TIFs as determined by the co-localization of 53BP1 and TRF2 to the overall 53BP1 foci detected. **p-value<0.01; one-way ANOVA with multiple-comparison post-hoc corrections.

Next, I used the experimental set up in which BJ cells expressing progerin or Lamin A through retroviral delivery were transfected with ASOs to test their proliferation. After 8 days of infection and selection, I pulsed cells with BrdU for 8 hours and stained for both BrdU and Ki67. Excitingly, both anti-teloG and anti-teloC, but not control ASO, restored proliferation rates in progerin-expressing cells (as independently measured by BrdU and Ki67) to the levels of control cells (**Figure 31**).

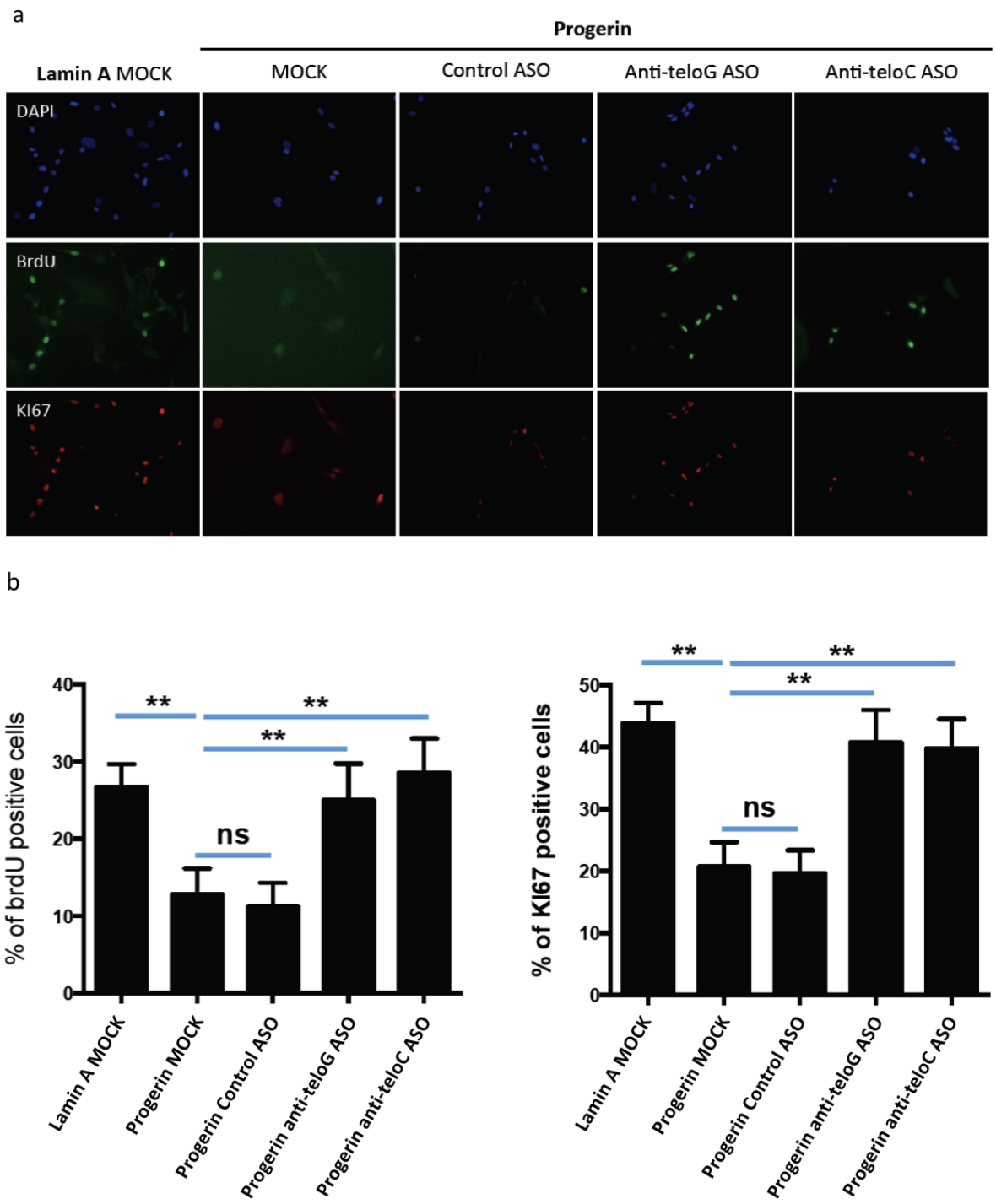

Figure 31. Telomeric ASOs improve the proliferation of progerin-expressing cells.

(a) BJ cells were transfected with the indicated ASOs and induced the expression of either progerin or Lamin A through retroviral delivery. After 8 days cells were pulsed with BrdU for 8 hours and stained for BrdU (green) and Ki67 (red). **(b)** Quantification of stainings shown in **a.** Bar graphs show the percentage of BrdU and Ki67-positive cells ± 95% confidence interval. **p-value<0.01, Chi-squared test. n=3 independent experiments. At least 300 cells were counted for each condition.

ASO treatments leaves Lamin A and progerin protein levels unaltered (**Figure 32**).

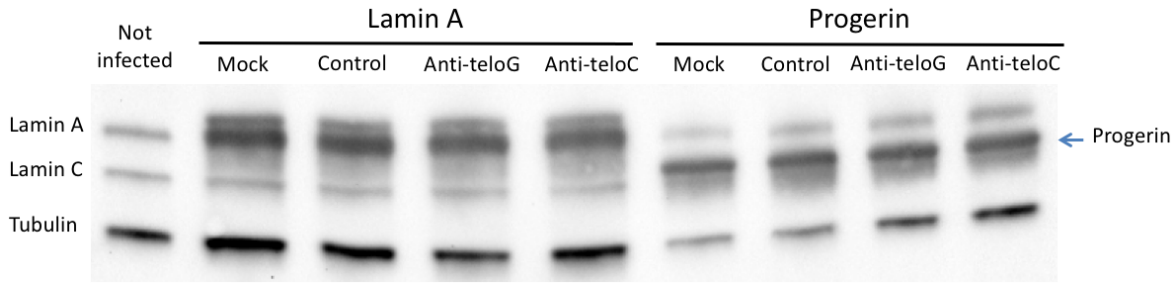

Figure 32. Lamin A and progerin protein levels remain unaltered upon telomeric ASO treatment.

BJ cells were transfected with the indicated ASOs and induced the expression of either progerin or Lamin A through retroviral delivery for 8 days. Representative western blot analysis shows Lamin A and Progerin expression in BJ cells transfected with the indicated ASO. Tubulin was used as loading control.

In parallel, we observed no obvious change in proliferation rates in Lamin A-expressing cells treated in the same way (**Figure 33**), suggesting a telomere-specific role of our ASOs in preventing proliferation inhibition mediated by tDDRNAs and tdilncRNAs induced upon progerin expression.

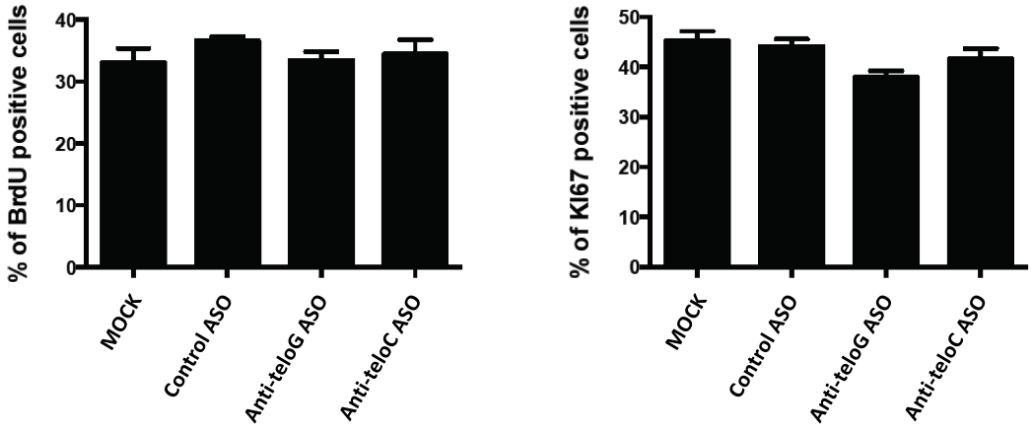

Figure 33. Unaltered proliferation rates in Lamin A-expressing cells upon ASO treatment.

Quantification of BrdU and Ki67 positive cells in Lamin A-transduced BJ cells transfected with the indicated ASO. 8 days after retroviral delivery, cells were pulsed with BrdU for 8 hours and subsequenty stained for BrdU and Ki67. Bar graphs show the percentage of BrdU and Ki67 positive cells ± 95% confidence interval. At least 100 cells were counted for each condition.

Unexpectedly, telomeric ASO treatment in progerin-expressing cells left unaltered SASP gene expression levels (**Figure 34**), suggesting a tDDRNA-independent and likely DDR-

independent mechanism for SASP control, and consistent with the results obtained in IR-induced senescent cells.

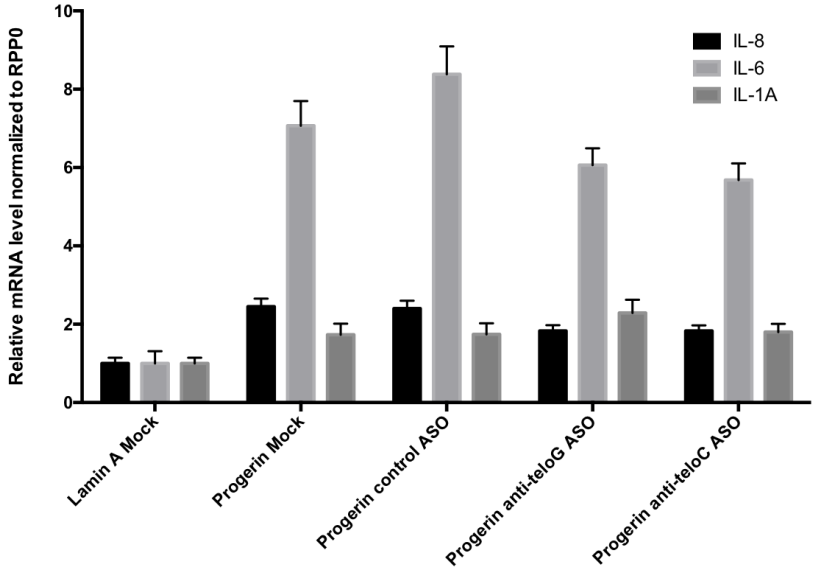

Figure 34. SASP mRNA levels are unaltered upon ASO treatment upon progerin expression.

RT-qPCR analysis of SASP (IL-8, IL-1A and IL-6) mRNA levels progerin-expressing BJ cells. Rplp0 (RPP0) mRNA and Lamin A control cells were used as normalizers. n=2 independent experiments. Error bars represent the s.e.m.

Lastly, I monitored the nuclear shape of progerin-expressing cells upon telomeric ASO treatment. In order to do so, I measured the circularity index of the nuclei tested (with a value of 1 indicating a perfect circle and as the value approaches 0, it indicates an increasingly elongated shape). Consistent with previous reports, progerin expression lead to a decrease of circularity compared to Lamin A expressing cells (**Figure 35**). More interestingly, the nuclear shape abnormalities driven by progerin remained unaltered upon ASO treatment (**Figure 35**).

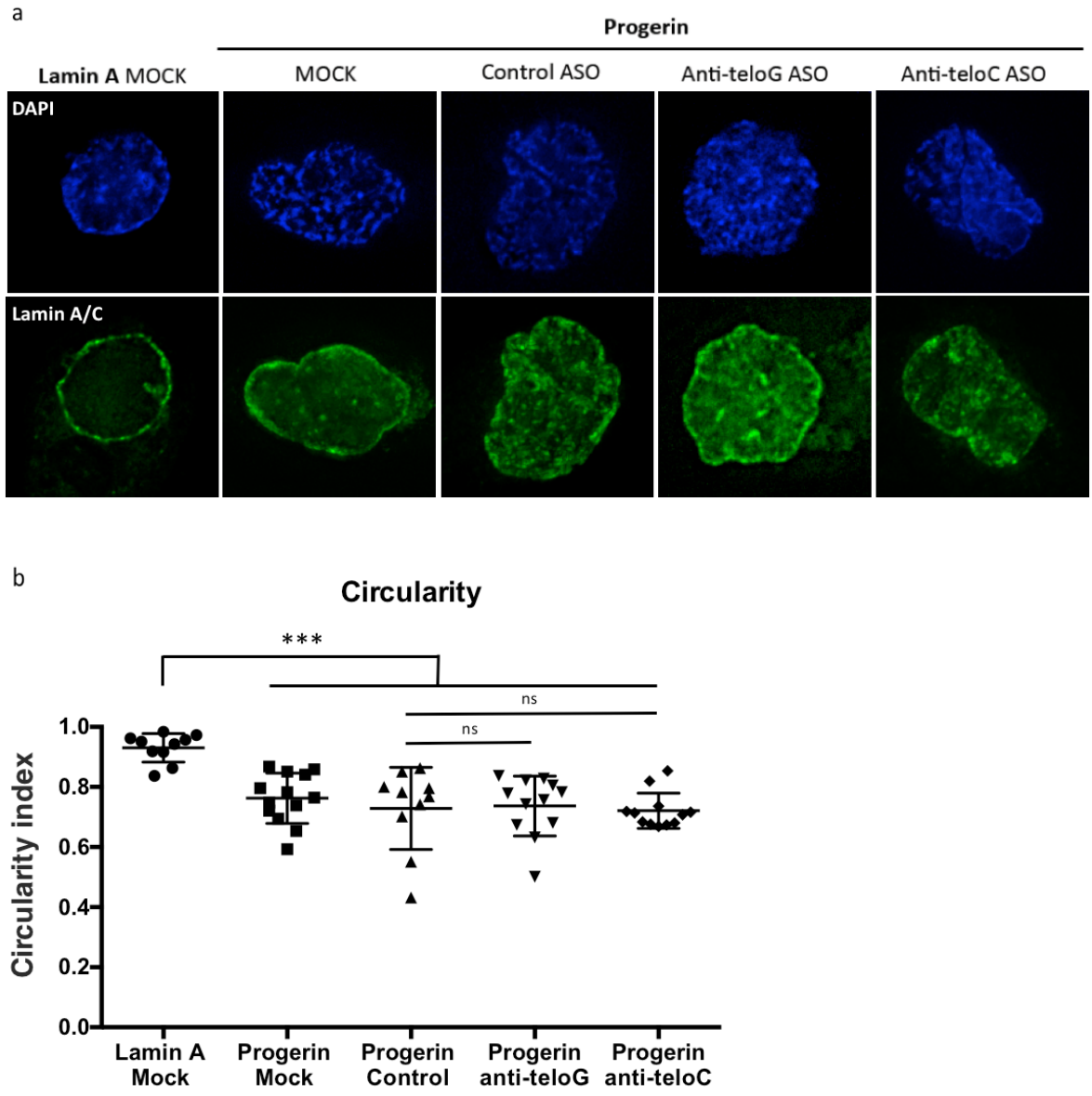

Figure 35. Progerin-driven nuclear shape abnormalities are unaltered upon ASO treatment.

(a) BJ cells were transfected with the indicated ASOs and induced the expression of either progerin or Lamin A through retroviral delivery. After 8 days, cells were stained for Lamin A/C (green). **(b)** Quantification of stainings shown in **a.** Each point in the scatter plot shows the circularity index of a nucleus. ***p-value <0.001, one-way ANOVA with multiple-comparison post-hoc corrections. n=1

3.4.4 Human primary HGPS cells accumulate tDDRNAs and their inhibition improves their proliferation.

To further test the role of telomeric transcripts in progerin-driven pathology, I used HGPS patient-derived fibroblasts; which better resembles the human pathology of progeria and

whose progerin protein expression levels, as opposed to the overexpression of progerin in BJ fibroblasts, are comparable to Lamin A and Lamin C proteins (Goldman et al., 2004).

I therefore transfected human primary HGPS fibroblasts with ASOs to test whether tDDRNA and tdilncRNAs inhibition modulates cell proliferation. To do so, I treated early-passage HGPS fibroblasts with either telomeric or control ASOs and monitored their growth by a resazurin-based cell viability assay (**Figure 36**). Importantly, to maintain a constant ASO concentration of 20 nM, every time cells became confluent I split and re-treated them until cell proliferation ceased.

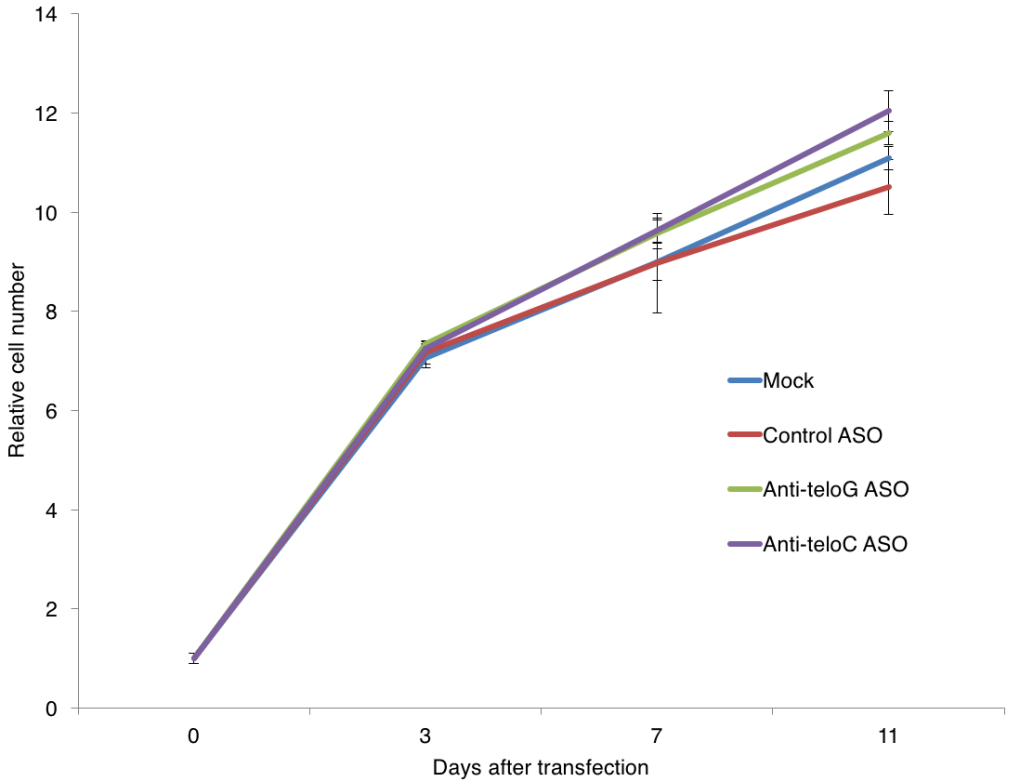

Figure 36. Telomeric ASO treatment improves proliferation rates by slowing down the growth decline of human primary HGPS fibroblasts.

Growth curve (normalised to day 0) of human primary HGPS cells treated or not with ASOs. Cell growth was monitored for 11 days until cells fully arrested their proliferation. n=1 experiment. Error bars of technical replicates represent the s.d.

Consistent with the reported growth decline phenotype, HGPS-cultured fibroblasts underwent a rapid growth deceleration in just a few days. Importantly, telomeric ASO

treatment moderately improved the proliferation rate of HGPS fibroblasts (**Figure 36**), consistent with the upregulation of both G-rich and C-rich tDDRNAs at the time points tested (**Figure 37**).

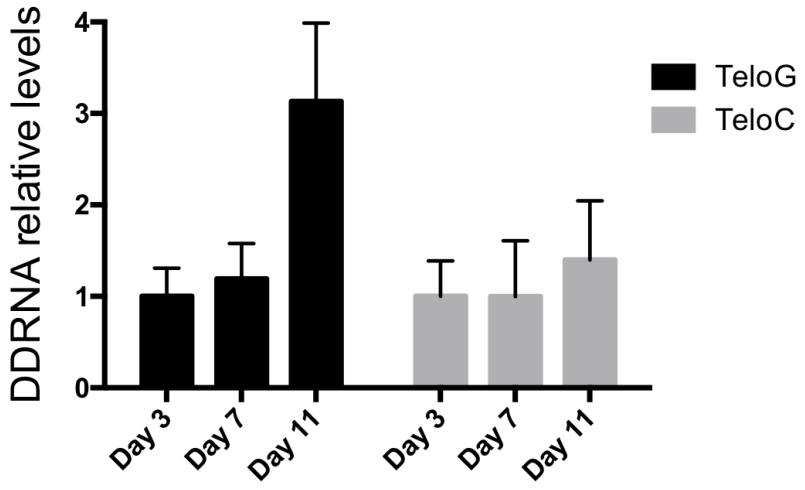

Figure 37. tDDRNA induction correlates with growth decline in human primary HGPS fibroblasts.
Mock-treated HGPS fibroblasts small RNA samples from HGPS ASO growth curves was gel-extracted (< 40 nt) and used for PCR amplification (as described on Figure 12) to detect tDDRNAs. n=1 experiment tDDRNA levels were normalized to mir17 and HGPS cells (day 3). Error bars of technical replicates represent the s.d.

Notably, this telomeric ASO-driven growth amelioration was accompanied by a decrease of p21 mRNA expression at late-passage HGPS cells (**Figure 38a**). In addition, and consistent with the results obtained in progerin-overexpressing BJ cells, ASO treatments left unaltered progerin mRNA levels (**Figure 38b**).

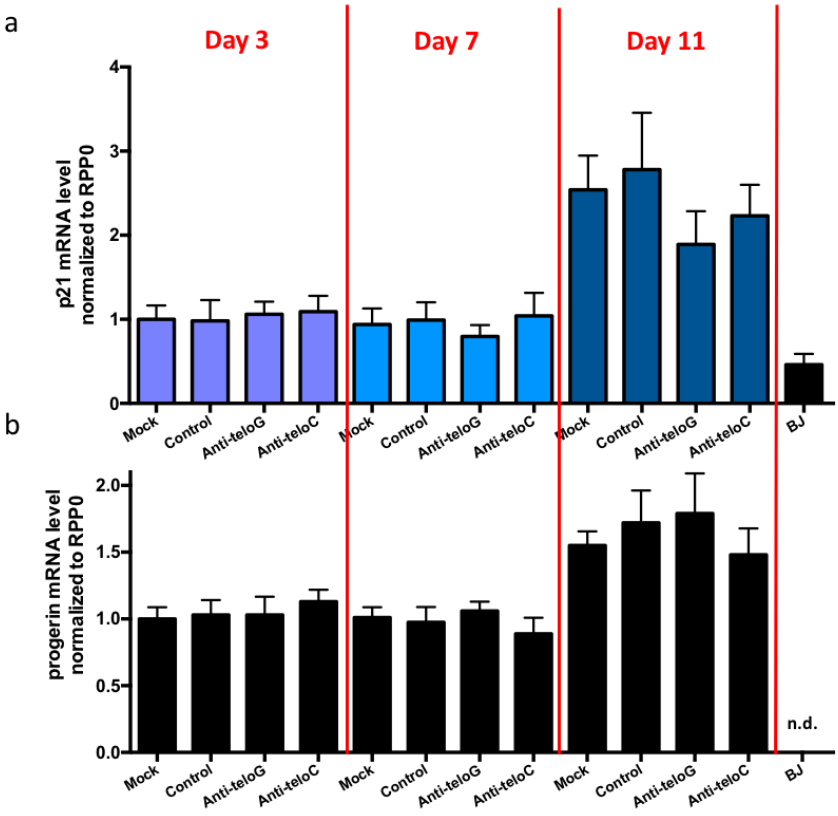

Figure 38. Telomeric ASO treatment partially prevents the induction of p21 mRNA in primary HGPS cells

RT-qPCR analysis of the p21 **(a)** and progerin **(b)** mRNA levels of human primary HGPS fibroblasts at different time points after ASO transfection. BJ cells RNA was used as negative control for progerin detection. Rplp0 (RPP0) mRNA was used as normalizer. n.d. = not detectable. n=1 experiment Error bars of technical replicates represent the s.d.

3.4.5 tDDRNAs and tdilncRNAs accumulate in a progeric inducible skin mouse model.

To validate the efficacy of our telomeric ASOs *in vivo* in a relevant HGPS animal model, in collaboration with the laboratory of Maria Eriksson at Karolinska Institutet (Sweden), we used an inducible skin mouse model derived from the breeding of K5tTA mice6 with mice expressing either human Lamin A gene or the most common HGPS mutation (1824C>T) under tet control. These resulting mice inducibly express human lamin A or progerin in epidermal keratinocytes (Sagelius et al., 2008). I therefore extracted RNA from skin tissue of control and HGPS mice at postnatal day 6 to monitor for tDDRNAs and

tdilncRNAs and observed increased teloG and teloC levels of both telomere transcripts in HGPS mice (**Figure 39**).

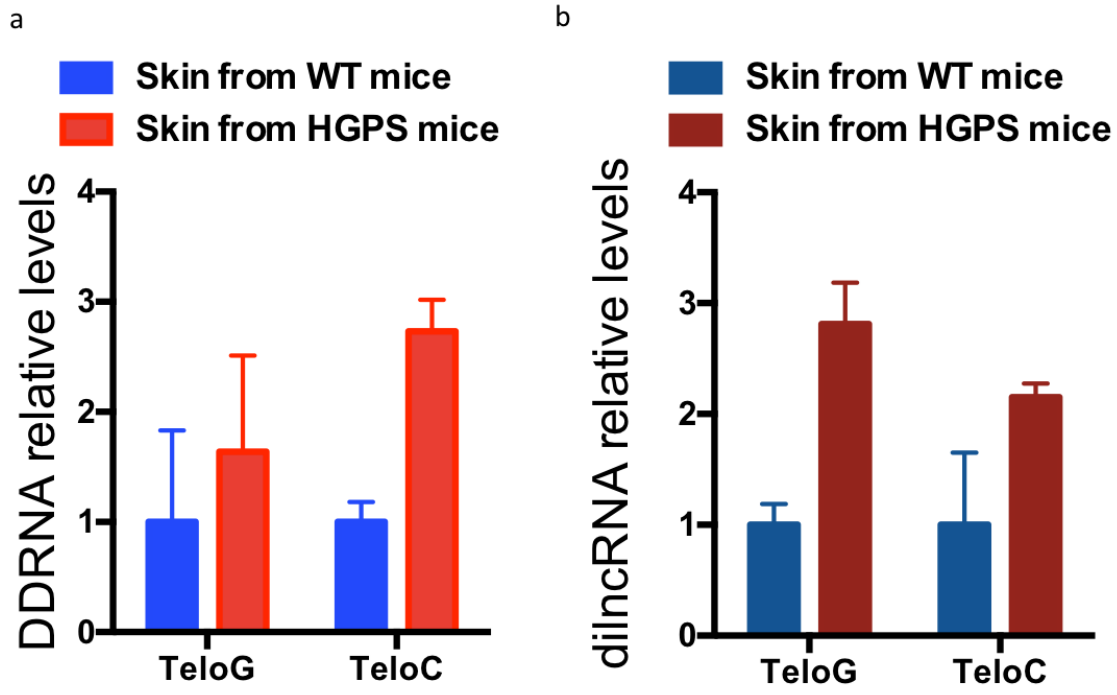

Figure 39. Accumulation of tDDRNAs and tdilncRNAs in a progeric inducible skin mouse model.

(a) Skin from Wild type (WT) and mutant HGPS mice was collected and total cell RNA extraction was performed. Small RNA was gel-extracted (< 40 nt) and used for PCR amplification (as described in Figure 12) to detect tDDRNAs. n=3 independent experiments. tDDRNA levels were normalized to mir17 and to the cells from skin of WT mice. **(b)** Total cell RNA extracted as in **a** was used as starting material to perform strand-specific RT–qPCR to detect tdilncRNAs. tdilncRNA levels were normalized to Rplp0 mRNA and to the cells from skin of WT mice. n=3 independent experiments.

3.4.6 Progerin-expressing mice treated with telomeric antisense oligonucleotides live longer.

To monitor lifespan in the HGPS skin mouse model, pregnant mice were injected with both anti-teloG and anti-teloC ASOs (15 mg/kg) or phosphate buffered saline (PBS) as control at embryonic day 17. After birth, new-born mice were injected intraperitoneally once every three days starting at postnatal day 2 (**Figure 40a**). As previously reported, progerin-expressing mice had a dramatically shorter lifespan compared to wild types (**Figure 40b** and (Sagelius et al., 2008)). Strikingly however, progerin-expressing mice

treated with anti-teloG ASO lived significantly longer than untreated controls (**Figure 40b**) while wild type mice did not show any effect in survival when injected with anti-teloG. Interestingly, anti-teloC ASO treatment left unaltered the lifespan of progerin-expressing mice (**Figure 40b**). Further studies will likely clarify the discrepancies observed between the effects of both telomeric ASOs in lifespan extension.

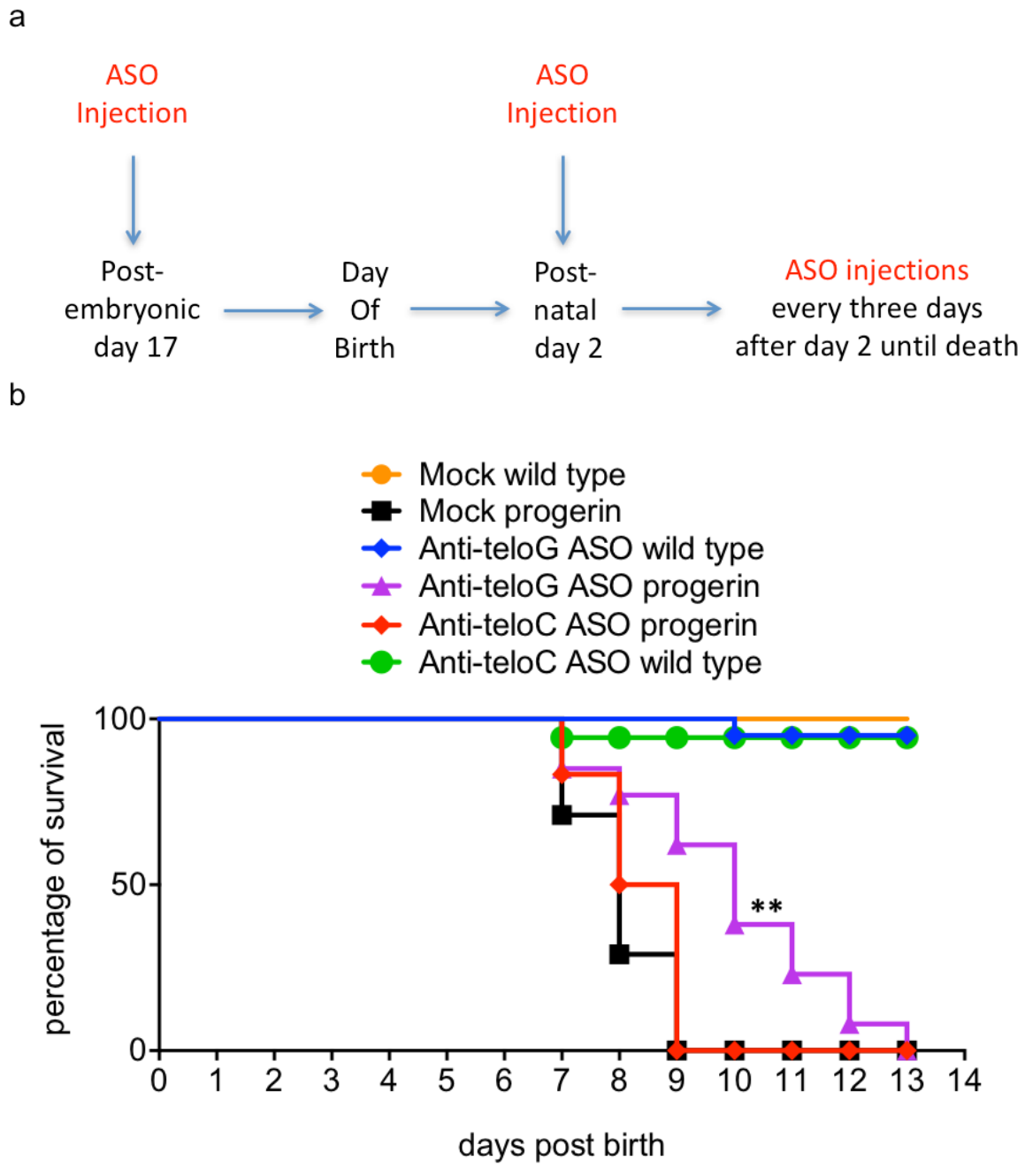

Figure 40. Progerin-expressing mice treated with telomeric ASOs live longer.

(a) Scheme of the experimental design set for ASO delivery in the HGPS skin mouse model. **(b)** Kaplan-Meier curve of wild type mice treated with vehicle (n=16, yellow), anti-teloG (n=20, blue) or anti-teloC ASOs (n=10, green); and progerin-expressing mice treated with vehicle (n=7, black), anti-teloG (n=13,

purple) or anti-teloC ASOs (n=7, red). Mice were injected intraperitoneally with 15 mg/kg of telomeric ASO. **p-value<0.01. Kaplan-Meier survival analysis. This experiment was performed in collaboration with Maria Eriksson at the Karolinska Institutet (Sweden).

Altogether these results demonstrate that sequence-specific targeting of tDDRNAs and tdilncRNAs by ASOs reduces the aging phenotype, such as cell proliferation defects, caused by progerin in cultured cells and in a HGPS animal model leading to lifespan extension.

4 DISCUSSION

4.1 The role of telomere transcription induced by telomere dysfunction.

4.1.1 A link between RNA and the DNA damage response.

It has been known for decades that RNA pol II shows high affinity for DNA ends (Dynan and Burgess, 1981); however, this notion had not been yet linked to any relevant biological function. Recently, our lab has demonstrated that transcriptionally active RNA pol II is recruited to DSBs, a mechanism facilitated by its interaction with the MRN complex (Michelini et al., 2017). According to our results, when a DSB arises, RNA pol II is recruited at the site of damage resulting in the generation of RNA transcripts (named dilncRNAs) resulting from the transcription from and toward the DSB site. In addition, DROSHA and DICER process paired dilncRNAs and generate DDRNAs, which in turn bind to their complementary unprocessed dilncRNA (**Figure 41)**(Michelini et al., 2017).

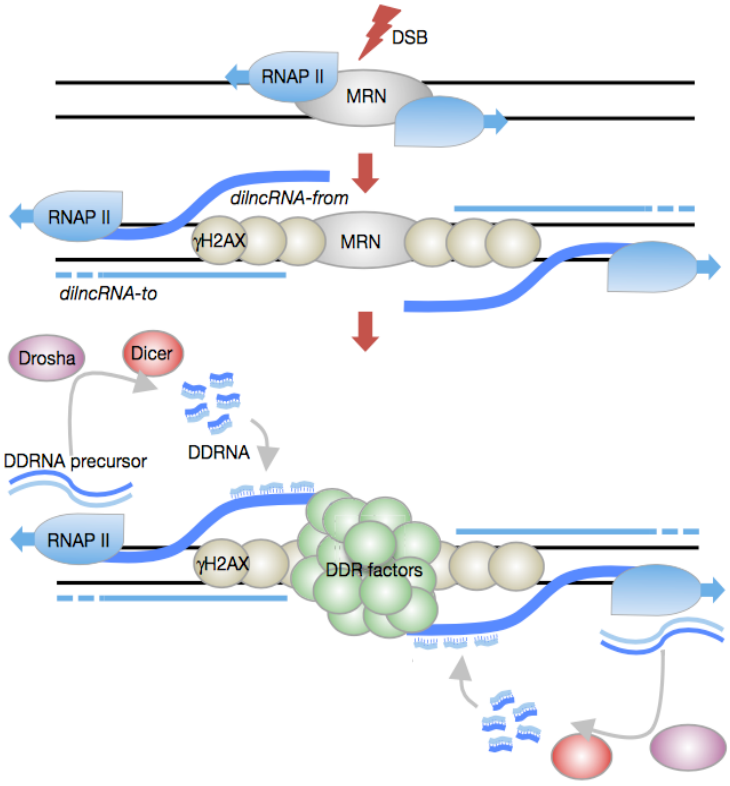

Adapted from (Michelini et al., 2017)

Figure 41. dilncRNAs orchestrate the DDR by interacting with DDRNAs at DSBs.

Upon DSB generation, the MRN complex recruits RNA pol II at the site of damage triggering a bidirectional synthesis of dilncRNAs from and towards the DSB. DROSHA and DICER endoribonucleases process the long double-stranded RNAs, likely formed by the outcome of paired or folded dilncRNAs, generating

DDRNAs that ultimately pair with unprocessed single-stranded dilncRNAs. Together, they allow the recruitment of 53BP1 leading to the formation of the DDR focus.

This DDRNA-driven mechanism which favours the secondary recruitment of DDR factors and therefore a full DDR activation, although not yet fully understood, is known to allow the recruitment of 53BP1 to DSBs by binding to DDRNAs (**Figure 41**) in a manner dependent on its tudor domain (Michelini et al., 2017).

4.1.2 Telomere transcription upon telomere dysfunction.

In line with the above-mentioned findings (section 4.1.1), Trf2-depleted MEFs ($Trf2^{F/F}$ MEFs treated with 4OHT for 48 hours), which undergo telomere dysfunction, are actively transcribed and generate double-stranded telomeric DDRNAs (**Figures 13** and **16**) and their precursor dilncRNAs (**Figure 17**). In addition, T19 human cells expressing the dominant negative form of TRF2, TRF2 ΔBΔM, recapitulate the tDDRNAs induction observed in mouse cells undergoing telomere dysfunction (**Figure 15**). Although PCR detection of a UUAGGG-*tandem* repeat containing RNA aimed to quantify telomeric G-rich dilncRNAs may also amplify the telomere transcript TERRA (Azzalin et al., 2007, Schoeftner and Blasco, 2008), C-rich telomere CCCUAA-repeat RNAs -transcripts arising at chromosome ends in the direction towards the centromere- have not been yet functionally characterized in mammals. Moreover, the upregulation of telomeric dilncRNA transcription induced by the removal of TRF2 and leading to DDR activation at telomeres is likely independent from TERRA transcription. This is supported by the fact that TERRA upregulation is not dependent on DNA damage signalling caused by TRF2 removal but rather caused by the absence of TRF2's homodimerization domain, which serves as a repressive mark for TERRA transcription (Porro et al., 2014). Furthermore, depletion of the telomeric proteins Rap1 or Taz1 (homologs of the mammalian proteins RAP1 and TRF1/2, respectively) in *Schizosaccharomyces pombe* strains have also been demonstrated to induce C-rich telomeric transcripts (Bah et al., 2012, Greenwood and Cooper, 2012), indicating an evolutionarily conserved increase of telomere transcription upon induction of

telomere dysfunction. These results are in agreement with RNA pol II recruitment at DSBs sites in *Schizosaccharomyces pombe* (Ohle et al., 2016), and with the reported enriched RNA pol II occupancy at telomeres upon induction of telomere dysfunction in human cells (Porro et al., 2014). The precise tDDRNA-dependent mechanism by which the DDR proteins are recruited to dysfunctional telomeres remains unclear, although previous reports suggest the involvement of 53BP1 in this process, as it has the ability to associate to RNA through its tudor domain (Pryde et al., 2005, Michelini et al., 2017).

The fact that tDDRNAs' biogenesis inhibition by DROSHA and DICER depletion and that sequence-specific ASOs against tDDRNAs and tdilncRNAs reduce DDR activation at telomeres (**Figures 20** and **21**; **22** and **29**, respectively) suggests that tDDRNAs and tdilncRNAs act in a sequence-specific manner ultimately allowing DDR signalling, consistent with previous reports that show comparable evidence at other genomic regions (Francia et al., 2012, Michelini et al., 2017).

4.2 Implications of tDDRNAs inhibition in cellular senescence.

The ability to detect tDDRNAs and their precursor tdilncRNAs and to inhibit telomeric transcripts by ASO delivery may have important implications in telomere-driven biological processes such as cellular senescence and aging (Jeyapalan et al., 2007, Herbig et al., 2006, Fumagalli et al., 2012, Hewitt et al., 2012, Waaijer et al., 2016) and in pathological conditions such as cancer and other telomere-driven medical conditions (also known as telomere syndromes) (Armanios and Blackburn, 2012).

Senescence induced by either critically short telomeres (replicative senescence) or irreparable telomeres after irradiation (IR-induced senescence) consistently induced the expression of tDDRNAs (**Figures 23** and **24**, respectively), indicating a role of tDDRNAs as potential biomarkers of DDR activation at dysfunctional telomeres in senescence.

ASO delivery in IR-induced senescent fibroblasts reduced the expression levels of p16 and p21 (**Figure 25a, b**), both markers known to establish and maintain the growth arrest that is typical of senescence (Jackson and Pereira-Smith, 2006, Campisi and d'Adda di Fagagna, 2007), indicating a potential role for tDDRNAs to allow cell growth arrest by controlling the ATM-p53-p21 and p16-pRB pathways. Interestingly, the expression of the SASP genes IL-6, IL-8 and IL-1A upon telomeric ASO treatment remains unaltered (**Figure 25c**), suggesting a tDDRNA/tdilncRNA-independent mechanism for SASP production.

Notably, it has recently been demonstrated that chromatin fragments leak out from the nuclei to the cytoplasm in primary human cells during senescence (Ivanov et al., 2013, Dou et al., 2015, Campisi, 2013), a phenomenon known to occur as a result of the loss of nuclear lamina protein lamin B1 (Shah et al., 2013, Shimi et al., 2011, Freund et al., 2012), which ultimately leads to compromised nuclear envelope integrity. However, the functional significance of these senescence-associated cytoplasmic chromatin fragments (CCFs) had remained elusive. More recently, several independent laboratories have demonstrated that CCFs activate the cGAS–STING pathway (Dou et al., 2017, Gluck et

al., 2017, Yang et al., 2017), an innate cytosolic DNA-sensing pathway which plays essential roles in preventing microbial infection and in triggering inflammation (Ishikawa et al., 2009, Barber, 2015, Ishikawa and Barber, 2008). Interestingly, these recent findings support the notion that the activation of cGAS–STING through CCFs' sensing promotes SASP production, as depletion of either cGAS or STING in human senescent cells fully abrogates SASP gene expression without affecting senescence maintenance, as measured by p16 and lamin B1 markers and SA-β-gal activity (Dou et al., 2017). Furthermore, overexpression of lamin B1 in senescent cells has little effect on the induction of γH2AX and p-ATM S1981, but significantly abrogates the formation of CCFs and the SASP gene expression (Dou et al., 2017). On the other hand, suppression of cGAS or STING upon senescence induction in human primary fibroblasts had no effect in DDR signaling as measured by pATM S1981 and γH2AX proteins levels (Dou et al., 2017). Although further studies have to be performed in order to elucidate the precise mechanism of SASP activation, the apparent DDR-independent mechanism by which CCFs induce SASP expression in senescence could explain why telomeric transripts' inhibition by ASO delivery had no apparent effect on IL-6, IL-8 and IL-1A mRNA expression in IR-induced senescent cells (**Figure 25c**). In line with these findings, confirmation of unaltered Lamin B1 levels upon telomeric transcripts' inhibition by ASO delivery in senescent cells may provide an explanation of why SASP levels are not affected, because unchanged low levels of Lamin B1 would lead to a persistent compromised integrity of the nuclear envelope (Shah et al., 2013, Shimi et al., 2011, Freund et al., 2012).

Although SASP expression is reported to partially rely on persistent DDR signaling (Rodier et al., 2009, Fumagalli and d'Adda di Fagagna, 2009), to what extent telomeric DDR is involved in this process is still unclear. A way to address this would require for instance ATM inhibition, as it would likely abrogate SASP production, in the same setup we used to test ASO treatments. Impaired SASP expression upon ATM inhibition but

unaltered SASP levels upon telomeric ASO treatment would suggest a telomeric DDR-independent mechanism by which SASP is generated in senescent cells.

4.3 Inhibition of progerin-driven telomere DDR signaling ameliorates the aging phenotype.

HGPS and other premature aging syndromes provide an opportunity to understand the mechanisms that drive aging. In agreement with the previously reported progerin-driven telomere dysfunction (Benson et al., 2010), overexpression of progerin in human skin fibroblasts leads to an increase of Telomere Induced Foci (TIF), as monitored by the co-localization events between TRF2 and 53BP1 (**Figure 29**). This increase of DDR signalling at the telomeres is consistent with the induction of tDDRNAs and their precursor tdilncRNA (**Figures 26** and **27**, respectively) as compared to control Lamin A-expressing cells.

Although no reports studying HGPS patient-derived cells have directly reported telomere dysfunction, these cells have been shown to undergo accelerated telomere shortening (Decker et al., 2009). Interestingly, passaging in culture of human primary HGPS fibroblasts throughout several population doublings shows a progressive accumulation of tDDRNAs' expression (**Figure 37**) and a gradual growth rate loss (**Figure 36**) associated with an increase of p21 mRNA level (**Figure 38 and 42**), altogether suggesting an increase of DDR activation at telomeres. However, further studies to monitor the co-localization events between DDR and telomere proteins are needed in order to confirm the potential progressive accumulation of progerin-driven dysfunctional telomeres in HGPS patient-derived fibroblasts.

The treatment with telomeric ASOs is able to specifically inhibit progerin-induced tDDRNAs and tdilncRNAs thus preventing DDR activation at dysfunctional telomeres (**Figure 29**), without affecting the signalling of DNA damage at other genomic regions (**Figure 30**). More excitingly, telomeric ASO treatment allows to rescue the proliferative capacity of progerin-overexpressing fibroblasts as monitored by Ki67 and BrdU positive cells (**Figure 31**), suggesting a role of tDDRNAs in regulating cell growth by controlling the signalling of progerin-induced telomere dysfunction (**Figure 42**). In line with these

observations, telomeric ASO treatment in human primary HGPS fibroblasts slows down their growth decline (**Figure 36)**, further indicating a role of telomere dysfunction also in patient-derived HGPS cells. This telomeric ASO-driven improved proliferation is concomitant with a reduction of p21 gene expression (**Figure 38)**, a decrease consistent to what is observed in IR-induced senescent cells (**Figure 25a**). Overall, these results strongly indicate a role of progerin-induced tDDRNAs and tdilncRNAs in allowing the activation of DDR at the telomeres that ultimately leads to a growth arrest by activating the ATM-p53-p21 pathway (**Figure 42**).

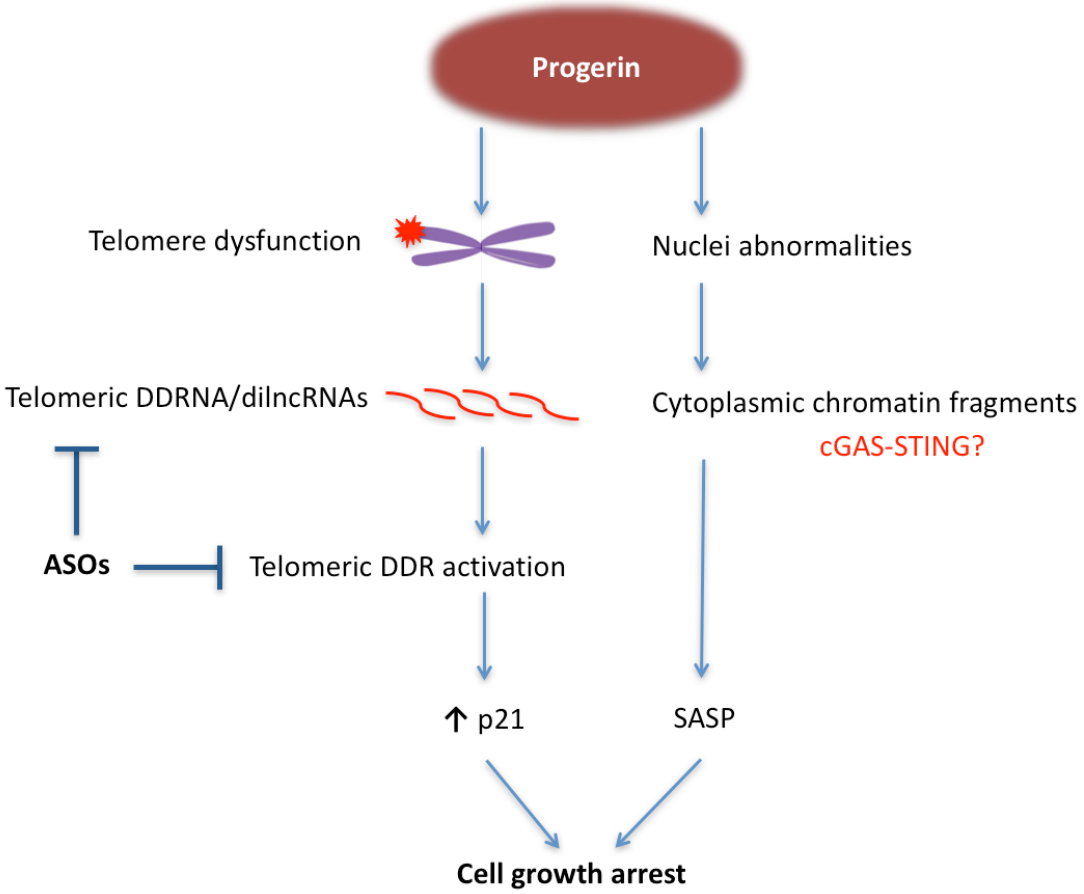

Figure 42. Model of progerin-driven telomere dysfunction: a major cause of growth decline.

Progerin expression causes accumulation of dysfunctional telomeres, which in turns leads to the induction of telomere transcripts ultimately allowing the full DDR activation at telomeres. Telomeric DDR induces p21 upregulation inducing cell growth arrest. Independently of telomere dysfunction, progerin induces SASP, likely due to the increase of cytoplasmic chromatin fragments induced as a consequence of nuclear shape abnormalities.

Interestingly, and consistent with IR-induced senescent cells, the expression of the SASP genes IL-6, IL-8 and IL-1A upon telomeric ASO treatment in progerin-expressing fibroblasts remains unaltered (**Figure 34**), suggesting a tDDRNA/tdilncRNAs-independent mechanism for SASP production as hypothesized on section 4.2 a process likely dependent on the cGAS–STING pathway. Consistent with the unaltered expression of SASP genes, progerin-driven nuclear shape abnormalities remained also unaffected upon telomeric ASO treatment (**Figure 35**). Further studies likely involving cGAS, STING or ATM depletion have to be performed in order to unravel the precise mechanism of progerin-induced SASP genes in HGPS.

Consistent with the progerin-driven tDDRNA and tdilncRNA induction observed *in vitro*, quantification of telomeric transcripts in an HGPS skin mouse model shows an increase of both tDDRNAs and their precursors as compared to wild type mice (**Figure 39**). The consistent induction of tDDRNAs and tdilncRNAs *in vitro* and *in vivo* in different HGPS models strongly indicate a role of telomere dysfunction in HGPS pathology. Finally, the observed *in vitro* telomeric ASO-driven amelioration of cell proliferation both in progerin-overexpressing human fibroblasts and in patient-derived cells is consistent with the increase of lifespan in the HGPS skin mouse model (**Figure 40**). Although further analyses need to be performed in order to understand the mechanism by which telomeric ASOs modulate cell proliferation at a single-cell level *in vivo*, this initial set of results are promising and suggest a potential use of telomeric ASOs as a therapeutic option worth exploring for HGPS patients.

4.4 Hutchinson-Gilford progeria syndrome: in search for a treatment.

Although several drugs have proven to show beneficial effects on a subset of progerin-driven features, aiming however only to control complications such as cardiovascular problems, no specific treatment is yet available to cure HGPS. In the recent years, several clinical trials have been carried out on HGPS children (Gordon et al., 2012, Rehman et al., 2015). Although there is still no approved drug for treatment of HGPS by the Food and Drug Administration (FDA), these trials are offering a promising future for HGPS patients (Rehman et al., 2015). However, the therapeutic strategies proposed so far, which include mTOR inhibitors (Cao et al., 2011) or farnesyltransferase inhibitors (FTIs, compounds that prevent the farnesylation of prelamin A) (Gordon et al., 2012) target cellular pathways important for the normal cell activity and their inhibition have severe toxic effects (Rehman et al., 2015). Differently, the use of an inhibitor of tDDRNAs allows the specific prevention of telomeric DDR, without affecting the cell proficiency in signalling and repairing DNA damage at other genomic locations.

ASOs have already been successfully used as effective FDA-approved drugs to treat different diseases (Stein and Castanotto, 2017, Wan and Dreyfuss, 2017). Furthermore, ASO-based approaches that correct aberrant LMNA splicing have already proven effective in a HGPS mouse model (Lee et al., 2016, Osorio et al., 2011), thus validating ASO-based approaches also in HGPS. However, the design and use of these splicing-correcting ASOs is restricted to individual HGPS mutations, since the disease can arise as a result of different LMNA mutations (De Sandre-Giovannoli et al., 2003, Eriksson et al., 2003, Moulson et al., 2007, Reunert et al., 2012, DeBoy et al., 2017, Bar et al., 2017). In contrast, a telomeric ASO approach has the potential to benefit any HGPS patient regardless of the genetic mutation, and even different progeric diseases, provided they are associated with telomeric DDR. Examples include atypical progeroid syndromes, autosomal recessive restrictive dermopathy and Nestor–Guillermo progeria syndrome.

As explained on section 1.4.2, progerin expression leads to a complex molecular and cellular response (**Figure 5**) that ultimately causes the HGPS phenotype. These progerin-driven pathological features are not entirely restricted to telomere dysfunction and this could explain why telomeric ASOs do not contribute to ameliorate a subset of HGPS features, which is for instance the case of progerin-driven SASP expression (**Figure 34**). In fact, many of the cellular pathways misregulated in HGPS are highly interdependent, making challenging the identification of cellular features directly affected by progerin and driving HGPS etiology. Importantly, a major progerin-driven defect is the limited cellular proliferative capacity of the cell, which is notably improved upon telomeric ASO treatment (**Figures 31**, **36** and **40**), which strongly places telomere dysfunction as a fundamental aspect in HGPS pathology.

Overall, these observations confirm a direct role of tDDRNAs in progerin-driven telomere dysfunction, and that their inhibition results in the amelioration of the aging phenotype of progerin-expressing cultured cells and increases the lifespan in a HGPS mouse model. The use of telomeric ASOs opens the possibility for additional therapeutics as a potential treatment for HGPS patients alone or in combination with other drugs.

Lastly, this telomeric ASO-based therapeutic strategy could potentially be extended to any genetic disease associated with telomere dysfunction and consequent DDR activation, such as dyskeratosis congenita, ataxia telangectasia, Werner syndrome, Bloom's syndrome, Hoyeraal–Hreidarsson syndrome, Revesz syndrome and Coats plus syndrome (Armanios and Blackburn, 2012).

References

ANDO, Y., TOMARU, Y., MORINAGA, A., BURROUGHS, A. M., KAWAJI, H., KUBOSAKI, A., KIMURA, R., TAGATA, M., INO, Y., HIRANO, H., CHIBA, J., SUZUKI, H., CARNINCI, P. & HAYASHIZAKI, Y. 2011. Nuclear pore complex protein mediated nuclear localization of dicer protein in human cells. *PLoS One,* 6**,** e23385.

ARMANIOS, M. & BLACKBURN, E. H. 2012. The telomere syndromes. *Nat Rev Genet,* 13**,** 693-704.

ARNOULT, N., VAN BENEDEN, A. & DECOTTIGNIES, A. 2012. Telomere length regulates TERRA levels through increased trimethylation of telomeric H3K9 and HP1alpha. *Nat Struct Mol Biol,* 19**,** 948-56.

ARORA, R., LEE, Y., WISCHNEWSKI, H., BRUN, C. M., SCHWARZ, T. & AZZALIN, C. M. 2014. RNaseH1 regulates TERRA-telomeric DNA hybrids and telomere maintenance in ALT tumour cells. *Nat Commun,* 5**,** 5220.

AZZALIN, C. M. & LINGNER, J. 2008. Telomeres: the silence is broken. *Cell Cycle,* 7**,** 1161-5.

AZZALIN, C. M., REICHENBACH, P., KHORIAULI, L., GIULOTTO, E. & LINGNER, J. 2007. Telomeric repeat containing RNA and RNA surveillance factors at mammalian chromosome ends. *Science,* 318**,** 798-801.

BAH, A., WISCHNEWSKI, H., SHCHEPACHEV, V. & AZZALIN, C. M. 2012. The telomeric transcriptome of Schizosaccharomyces pombe. *Nucleic Acids Res,* 40**,** 2995-3005.

BALL, H. L., MYERS, J. S. & CORTEZ, D. 2005. ATRIP binding to replication protein A-single-stranded DNA promotes ATR-ATRIP localization but is dispensable for Chk1 phosphorylation. *Mol Biol Cell,* 16**,** 2372-81.

BAR, D. Z., ARLT, M. F., BRAZIER, J. F., NORRIS, W. E., CAMPBELL, S. E., CHINES, P., LARRIEU, D., JACKSON, S. P., COLLINS, F. S., GLOVER, T. W. & GORDON, L. B. 2017. A novel somatic mutation achieves partial rescue in a child with Hutchinson-Gilford progeria syndrome. *J Med Genet,* 54**,** 212-216.

BARBER, G. N. 2015. STING: infection, inflammation and cancer. *Nat Rev Immunol,* 15**,** 760-70.

BARTEK, J. & LUKAS, J. 2007. DNA damage checkpoints: from initiation to recovery or adaptation. *Curr Opin Cell Biol,* 19**,** 238-45.

BARTHEL, F. P., WEI, W., TANG, M., MARTINEZ-LEDESMA, E., HU, X., AMIN, S. B., AKDEMIR, K. C., SETH, S., SONG, X., WANG, Q., LICHTENBERG, T., HU, J., ZHANG, J., ZHENG, S. & VERHAAK, R. G. 2017. Systematic analysis of telomere length and somatic alterations in 31 cancer types. *Nat Genet,* 49**,** 349-357.

BAUMANN, P. & CECH, T. R. 2001. Pot1, the putative telomere end-binding protein in fission yeast and humans. *Science,* 292**,** 1171-5.

BEKKER-JENSEN, S., LUKAS, C., KITAGAWA, R., MELANDER, F., KASTAN, M. B., BARTEK, J. & LUKAS, J. 2006. Spatial organization of the mammalian genome surveillance machinery in response to DNA strand breaks. *J Cell Biol,* 173**,** 195-206.

BEKKER-JENSEN, S., LUKAS, C., MELANDER, F., BARTEK, J. & LUKAS, J. 2005. Dynamic assembly and sustained retention of 53BP1 at the sites of DNA damage are controlled by Mdc1/NFBD1. *J Cell Biol,* 170**,** 201-11.

BENETTI, R., SCHOEFTNER, S., MUNOZ, P. & BLASCO, M. A. 2008. Role of TRF2 in the assembly of telomeric chromatin. *Cell Cycle,* 7**,** 3461-8.

BENSIMON, A., SCHMIDT, A., ZIV, Y., ELKON, R., WANG, S. Y., CHEN, D. J., AEBERSOLD, R. & SHILOH, Y. 2010. ATM-dependent and -independent dynamics of the nuclear phosphoproteome after DNA damage. *Sci Signal,* 3**,** rs3.

BENSON, E. K., LEE, S. W. & AARONSON, S. A. 2010. Role of progerin-induced telomere dysfunction in HGPS premature cellular senescence. *J Cell Sci,* 123**,** 2605-12.

BILLY, E., BRONDANI, V., ZHANG, H., MULLER, U. & FILIPOWICZ, W. 2001. Specific interference with gene expression induced by long, double-stranded RNA in mouse embryonal teratocarcinoma cell lines. *Proc Natl Acad Sci U S A,* 98**,** 14428-33.

BRANDSMA, I. & GENT, D. C. 2012. Pathway choice in DNA double strand break repair: observations of a balancing act. *Genome Integr,* 3**,** 9.

BROCCOLI, D., SMOGORZEWSKA, A., CHONG, L. & DE LANGE, T. 1997. Human telomeres contain two distinct Myb-related proteins, TRF1 and TRF2. *Nat Genet,* 17**,** 231-5.

BURGER, K., SCHLACKOW, M., POTTS, M., HESTER, S., MOHAMMED, S. & GULLEROVA, M. 2017. Nuclear phosphorylated Dicer processes double-stranded RNA in response to DNA damage. *J Cell Biol,* 216**,** 2373-2389.

CAMPISI, J. 2001. Cellular senescence as a tumor-suppressor mechanism. *Trends Cell Biol,* 11**,** S27-31.

CAMPISI, J. 2013. Aging, cellular senescence, and cancer. *Annu Rev Physiol,* 75**,** 685-705.

CAMPISI, J. & D'ADDA DI FAGAGNA, F. 2007. Cellular senescence: when bad things happen to good cells. *Nat Rev Mol Cell Biol,* 8**,** 729-40.

CAO, K., CAPELL, B. C., ERDOS, M. R., DJABALI, K. & COLLINS, F. S. 2007. A lamin A protein isoform overexpressed in Hutchinson-Gilford progeria syndrome interferes with mitosis in progeria and normal cells. *Proc Natl Acad Sci U S A,* 104**,** 4949-54.

CAO, K., GRAZIOTTO, J. J., BLAIR, C. D., MAZZULLI, J. R., ERDOS, M. R., KRAINC, D. & COLLINS, F. S. 2011. Rapamycin reverses cellular phenotypes and enhances mutant protein clearance in Hutchinson-Gilford progeria syndrome cells. *Sci Transl Med,* 3**,** 89ra58.

CAWTHON, R. M. 2002. Telomere measurement by quantitative PCR. *Nucleic Acids Res,* 30**,** e47.

CELLI, G. B. & DE LANGE, T. 2005. DNA processing is not required for ATM-mediated telomere damage response after TRF2 deletion. *Nat Cell Biol,* 7**,** 712-8.

CELLI, G. B., DENCHI, E. L. & DE LANGE, T. 2006. Ku70 stimulates fusion of dysfunctional telomeres yet protects chromosome ends from homologous recombination. *Nat Cell Biol,* 8**,** 885-90.

CHAKRABORTY, A., TAPRYAL, N., VENKOVA, T., HORIKOSHI, N., PANDITA, R. K., SARKER, A. H., SARKAR, P. S., PANDITA, T. K. & HAZRA, T. K. 2016. Classical non-homologous end-joining pathway utilizes nascent RNA for error-free double-strand break repair of transcribed genes. *Nat Commun,* 7**,** 13049.

CHANG, H. H. Y., PANNUNZIO, N. R., ADACHI, N. & LIEBER, M. R. 2017. Non-homologous DNA end joining and alternative pathways to double-strand break repair. *Nat Rev Mol Cell Biol,* 18**,** 495-506.

CHAPMAN, J. R., TAYLOR, M. R. & BOULTON, S. J. 2012. Playing the end game: DNA double-strand break repair pathway choice. *Mol Cell,* 47**,** 497-510.

CHEN, C., GU, P., WU, J., CHEN, X., NIU, S., SUN, H., WU, L., LI, N., PENG, J., SHI, S., FAN, C., HUANG, M., WONG, C. C., GONG, Q., KUMAR-SINHA, C., ZHANG, R., PUSZTAI, L., RAI, R., CHANG, S. & LEI, M. 2017. Structural insights into POT1-TPP1 interaction and POT1 C-terminal mutations in human cancer. *Nat Commun,* 8**,** 14929.

CHEN, L. Y., REDON, S. & LINGNER, J. 2012. The human CST complex is a terminator of telomerase activity. *Nature,* 488**,** 540-4.
CHEN, Y., RAI, R., ZHOU, Z. R., KANOH, J., RIBEYRE, C., YANG, Y., ZHENG, H., DAMAY, P., WANG, F., TSUJII, H., HIRAOKA, Y., SHORE, D., HU, H. Y., CHANG, S. & LEI, M. 2011. A conserved motif within RAP1 has diversified roles in telomere protection and regulation in different organisms. *Nat Struct Mol Biol,* 18**,** 213-21.
CHO, N. W., DILLEY, R. L., LAMPSON, M. A. & GREENBERG, R. A. 2014. Interchromosomal homology searches drive directional ALT telomere movement and synapsis. *Cell,* 159**,** 108-121.
CHOJNOWSKI, A., ONG, P. F., WONG, E. S., LIM, J. S., MUTALIF, R. A., NAVASANKARI, R., DUTTA, B., YANG, H., LIOW, Y. Y., SZE, S. K., BOUDIER, T., WRIGHT, G. D., COLMAN, A., BURKE, B., STEWART, C. L. & DREESEN, O. 2015. Progerin reduces LAP2alpha-telomere association in Hutchinson-Gilford progeria. *Elife,* 4.
CHU, H. P., CIFUENTES-ROJAS, C., KESNER, B., AEBY, E., LEE, H. G., WEI, C., OH, H. J., BOUKHALI, M., HAAS, W. & LEE, J. T. 2017. TERRA RNA Antagonizes ATRX and Protects Telomeres. *Cell,* 170**,** 86-101 e16.
CIMPRICH, K. A. & CORTEZ, D. 2008. ATR: an essential regulator of genome integrity. *Nat Rev Mol Cell Biol,* 9**,** 616-27.
CLYNES, D., JELINSKA, C., XELLA, B., AYYUB, H., SCOTT, C., MITSON, M., TAYLOR, S., HIGGS, D. R. & GIBBONS, R. J. 2015. Suppression of the alternative lengthening of telomere pathway by the chromatin remodelling factor ATRX. *Nat Commun,* 6**,** 7538.
COLLADO, M. & SERRANO, M. 2010. Senescence in tumours: evidence from mice and humans. *Nat Rev Cancer,* 10**,** 51-7.
COPPE, J. P., KAUSER, K., CAMPISI, J. & BEAUSEJOUR, C. M. 2006. Secretion of vascular endothelial growth factor by primary human fibroblasts at senescence. *J Biol Chem,* 281**,** 29568-74.
D'ADDA DI FAGAGNA, F. 2014. A direct role for small non-coding RNAs in DNA damage response. *Trends Cell Biol,* 24**,** 171-8.
D'ADDA DI FAGAGNA, F., REAPER, P. M., CLAY-FARRACE, L., FIEGLER, H., CARR, P., VON ZGLINICKI, T., SARETZKI, G., CARTER, N. P. & JACKSON, S. P. 2003. A DNA damage checkpoint response in telomere-initiated senescence. *Nature,* 426**,** 194-8.
DAGG, R. A., PICKETT, H. A., NEUMANN, A. A., NAPIER, C. E., HENSON, J. D., TEBER, E. T., ARTHUR, J. W., REYNOLDS, C. P., MURRAY, J., HABER, M., SOBINOFF, A. P., LAU, L. M. S. & REDDEL, R. R. 2017. Extensive Proliferation of Human Cancer Cells with Ever-Shorter Telomeres. *Cell Rep,* 19**,** 2544-2556.
DE LANGE, T. 2005. Shelterin: the protein complex that shapes and safeguards human telomeres. *Genes Dev,* 19**,** 2100-10.
DE SANDRE-GIOVANNOLI, A., BERNARD, R., CAU, P., NAVARRO, C., AMIEL, J., BOCCACCIO, I., LYONNET, S., STEWART, C. L., MUNNICH, A., LE MERRER, M. & LEVY, N. 2003. Lamin a truncation in Hutchinson-Gilford progeria. *Science,* 300**,** 2055.
DEBOY, E., PUTTARAJU, M., JAILWALA, P., KASOJI, M., CAM, M. & MISTELI, T. 2017. Identification of novel RNA isoforms of LMNA. *Nucleus***,** 1-10.
DECKER, M. L., CHAVEZ, E., VULTO, I. & LANSDORP, P. M. 2009. Telomere length in Hutchinson-Gilford progeria syndrome. *Mech Ageing Dev,* 130**,** 377-83.
DEMARIA, M., OHTANI, N., YOUSSEF, S. A., RODIER, F., TOUSSAINT, W., MITCHELL, J. R., LABERGE, R. M., VIJG, J., VAN STEEG, H., DOLLE, M. E., HOEIJMAKERS, J. H., DE BRUIN, A., HARA, E. & CAMPISI, J. 2014. An

essential role for senescent cells in optimal wound healing through secretion of PDGF-AA. *Dev Cell,* 31**,** 722-33.

DENCHI, E. L. & DE LANGE, T. 2007. Protection of telomeres through independent control of ATM and ATR by TRF2 and POT1. *Nature,* 448**,** 1068-71.

DI MICCO, R., FUMAGALLI, M. & D'ADDA DI FAGAGNA, F. 2007. Breaking news: high-speed race ends in arrest--how oncogenes induce senescence. *Trends Cell Biol,* 17**,** 529-36.

DILLEY, R. L., VERMA, P., CHO, N. W., WINTERS, H. D., WONDISFORD, A. R. & GREENBERG, R. A. 2016. Break-induced telomere synthesis underlies alternative telomere maintenance. *Nature,* 539**,** 54-58.

DIMITROVA, N. & DE LANGE, T. 2009. Cell cycle-dependent role of MRN at dysfunctional telomeres: ATM signaling-dependent induction of nonhomologous end joining (NHEJ) in G1 and resection-mediated inhibition of NHEJ in G2. *Mol Cell Biol,* 29**,** 5552-63.

DIMRI, G. P., LEE, X., BASILE, G., ACOSTA, M., SCOTT, G., ROSKELLEY, C., MEDRANO, E. E., LINSKENS, M., RUBELJ, I., PEREIRA-SMITH, O. & ET AL. 1995. A biomarker that identifies senescent human cells in culture and in aging skin in vivo. *Proc Natl Acad Sci U S A,* 92**,** 9363-7.

DOKSANI, Y., WU, J. Y., DE LANGE, T. & ZHUANG, X. 2013. Super-resolution fluorescence imaging of telomeres reveals TRF2-dependent T-loop formation. *Cell,* 155**,** 345-356.

DOU, Z., GHOSH, K., VIZIOLI, M. G., ZHU, J., SEN, P., WANGENSTEEN, K. J., SIMITHY, J., LAN, Y., LIN, Y., ZHOU, Z., CAPELL, B. C., XU, C., XU, M., KIECKHAEFER, J. E., JIANG, T., SHOSHKES-CARMEL, M., TANIM, K., BARBER, G. N., SEYKORA, J. T., MILLAR, S. E., KAESTNER, K. H., GARCIA, B. A., ADAMS, P. D. & BERGER, S. L. 2017. Cytoplasmic chromatin triggers inflammation in senescence and cancer. *Nature,* 550**,** 402-406.

DOU, Z., XU, C., DONAHUE, G., SHIMI, T., PAN, J. A., ZHU, J., IVANOV, A., CAPELL, B. C., DRAKE, A. M., SHAH, P. P., CATANZARO, J. M., RICKETTS, M. D., LAMARK, T., ADAM, S. A., MARMORSTEIN, R., ZONG, W. X., JOHANSEN, T., GOLDMAN, R. D., ADAMS, P. D. & BERGER, S. L. 2015. Autophagy mediates degradation of nuclear lamina. *Nature,* 527**,** 105-9.

DOYLE, M., BADERTSCHER, L., JASKIEWICZ, L., GUTTINGER, S., JURADO, S., HUGENSCHMIDT, T., KUTAY, U. & FILIPOWICZ, W. 2013. The double-stranded RNA binding domain of human Dicer functions as a nuclear localization signal. *RNA,* 19**,** 1238-52.

DYNAN, W. S. & BURGESS, R. R. 1981. In vitro transcription by wheat germ RNA polymerase II. Initiation of RNA synthesis on relaxed, closed circular template. *J Biol Chem,* 256**,** 5866-73.

EPISKOPOU, H., DRASKOVIC, I., VAN BENEDEN, A., TILMAN, G., MATTIUSSI, M., GOBIN, M., ARNOULT, N., LONDONO-VALLEJO, A. & DECOTTIGNIES, A. 2014. Alternative Lengthening of Telomeres is characterized by reduced compaction of telomeric chromatin. *Nucleic Acids Res,* 42**,** 4391-405.

ERIKSSON, M., BROWN, W. T., GORDON, L. B., GLYNN, M. W., SINGER, J., SCOTT, L., ERDOS, M. R., ROBBINS, C. M., MOSES, T. Y., BERGLUND, P., DUTRA, A., PAK, E., DURKIN, S., CSOKA, A. B., BOEHNKE, M., GLOVER, T. W. & COLLINS, F. S. 2003. Recurrent de novo point mutations in lamin A cause Hutchinson-Gilford progeria syndrome. *Nature,* 423**,** 293-8.

ESPADA, J., VARELA, I., FLORES, I., UGALDE, A. P., CADINANOS, J., PENDAS, A. M., STEWART, C. L., TRYGGVASON, K., BLASCO, M. A., FREIJE, J. M. & LOPEZ-OTIN, C. 2008. Nuclear envelope defects cause stem cell dysfunction in premature-aging mice. *J Cell Biol,* 181**,** 27-35.

FERETZAKI, M. & LINGNER, J. 2017. A practical qPCR approach to detect TERRA, the elusive telomeric repeat-containing RNA. *Methods,* 114**,** 39-45.
FEUERHAHN, S., IGLESIAS, N., PANZA, A., PORRO, A. & LINGNER, J. 2010. TERRA biogenesis, turnover and implications for function. *FEBS Lett,* 584**,** 3812-8.
FRANCIA, S., CABRINI, M., MATTI, V., OLDANI, A. & D'ADDA DI FAGAGNA, F. 2016. DICER, DROSHA and DNA damage response RNAs are necessary for the secondary recruitment of DNA damage response factors. *J Cell Sci,* 129**,** 1468-76.
FRANCIA, S., MICHELINI, F., SAXENA, A., TANG, D., DE HOON, M., ANELLI, V., MIONE, M., CARNINCI, P. & D'ADDA DI FAGAGNA, F. 2012. Site-specific DICER and DROSHA RNA products control the DNA-damage response. *Nature,* 488**,** 231-5.
FRESCAS, D. & DE LANGE, T. 2014. A TIN2 dyskeratosis congenita mutation causes telomerase-independent telomere shortening in mice. *Genes Dev,* 28**,** 153-66.
FREUND, A., LABERGE, R. M., DEMARIA, M. & CAMPISI, J. 2012. Lamin B1 loss is a senescence-associated biomarker. *Mol Biol Cell,* 23**,** 2066-75.
FUMAGALLI, M. & D'ADDA DI FAGAGNA, F. 2009. SASPense and DDRama in cancer and ageing. *Nat Cell Biol,* 11**,** 921-3.
FUMAGALLI, M., ROSSIELLO, F., CLERICI, M., BAROZZI, S., CITTARO, D., KAPLUNOV, J. M., BUCCI, G., DOBREVA, M., MATTI, V., BEAUSEJOUR, C. M., HERBIG, U., LONGHESE, M. P. & D'ADDA DI FAGAGNA, F. 2012. Telomeric DNA damage is irreparable and causes persistent DNA-damage-response activation. *Nat Cell Biol,* 14**,** 355-65.
GALBIATI, A., BEAUSEJOUR, C. & D'ADDA DI FAGAGNA, F. 2017. A novel single-cell method provides direct evidence of persistent DNA damage in senescent cells and aged mammalian tissues. *Aging Cell,* 16**,** 422-427.
GLUCK, S., GUEY, B., GULEN, M. F., WOLTER, K., KANG, T. W., SCHMACKE, N. A., BRIDGEMAN, A., REHWINKEL, J., ZENDER, L. & ABLASSER, A. 2017. Innate immune sensing of cytosolic chromatin fragments through cGAS promotes senescence. *Nat Cell Biol,* 19**,** 1061-1070.
GOLDMAN, D. P., CUTLER, D., ROWE, J. W., MICHAUD, P. C., SULLIVAN, J., PENEVA, D. & OLSHANSKY, S. J. 2013. Substantial health and economic returns from delayed aging may warrant a new focus for medical research. *Health Aff (Millwood),* 32**,** 1698-705.
GOLDMAN, R. D., SHUMAKER, D. K., ERDOS, M. R., ERIKSSON, M., GOLDMAN, A. E., GORDON, L. B., GRUENBAUM, Y., KHUON, S., MENDEZ, M., VARGA, R. & COLLINS, F. S. 2004. Accumulation of mutant lamin A causes progressive changes in nuclear architecture in Hutchinson-Gilford progeria syndrome. *Proc Natl Acad Sci U S A,* 101**,** 8963-8.
GONZALO, S. & KREIENKAMP, R. 2015. DNA repair defects and genome instability in Hutchinson-Gilford Progeria Syndrome. *Curr Opin Cell Biol,* 34**,** 75-83.
GONZALO, S., KREIENKAMP, R. & ASKJAER, P. 2017. Hutchinson-Gilford Progeria Syndrome: A premature aging disease caused by LMNA gene mutations. *Ageing Res Rev,* 33**,** 18-29.
GOODARZI, A. A., YU, Y., RIBALLO, E., DOUGLAS, P., WALKER, S. A., YE, R., HARER, C., MARCHETTI, C., MORRICE, N., JEGGO, P. A. & LEES-MILLER, S. P. 2006. DNA-PK autophosphorylation facilitates Artemis endonuclease activity. *EMBO J,* 25**,** 3880-9.
GORDON, L. B., KLEINMAN, M. E., MILLER, D. T., NEUBERG, D. S., GIOBBIE-HURDER, A., GERHARD-HERMAN, M., SMOOT, L. B., GORDON, C. M., CLEVELAND, R., SNYDER, B. D., FLIGOR, B., BISHOP, W. R., STATKEVICH, P., REGEN, A., SONIS, A., RILEY, S., PLOSKI, C., CORREIA, A., QUINN, N., ULLRICH, N. J., NAZARIAN, A., LIANG, M. G., HUH, S. Y.,

SCHWARTZMAN, A. & KIERAN, M. W. 2012. Clinical trial of a farnesyltransferase inhibitor in children with Hutchinson-Gilford progeria syndrome. *Proc Natl Acad Sci U S A,* 109**,** 16666-71.

GRAWUNDER, U., WILM, M., WU, X., KULESZA, P., WILSON, T. E., MANN, M. & LIEBER, M. R. 1997. Activity of DNA ligase IV stimulated by complex formation with XRCC4 protein in mammalian cells. *Nature,* 388**,** 492-5.

GREENWOOD, J. & COOPER, J. P. 2012. Non-coding telomeric and subtelomeric transcripts are differentially regulated by telomeric and heterochromatin assembly factors in fission yeast. *Nucleic Acids Res,* 40**,** 2956-63.

GREIDER, C. W. 1993. Telomerase and telomere-length regulation: lessons from small eukaryotes to mammals. *Cold Spring Harb Symp Quant Biol,* 58**,** 719-23.

GRIFFITH, J. D., COMEAU, L., ROSENFIELD, S., STANSEL, R. M., BIANCHI, A., MOSS, H. & DE LANGE, T. 1999. Mammalian telomeres end in a large duplex loop. *Cell,* 97**,** 503-14.

GU, J., LI, S., ZHANG, X., WANG, L. C., NIEWOLIK, D., SCHWARZ, K., LEGERSKI, R. J., ZANDI, E. & LIEBER, M. R. 2010. DNA-PKcs regulates a single-stranded DNA endonuclease activity of Artemis. *DNA Repair (Amst),* 9**,** 429-37.

GULLEROVA, M. & PROUDFOOT, N. J. 2012. Convergent transcription induces transcriptional gene silencing in fission yeast and mammalian cells. *Nat Struct Mol Biol,* 19**,** 1193-201.

HARLEY, C. B., FUTCHER, A. B. & GREIDER, C. W. 1990. Telomeres shorten during ageing of human fibroblasts. *Nature,* 345**,** 458-60.

HARPER, J. W. & ELLEDGE, S. J. 2007. The DNA damage response: ten years after. *Mol Cell,* 28**,** 739-45.

HARRISON, J. C. & HABER, J. E. 2006. Surviving the breakup: the DNA damage checkpoint. *Annu Rev Genet,* 40**,** 209-35.

HAYFLICK, L. 1965. The Limited in Vitro Lifetime of Human Diploid Cell Strains. *Exp Cell Res,* 37**,** 614-36.

HE, L. & HANNON, G. J. 2004. MicroRNAs: small RNAs with a big role in gene regulation. *Nat Rev Genet,* 5**,** 522-31.

HEAPHY, C. M., DE WILDE, R. F., JIAO, Y., KLEIN, A. P., EDIL, B. H., SHI, C., BETTEGOWDA, C., RODRIGUEZ, F. J., EBERHART, C. G., HEBBAR, S., OFFERHAUS, G. J., MCLENDON, R., RASHEED, B. A., HE, Y., YAN, H., BIGNER, D. D., OBA-SHINJO, S. M., MARIE, S. K., RIGGINS, G. J., KINZLER, K. W., VOGELSTEIN, B., HRUBAN, R. H., MAITRA, A., PAPADOPOULOS, N. & MEEKER, A. K. 2011. Altered telomeres in tumors with ATRX and DAXX mutations. *Science,* 333**,** 425.

HEMANN, M. T., STRONG, M. A., HAO, L. Y. & GREIDER, C. W. 2001. The shortest telomere, not average telomere length, is critical for cell viability and chromosome stability. *Cell,* 107**,** 67-77.

HENNEKAM, R. C. 2006. Hutchinson-Gilford progeria syndrome: review of the phenotype. *Am J Med Genet A,* 140**,** 2603-24.

HENSON, J. D., CAO, Y., HUSCHTSCHA, L. I., CHANG, A. C., AU, A. Y., PICKETT, H. A. & REDDEL, R. R. 2009. DNA C-circles are specific and quantifiable markers of alternative-lengthening-of-telomeres activity. *Nat Biotechnol,* 27**,** 1181-5.

HERBIG, U., FERREIRA, M., CONDEL, L., CAREY, D. & SEDIVY, J. M. 2006. Cellular senescence in aging primates. *Science,* 311**,** 1257.

HERBIG, U., JOBLING, W. A., CHEN, B. P., CHEN, D. J. & SEDIVY, J. M. 2004. Telomere shortening triggers senescence of human cells through a pathway involving ATM, p53, and p21(CIP1), but not p16(INK4a). *Mol Cell,* 14**,** 501-13.

HEWITT, G., JURK, D., MARQUES, F. D., CORREIA-MELO, C., HARDY, T., GACKOWSKA, A., ANDERSON, R., TASCHUK, M., MANN, J. & PASSOS, J.

F. 2012. Telomeres are favoured targets of a persistent DNA damage response in ageing and stress-induced senescence. *Nat Commun,* 3**,** 708.
HOCKEMEYER, D., PALM, W., ELSE, T., DANIELS, J. P., TAKAI, K. K., YE, J. Z., KEEGAN, C. E., DE LANGE, T. & HAMMER, G. D. 2007. Telomere protection by mammalian Pot1 requires interaction with Tpp1. *Nat Struct Mol Biol,* 14**,** 754-61.
HOCKEMEYER, D., PALM, W., WANG, R. C., COUTO, S. S. & DE LANGE, T. 2008. Engineered telomere degradation models dyskeratosis congenita. *Genes Dev,* 22**,** 1773-85.
IACOVONI, J. S., CARON, P., LASSADI, I., NICOLAS, E., MASSIP, L., TROUCHE, D. & LEGUBE, G. 2010. High-resolution profiling of gammaH2AX around DNA double strand breaks in the mammalian genome. *EMBO J,* 29**,** 1446-57.
IANNELLI, F., GALBIATI, A., CAPOZZO, I., NGUYEN, Q., MAGNUSON, B., MICHELINI, F., D'ALESSANDRO, G., CABRINI, M., RONCADOR, M., FRANCIA, S., CROSETTO, N., LJUNGMAN, M., CARNINCI, P. & D'ADDA DI FAGAGNA, F. 2017. A damaged genome's transcriptional landscape through multilayered expression profiling around in situ-mapped DNA double-strand breaks. *Nat Commun,* 8**,** 15656.
ILIAKIS, G., WANG, Y., GUAN, J. & WANG, H. 2003. DNA damage checkpoint control in cells exposed to ionizing radiation. *Oncogene,* 22**,** 5834-47.
ISHIKAWA, H. & BARBER, G. N. 2008. STING is an endoplasmic reticulum adaptor that facilitates innate immune signalling. *Nature,* 455**,** 674-8.
ISHIKAWA, H., MA, Z. & BARBER, G. N. 2009. STING regulates intracellular DNA-mediated, type I interferon-dependent innate immunity. *Nature,* 461**,** 788-92.
IVANOV, A., PAWLIKOWSKI, J., MANOHARAN, I., VAN TUYN, J., NELSON, D. M., RAI, T. S., SHAH, P. P., HEWITT, G., KOROLCHUK, V. I., PASSOS, J. F., WU, H., BERGER, S. L. & ADAMS, P. D. 2013. Lysosome-mediated processing of chromatin in senescence. *J Cell Biol,* 202**,** 129-43.
JACKSON, J. G. & PEREIRA-SMITH, O. M. 2006. p53 is preferentially recruited to the promoters of growth arrest genes p21 and GADD45 during replicative senescence of normal human fibroblasts. *Cancer Res,* 66**,** 8356-60.
JAZAYERI, A., FALCK, J., LUKAS, C., BARTEK, J., SMITH, G. C., LUKAS, J. & JACKSON, S. P. 2006. ATM- and cell cycle-dependent regulation of ATR in response to DNA double-strand breaks. *Nat Cell Biol,* 8**,** 37-45.
JEYAPALAN, J. C., FERREIRA, M., SEDIVY, J. M. & HERBIG, U. 2007. Accumulation of senescent cells in mitotic tissue of aging primates. *Mech Ageing Dev,* 128**,** 36-44.
JUN, H. I., LIU, J., JEONG, H., KIM, J. K. & QIAO, F. 2013. Tpz1 controls a telomerase-nonextendible telomeric state and coordinates switching to an extendible state via Ccq1. *Genes Dev,* 27**,** 1917-31.
KARPENSHIF, Y. & BERNSTEIN, K. A. 2012. From yeast to mammals: recent advances in genetic control of homologous recombination. *DNA Repair (Amst),* 11**,** 781-8.
KHANNA, K. K. & JACKSON, S. P. 2001. DNA double-strand breaks: signaling, repair and the cancer connection. *Nat Genet,* 27**,** 247-54.
KIRKLAND, J. L. 2016. Translating the Science of Aging into Therapeutic Interventions. *Cold Spring Harb Perspect Med,* 6**,** a025908.
KRISHNAMURTHY, J., TORRICE, C., RAMSEY, M. R., KOVALEV, G. I., AL-REGAIEY, K., SU, L. & SHARPLESS, N. E. 2004. Ink4a/Arf expression is a biomarker of aging. *J Clin Invest,* 114**,** 1299-307.
KUDLOW, B. A., STANFEL, M. N., BURTNER, C. R., JOHNSTON, E. D. & KENNEDY, B. K. 2008. Suppression of proliferative defects associated with processing-defective lamin A mutants by hTERT or inactivation of p53. *Mol Biol Cell,* 19**,** 5238-48.

LAVASANI, M., ROBINSON, A. R., LU, A., SONG, M., FEDUSKA, J. M., AHANI, B., TILSTRA, J. S., FELDMAN, C. H., ROBBINS, P. D., NIEDERNHOFER, L. J. & HUARD, J. 2012. Muscle-derived stem/progenitor cell dysfunction limits healthspan and lifespan in a murine progeria model. *Nat Commun,* 3**,** 608.

LEE, H. C., AALTO, A. P., YANG, Q., CHANG, S. S., HUANG, G., FISHER, D., CHA, J., PORANEN, M. M., BAMFORD, D. H. & LIU, Y. 2010. The DNA/RNA-dependent RNA polymerase QDE-1 generates aberrant RNA and dsRNA for RNAi in a process requiring replication protein A and a DNA helicase. *PLoS Biol,* 8.

LEE, H. C., CHANG, S. S., CHOUDHARY, S., AALTO, A. P., MAITI, M., BAMFORD, D. H. & LIU, Y. 2009. qiRNA is a new type of small interfering RNA induced by DNA damage. *Nature,* 459**,** 274-7.

LEE, S. J., JUNG, Y. S., YOON, M. H., KANG, S. M., OH, A. Y., LEE, J. H., JUN, S. Y., WOO, T. G., CHUN, H. Y., KIM, S. K., CHUNG, K. J., LEE, H. Y., LEE, K., JIN, G., NA, M. K., HA, N. C., BARCENA, C., FREIJE, J. M., LOPEZ-OTIN, C., SONG, G. Y. & PARK, B. J. 2016. Interruption of progerin-lamin A/C binding ameliorates Hutchinson-Gilford progeria syndrome phenotype. *J Clin Invest,* 126**,** 3879-3893.

LEI, M., PODELL, E. R. & CECH, T. R. 2004. Structure of human POT1 bound to telomeric single-stranded DNA provides a model for chromosome end-protection. *Nat Struct Mol Biol,* 11**,** 1223-9.

LI, J. S., MIRALLES FUSTE, J., SIMAVORIAN, T., BARTOCCI, C., TSAI, J., KARLSEDER, J. & LAZZERINI DENCHI, E. 2017. TZAP: A telomere-associated protein involved in telomere length control. *Science,* 355**,** 638-641.

LI, X. & HEYER, W. D. 2009. RAD54 controls access to the invading 3'-OH end after RAD51-mediated DNA strand invasion in homologous recombination in Saccharomyces cerevisiae. *Nucleic Acids Res,* 37**,** 638-46.

LIEBER, M. R. 2010. The mechanism of double-strand DNA break repair by the nonhomologous DNA end-joining pathway. *Annu Rev Biochem,* 79**,** 181-211.

LINDAHL, T. & BARNES, D. E. 2000. Repair of endogenous DNA damage. *Cold Spring Harb Symp Quant Biol,* 65**,** 127-33.

LIU, B., WANG, J., CHAN, K. M., TJIA, W. M., DENG, W., GUAN, X., HUANG, J. D., LI, K. M., CHAU, P. Y., CHEN, D. J., PEI, D., PENDAS, A. M., CADINANOS, J., LOPEZ-OTIN, C., TSE, H. F., HUTCHISON, C., CHEN, J., CAO, Y., CHEAH, K. S., TRYGGVASON, K. & ZHOU, Z. 2005. Genomic instability in laminopathy-based premature aging. *Nat Med,* 11**,** 780-5.

LIU, W. & SHARPLESS, N. E. 2012. Senescence-escape in melanoma. *Pigment Cell Melanoma Res,* 25**,** 408-9.

LONDONO-VALLEJO, J. A., DER-SARKISSIAN, H., CAZES, L., BACCHETTI, S. & REDDEL, R. R. 2004. Alternative lengthening of telomeres is characterized by high rates of telomeric exchange. *Cancer Res,* 64**,** 2324-7.

LOVEJOY, C. A., LI, W., REISENWEBER, S., THONGTHIP, S., BRUNO, J., DE LANGE, T., DE, S., PETRINI, J. H., SUNG, P. A., JASIN, M., ROSENBLUH, J., ZWANG, Y., WEIR, B. A., HATTON, C., IVANOVA, E., MACCONAILL, L., HANNA, M., HAHN, W. C., LUE, N. F., REDDEL, R. R., JIAO, Y., KINZLER, K., VOGELSTEIN, B., PAPADOPOULOS, N., MEEKER, A. K. & CONSORTIUM, A. L. T. S. C. 2012. Loss of ATRX, genome instability, and an altered DNA damage response are hallmarks of the alternative lengthening of telomeres pathway. *PLoS Genet,* 8**,** e1002772.

LUKE, B., PANZA, A., REDON, S., IGLESIAS, N., LI, Z. & LINGNER, J. 2008. The Rat1p 5' to 3' exonuclease degrades telomeric repeat-containing RNA and promotes telomere elongation in Saccharomyces cerevisiae. *Mol Cell,* 32**,** 465-77.

MAKAROV, V. L., HIROSE, Y. & LANGMORE, J. P. 1997. Long G tails at both ends of human chromosomes suggest a C strand degradation mechanism for telomere shortening. *Cell,* 88**,** 657-66.

MARTIN, M., TERRADAS, M., ILIAKIS, G., TUSELL, L. & GENESCA, A. 2009. Breaks invisible to the DNA damage response machinery accumulate in ATM-deficient cells. *Genes Chromosomes Cancer,* 48**,** 745-59.

MARTINEZ, P., THANASOULA, M., CARLOS, A. R., GOMEZ-LOPEZ, G., TEJERA, A. M., SCHOEFTNER, S., DOMINGUEZ, O., PISANO, D. G., TARSOUNAS, M. & BLASCO, M. A. 2010. Mammalian Rap1 controls telomere function and gene expression through binding to telomeric and extratelomeric sites. *Nat Cell Biol,* 12**,** 768-80.

MARTINEZ, P., THANASOULA, M., MUNOZ, P., LIAO, C., TEJERA, A., MCNEES, C., FLORES, J. M., FERNANDEZ-CAPETILLO, O., TARSOUNAS, M. & BLASCO, M. A. 2009. Increased telomere fragility and fusions resulting from TRF1 deficiency lead to degenerative pathologies and increased cancer in mice. *Genes Dev,* 23**,** 2060-75.

MCCLOREY, G. & WOOD, M. J. 2015. An overview of the clinical application of antisense oligonucleotides for RNA-targeting therapies. *Curr Opin Pharmacol,* 24**,** 52-8.

MICHALIK, K. M., BOTTCHER, R. & FORSTEMANN, K. 2012. A small RNA response at DNA ends in Drosophila. *Nucleic Acids Res,* 40**,** 9596-603.

MICHELINI, F., PITCHIAYA, S., VITELLI, V., SHARMA, S., GIOIA, U., PESSINA, F., CABRINI, M., WANG, Y., CAPOZZO, I., IANNELLI, F., MATTI, V., FRANCIA, S., SHIVASHANKAR, G. V., WALTER, N. G. & D'ADDA DI FAGAGNA, F. 2017. Damage-induced lncRNAs control the DNA damage response through interaction with DDRNAs at individual double-strand breaks. *Nat Cell Biol,* 19**,** 1400-1411.

MOON, A. F., PRYOR, J. M., RAMSDEN, D. A., KUNKEL, T. A., BEBENEK, K. & PEDERSEN, L. C. 2014. Sustained active site rigidity during synthesis by human DNA polymerase mu. *Nat Struct Mol Biol,* 21**,** 253-60.

MORRICAL, S. W. 2015. DNA-pairing and annealing processes in homologous recombination and homology-directed repair. *Cold Spring Harb Perspect Biol,* 7**,** a016444.

MOULSON, C. L., FONG, L. G., GARDNER, J. M., FARBER, E. A., GO, G., PASSARIELLO, A., GRANGE, D. K., YOUNG, S. G. & MINER, J. H. 2007. Increased progerin expression associated with unusual LMNA mutations causes severe progeroid syndromes. *Hum Mutat,* 28**,** 882-9.

MUNOZ, P., BLANCO, R., DE CARCER, G., SCHOEFTNER, S., BENETTI, R., FLORES, J. M., MALUMBRES, M. & BLASCO, M. A. 2009. TRF1 controls telomere length and mitotic fidelity in epithelial homeostasis. *Mol Cell Biol,* 29**,** 1608-25.

MUNOZ-ESPIN, D., CANAMERO, M., MARAVER, A., GOMEZ-LOPEZ, G., CONTRERAS, J., MURILLO-CUESTA, S., RODRIGUEZ-BAEZA, A., VARELA-NIETO, I., RUBERTE, J., COLLADO, M. & SERRANO, M. 2013. Programmed cell senescence during mammalian embryonic development. *Cell,* 155**,** 1104-18.

NAPIER, C. E., HUSCHTSCHA, L. I., HARVEY, A., BOWER, K., NOBLE, J. R., HENDRICKSON, E. A. & REDDEL, R. R. 2015. ATRX represses alternative lengthening of telomeres. *Oncotarget,* 6**,** 16543-58.

NARITA, M., NUNEZ, S., HEARD, E., NARITA, M., LIN, A. W., HEARN, S. A., SPECTOR, D. L., HANNON, G. J. & LOWE, S. W. 2003. Rb-mediated heterochromatin formation and silencing of E2F target genes during cellular senescence. *Cell,* 113**,** 703-16.

O'SULLIVAN, R. J. & KARLSEDER, J. 2010. Telomeres: protecting chromosomes against genome instability. *Nat Rev Mol Cell Biol,* 11**,** 171-81.

OHLE, C., TESORERO, R., SCHERMANN, G., DOBREV, N., SINNING, I. & FISCHER, T. 2016. Transient RNA-DNA Hybrids Are Required for Efficient Double-Strand Break Repair. *Cell,* 167**,** 1001-1013 e7.

OHRT, T., MUETZE, J., SVOBODA, P. & SCHWILLE, P. 2012. Intracellular localization and routing of miRNA and RNAi pathway components. *Curr Top Med Chem,* 12**,** 79-88.

OKAMOTO, K., BARTOCCI, C., OUZOUNOV, I., DIEDRICH, J. K., YATES, J. R., 3RD & DENCHI, E. L. 2013. A two-step mechanism for TRF2-mediated chromosome-end protection. *Nature,* 494**,** 502-5.

OSORIO, F. G., NAVARRO, C. L., CADINANOS, J., LOPEZ-MEJIA, I. C., QUIROS, P. M., BARTOLI, C., RIVERA, J., TAZI, J., GUZMAN, G., VARELA, I., DEPETRIS, D., DE CARLOS, F., COBO, J., ANDRES, V., DE SANDRE-GIOVANNOLI, A., FREIJE, J. M., LEVY, N. & LOPEZ-OTIN, C. 2011. Splicing-directed therapy in a new mouse model of human accelerated aging. *Sci Transl Med,* 3**,** 106ra107.

PACHECO, L. M., GOMEZ, L. A., DIAS, J., ZIEBARTH, N. M., HOWARD, G. A. & SCHILLER, P. C. 2014. Progerin expression disrupts critical adult stem cell functions involved in tissue repair. *Aging (Albany NY),* 6**,** 1049-63.

PALM, W., HOCKEMEYER, D., KIBE, T. & DE LANGE, T. 2009. Functional dissection of human and mouse POT1 proteins. *Mol Cell Biol,* 29**,** 471-82.

PANKOTAI, T., BONHOMME, C., CHEN, D. & SOUTOGLOU, E. 2012. DNAPKcs-dependent arrest of RNA polymerase II transcription in the presence of DNA breaks. *Nat Struct Mol Biol,* 19**,** 276-82.

POLO, S. E. & JACKSON, S. P. 2011. Dynamics of DNA damage response proteins at DNA breaks: a focus on protein modifications. *Genes Dev,* 25**,** 409-33.

PORRO, A., FEUERHAHN, S., DELAFONTAINE, J., RIETHMAN, H., ROUGEMONT, J. & LINGNER, J. 2014. Functional characterization of the TERRA transcriptome at damaged telomeres. *Nat Commun,* 5**,** 5379.

POVIRK, L. F. 1996. DNA damage and mutagenesis by radiomimetic DNA-cleaving agents: bleomycin, neocarzinostatin and other enediynes. *Mutat Res,* 355**,** 71-89.

PROKOCIMER, M., BARKAN, R. & GRUENBAUM, Y. 2013. Hutchinson-Gilford progeria syndrome through the lens of transcription. *Aging Cell,* 12**,** 533-43.

PROVOST, P., DISHART, D., DOUCET, J., FRENDEWEY, D., SAMUELSSON, B. & RADMARK, O. 2002. Ribonuclease activity and RNA binding of recombinant human Dicer. *EMBO J,* 21**,** 5864-74.

PRYDE, F., KHALILI, S., ROBERTSON, K., SELFRIDGE, J., RITCHIE, A. M., MELTON, D. W., JULLIEN, D. & ADACHI, Y. 2005. 53BP1 exchanges slowly at the sites of DNA damage and appears to require RNA for its association with chromatin. *J Cell Sci,* 118**,** 2043-55.

RASTOGI, R. P., RICHA, KUMAR, A., TYAGI, M. B. & SINHA, R. P. 2010. Molecular mechanisms of ultraviolet radiation-induced DNA damage and repair. *J Nucleic Acids,* 2010**,** 592980.

REDON, S., REICHENBACH, P. & LINGNER, J. 2010. The non-coding RNA TERRA is a natural ligand and direct inhibitor of human telomerase. *Nucleic Acids Res,* 38**,** 5797-806.

REHMAN, N. A., REHMAN, A. A., ASHRAF, I. N. & AHMED, S. 2015. Can Hutchinson-Gilford progeria syndrome be cured in the future? *Intractable Rare Dis Res,* 4**,** 111-2.

REUNERT, J., WENTZELL, R., WALTER, M., JAKUBICZKA, S., ZENKER, M., BRUNE, T., RUST, S. & MARQUARDT, T. 2012. Neonatal progeria: increased

ratio of progerin to lamin A leads to progeria of the newborn. *Eur J Hum Genet,* 20**,** 933-7.

RIVERA-TORRES, J., ACIN-PEREZ, R., CABEZAS-SANCHEZ, P., OSORIO, F. G., GONZALEZ-GOMEZ, C., MEGIAS, D., CAMARA, C., LOPEZ-OTIN, C., ENRIQUEZ, J. A., LUQUE-GARCIA, J. L. & ANDRES, V. 2013. Identification of mitochondrial dysfunction in Hutchinson-Gilford progeria syndrome through use of stable isotope labeling with amino acids in cell culture. *J Proteomics,* 91**,** 466-77.

RODIER, F., COPPE, J. P., PATIL, C. K., HOEIJMAKERS, W. A., MUNOZ, D. P., RAZA, S. R., FREUND, A., CAMPEAU, E., DAVALOS, A. R. & CAMPISI, J. 2009. Persistent DNA damage signalling triggers senescence-associated inflammatory cytokine secretion. *Nat Cell Biol,* 11**,** 973-9.

ROSENGARDTEN, Y., MCKENNA, T., GROCHOVA, D. & ERIKSSON, M. 2011. Stem cell depletion in Hutchinson-Gilford progeria syndrome. *Aging Cell,* 10**,** 1011-20.

ROSSIELLO, F., AGUADO, J., SEPE, S., IANNELLI, F., NGUYEN, Q., PITCHIAYA, S., CARNINCI, P. & D'ADDA DI FAGAGNA, F. 2017. DNA damage response inhibition at dysfunctional telomeres by modulation of telomeric DNA damage response RNAs. *Nat Commun,* 8**,** 13980.

SAGELIUS, H., ROSENGARDTEN, Y., HANIF, M., ERDOS, M. R., ROZELL, B., COLLINS, F. S. & ERIKSSON, M. 2008. Targeted transgenic expression of the mutation causing Hutchinson-Gilford progeria syndrome leads to proliferative and degenerative epidermal disease. *J Cell Sci,* 121**,** 969-78.

SAITO, S., KUROSAWA, A. & ADACHI, N. 2016. Mutations in XRCC4 cause primordial dwarfism without causing immunodeficiency. *J Hum Genet,* 61**,** 679-85.

SARETZKI, G. 2014. Extra-telomeric functions of human telomerase: cancer, mitochondria and oxidative stress. *Curr Pharm Des,* 20**,** 6386-403.

SCAFFIDI, P. & MISTELI, T. 2008. Lamin A-dependent misregulation of adult stem cells associated with accelerated ageing. *Nat Cell Biol,* 10**,** 452-9.

SCHMIDTS, I., BOTTCHER, R., MIRKOVIC-HOSLE, M. & FORSTEMANN, K. 2016. Homology directed repair is unaffected by the absence of siRNAs in Drosophila melanogaster. *Nucleic Acids Res,* 44**,** 8261-71.

SCHOEFTNER, S. & BLASCO, M. A. 2008. Developmentally regulated transcription of mammalian telomeres by DNA-dependent RNA polymerase II. *Nat Cell Biol,* 10**,** 228-36.

SEDELNIKOVA, O. A., HORIKAWA, I., ZIMONJIC, D. B., POPESCU, N. C., BONNER, W. M. & BARRETT, J. C. 2004. Senescing human cells and ageing mice accumulate DNA lesions with unrepairable double-strand breaks. *Nat Cell Biol,* 6**,** 168-70.

SFEIR, A., KOSIYATRAKUL, S. T., HOCKEMEYER, D., MACRAE, S. L., KARLSEDER, J., SCHILDKRAUT, C. L. & DE LANGE, T. 2009. Mammalian telomeres resemble fragile sites and require TRF1 for efficient replication. *Cell,* 138**,** 90-103.

SFEIR, A. & SYMINGTON, L. S. 2015. Microhomology-Mediated End Joining: A Back-up Survival Mechanism or Dedicated Pathway? *Trends Biochem Sci,* 40**,** 701-14.

SHAH, P. P., DONAHUE, G., OTTE, G. L., CAPELL, B. C., NELSON, D. M., CAO, K., AGGARWALA, V., CRUICKSHANKS, H. A., RAI, T. S., MCBRYAN, T., GREGORY, B. D., ADAMS, P. D. & BERGER, S. L. 2013. Lamin B1 depletion in senescent cells triggers large-scale changes in gene expression and the chromatin landscape. *Genes Dev,* 27**,** 1787-99.

SHANBHAG, N. M., RAFALSKA-METCALF, I. U., BALANE-BOLIVAR, C., JANICKI, S. M. & GREENBERG, R. A. 2010. ATM-dependent chromatin

changes silence transcription in cis to DNA double-strand breaks. *Cell,* 141**,** 970-81.
SHILOH, Y. 2003. ATM and related protein kinases: safeguarding genome integrity. *Nat Rev Cancer,* 3**,** 155-68.
SHILOH, Y. & ZIV, Y. 2013. The ATM protein kinase: regulating the cellular response to genotoxic stress, and more. *Nat Rev Mol Cell Biol,* 14**,** 197-210.
SHIMI, T., BUTIN-ISRAELI, V., ADAM, S. A., HAMANAKA, R. B., GOLDMAN, A. E., LUCAS, C. A., SHUMAKER, D. K., KOSAK, S. T., CHANDEL, N. S. & GOLDMAN, R. D. 2011. The role of nuclear lamin B1 in cell proliferation and senescence. *Genes Dev,* 25**,** 2579-93.
ST LAURENT, G., WAHLESTEDT, C. & KAPRANOV, P. 2015. The Landscape of long noncoding RNA classification. *Trends Genet,* 31**,** 239-51.
STEIN, C. A. & CASTANOTTO, D. 2017. FDA-Approved Oligonucleotide Therapies in 2017. *Mol Ther,* 25**,** 1069-1075.
STORER, M., MAS, A., ROBERT-MORENO, A., PECORARO, M., ORTELLS, M. C., DI GIACOMO, V., YOSEF, R., PILPEL, N., KRIZHANOVSKY, V., SHARPE, J. & KEYES, W. M. 2013. Senescence is a developmental mechanism that contributes to embryonic growth and patterning. *Cell,* 155**,** 1119-30.
STUCKI, M., CLAPPERTON, J. A., MOHAMMAD, D., YAFFE, M. B., SMERDON, S. J. & JACKSON, S. P. 2005. MDC1 directly binds phosphorylated histone H2AX to regulate cellular responses to DNA double-strand breaks. *Cell,* 123**,** 1213-26.
SULLI, G., DI MICCO, R. & D'ADDA DI FAGAGNA, F. 2012. Crosstalk between chromatin state and DNA damage response in cellular senescence and cancer. *Nat Rev Cancer,* 12**,** 709-20.
SUN, Y., JIANG, X., CHEN, S., FERNANDES, N. & PRICE, B. D. 2005. A role for the Tip60 histone acetyltransferase in the acetylation and activation of ATM. *Proc Natl Acad Sci U S A,* 102**,** 13182-7.
TAKAI, K. K., KIBE, T., DONIGIAN, J. R., FRESCAS, D. & DE LANGE, T. 2011. Telomere protection by TPP1/POT1 requires tethering to TIN2. *Mol Cell,* 44**,** 647-59.
TCHKONIA, T., ZHU, Y., VAN DEURSEN, J., CAMPISI, J. & KIRKLAND, J. L. 2013. Cellular senescence and the senescent secretory phenotype: therapeutic opportunities. *J Clin Invest,* 123**,** 966-72.
TEIXEIRA, M. T., ARNERIC, M., SPERISEN, P. & LINGNER, J. 2004. Telomere length homeostasis is achieved via a switch between telomerase- extendible and -nonextendible states. *Cell,* 117**,** 323-35.
VALKO, M., RHODES, C. J., MONCOL, J., IZAKOVIC, M. & MAZUR, M. 2006. Free radicals, metals and antioxidants in oxidative stress-induced cancer. *Chem Biol Interact,* 160**,** 1-40.
VAN STEENSEL, B. & DE LANGE, T. 1997. Control of telomere length by the human telomeric protein TRF1. *Nature,* 385**,** 740-3.
VAN STEENSEL, B., SMOGORZEWSKA, A. & DE LANGE, T. 1998. TRF2 protects human telomeres from end-to-end fusions. *Cell,* 92**,** 401-13.
VICECONTE, N., DHEUR, M. S., MAJEROVA, E., PIERREUX, C. E., BAURAIN, J. F., VAN BAREN, N. & DECOTTIGNIES, A. 2017. Highly Aggressive Metastatic Melanoma Cells Unable to Maintain Telomere Length. *Cell Rep,* 19**,** 2529-2543.
VICKERS, K. C., ROTETA, L. A., HUCHESON-DILKS, H., HAN, L. & GUO, Y. 2015. Mining diverse small RNA species in the deep transcriptome. *Trends Biochem Sci,* 40**,** 4-7.
VON ZGLINICKI, T., SARETZKI, G., LADHOFF, J., D'ADDA DI FAGAGNA, F. & JACKSON, S. P. 2005. Human cell senescence as a DNA damage response. *Mech Ageing Dev,* 126**,** 111-7.

WAAIJER, M. E., CROCO, E., WESTENDORP, R. G., SLAGBOOM, P. E., SEDIVY, J. M., LORENZINI, A. & MAIER, A. B. 2016. DNA damage markers in dermal fibroblasts in vitro reflect chronological donor age. *Aging (Albany NY),* 8**,** 147-57.

WAN, L. & DREYFUSS, G. 2017. Splicing-Correcting Therapy for SMA. *Cell,* 170**,** 5.

WARD, I. M. & CHEN, J. 2001. Histone H2AX is phosphorylated in an ATR-dependent manner in response to replicational stress. *J Biol Chem,* 276**,** 47759-62.

WARD, J. F. 1988. DNA damage produced by ionizing radiation in mammalian cells: identities, mechanisms of formation, and reparability. *Prog Nucleic Acid Res Mol Biol,* 35**,** 95-125.

WATSON, J. D. 1972. Origin of concatemeric T7 DNA. *Nat New Biol,* 239**,** 197-201.

WEI, W., BA, Z., GAO, M., WU, Y., MA, Y., AMIARD, S., WHITE, C. I., RENDTLEW DANIELSEN, J. M., YANG, Y. G. & QI, Y. 2012. A role for small RNAs in DNA double-strand break repair. *Cell,* 149**,** 101-12.

WRIGHT, W. E., PIATYSZEK, M. A., RAINEY, W. E., BYRD, W. & SHAY, J. W. 1996. Telomerase activity in human germline and embryonic tissues and cells. *Dev Genet,* 18**,** 173-9.

WU, L. & HICKSON, I. D. 2003. The Bloom's syndrome helicase suppresses crossing over during homologous recombination. *Nature,* 426**,** 870-4.

WU, L., MULTANI, A. S., HE, H., COSME-BLANCO, W., DENG, Y., DENG, J. M., BACHILO, O., PATHAK, S., TAHARA, H., BAILEY, S. M., DENG, Y., BEHRINGER, R. R. & CHANG, S. 2006. Pot1 deficiency initiates DNA damage checkpoint activation and aberrant homologous recombination at telomeres. *Cell,* 126**,** 49-62.

WU, P., TAKAI, H. & DE LANGE, T. 2012. Telomeric 3' overhangs derive from resection by Exo1 and Apollo and fill-in by POT1b-associated CST. *Cell,* 150**,** 39-52.

WYATT, D. W., FENG, W., CONLIN, M. P., YOUSEFZADEH, M. J., ROBERTS, S. A., MIECZKOWSKI, P., WOOD, R. D., GUPTA, G. P. & RAMSDEN, D. A. 2016. Essential Roles for Polymerase theta-Mediated End Joining in the Repair of Chromosome Breaks. *Mol Cell,* 63**,** 662-673.

WYATT, H. D. & WEST, S. C. 2014. Holliday junction resolvases. *Cold Spring Harb Perspect Biol,* 6**,** a023192.

XI, L. & CECH, T. R. 2014. Inventory of telomerase components in human cells reveals multiple subpopulations of hTR and hTERT. *Nucleic Acids Res,* 42**,** 8565-77.

XIN, H., LIU, D., WAN, M., SAFARI, A., KIM, H., SUN, W., O'CONNOR, M. S. & SONGYANG, Z. 2007. TPP1 is a homologue of ciliate TEBP-beta and interacts with POT1 to recruit telomerase. *Nature,* 445**,** 559-62.

XU, M., PALMER, A. K., DING, H., WEIVODA, M. M., PIRTSKHALAVA, T., WHITE, T. A., SEPE, A., JOHNSON, K. O., STOUT, M. B., GIORGADZE, N., JENSEN, M. D., LEBRASSEUR, N. K., TCHKONIA, T. & KIRKLAND, J. L. 2015a. Targeting senescent cells enhances adipogenesis and metabolic function in old age. *Elife,* 4**,** e12997.

XU, M., TCHKONIA, T., DING, H., OGRODNIK, M., LUBBERS, E. R., PIRTSKHALAVA, T., WHITE, T. A., JOHNSON, K. O., STOUT, M. B., MEZERA, V., GIORGADZE, N., JENSEN, M. D., LEBRASSEUR, N. K. & KIRKLAND, J. L. 2015b. JAK inhibition alleviates the cellular senescence-associated secretory phenotype and frailty in old age. *Proc Natl Acad Sci U S A,* 112**,** E6301-10.

YANG, H., WANG, H., REN, J., CHEN, Q. & CHEN, Z. J. 2017. cGAS is essential for cellular senescence. *Proc Natl Acad Sci U S A,* 114**,** E4612-E4620.

YE, J. Z., DONIGIAN, J. R., VAN OVERBEEK, M., LOAYZA, D., LUO, Y., KRUTCHINSKY, A. N., CHAIT, B. T. & DE LANGE, T. 2004. TIN2 binds TRF1

and TRF2 simultaneously and stabilizes the TRF2 complex on telomeres. *J Biol Chem,* 279**,** 47264-71.

ZELENSKY, A., KANAAR, R. & WYMAN, C. 2014. Mediators of homologous DNA pairing. *Cold Spring Harb Perspect Biol,* 6**,** a016451.

ZHA, S., GUO, C., BOBOILA, C., OKSENYCH, V., CHENG, H. L., ZHANG, Y., WESEMANN, D. R., YUEN, G., PATEL, H., GOFF, P. H., DUBOIS, R. L. & ALT, F. W. 2011. ATM damage response and XLF repair factor are functionally redundant in joining DNA breaks. *Nature,* 469**,** 250-4.

ZHANG, J., LIAN, Q., ZHU, G., ZHOU, F., SUI, L., TAN, C., MUTALIF, R. A., NAVASANKARI, R., ZHANG, Y., TSE, H. F., STEWART, C. L. & COLMAN, A. 2011. A human iPSC model of Hutchinson Gilford Progeria reveals vascular smooth muscle and mesenchymal stem cell defects. *Cell Stem Cell,* 8**,** 31-45.

ZHONG, F. L., BATISTA, L. F., FREUND, A., PECH, M. F., VENTEICHER, A. S. & ARTANDI, S. E. 2012. TPP1 OB-fold domain controls telomere maintenance by recruiting telomerase to chromosome ends. *Cell,* 150**,** 481-94.

ZHU, Y., TCHKONIA, T., PIRTSKHALAVA, T., GOWER, A. C., DING, H., GIORGADZE, N., PALMER, A. K., IKENO, Y., HUBBARD, G. B., LENBURG, M., O'HARA, S. P., LARUSSO, N. F., MILLER, J. D., ROOS, C. M., VERZOSA, G. C., LEBRASSEUR, N. K., WREN, J. D., FARR, J. N., KHOSLA, S., STOUT, M. B., MCGOWAN, S. J., FUHRMANN-STROISSNIGG, H., GURKAR, A. U., ZHAO, J., COLANGELO, D., DORRONSORO, A., LING, Y. Y., BARGHOUTHY, A. S., NAVARRO, D. C., SANO, T., ROBBINS, P. D., NIEDERNHOFER, L. J. & KIRKLAND, J. L. 2015. The Achilles' heel of senescent cells: from transcriptome to senolytic drugs. *Aging Cell,* 14**,** 644-58.

ZOU, L. & ELLEDGE, S. J. 2003. Sensing DNA damage through ATRIP recognition of RPA-ssDNA complexes. *Science,* 300**,** 1542-8.

Acknowledgements

I would like to thank a number of people that supported me during my PhD.

To Dr. Fabrizio d'Adda di Fagagna, who believed in me and granted me the possibility to join his laboratory, and for his full support and dedication throughout my PhD.

To Prof. Marco Foiani and Prof. Joachim Lingner, for accepting to be my PhD co-supervisors and for dedicating their time to discuss my data and give relevant suggestions to improve the quality of my research.

To Dr. Anabelle Decottignies and Dr. Ylli Doksani, for accepting to be my PhD dissertation examiners and for reading my thesis.

To all FDA members, for making the lab a great environment to work in, which often lead to long and fruitful scientific discussions. In particular Francesca, Corey and iFabio, for their support and constant willingness to help throughout all my PhD. I am especially thankful to Quan, for his support and help during my stay in Japan and throughout all the process of putting together the TEsR story.

To all the good friends I have met outside the lab, in particular Smbat and Chris, for making these years in Milan unforgettable, their friendship grows every day.

A Dominika, por estar siempre ahí, por ser un apoyo incondicional.

Y, por último, mi mayor agradecimiento va a mi familia. Gracias a ella he llegado hasta aquí. Por el esfuerzo de mis padres de querer siempre lo mejor para mí. Estoy por siempre agradecido.